The Dissertation Committee for Mehrdad Vatani Certifies that this is the approved version of the following dissertation:

A VOLTAGE-ONLY METHOD FOR ESTIMATING THE LOCATION OF TRANSMISSION FAULTS

Committee:

Mack Grady, Supervisor

Mircea Driga

Aristotle Arapostathis

Edward Powers

William Guy

A VOLTAGE-ONLY METHOD FOR ESTIMATING THE LOCATION OF TRANSMISSION FAULTS

by

Mehrdad Vatani, B.S.; M.B.A.; M.S.E.

Dissertation

Presented to the Faculty of the Graduate School of

The University of Texas at Austin

in Partial Fulfillment

of the Requirements

for the Degree of

Doctor of Philosophy

The University of Texas at Austin

December 2006

To my father

To Ladan

To my mother and my family

Acknowledgements

The author is grateful to his supervisor and mentor Dr. W. Mack Grady for his guidance, inspiration, and continuous support throughout the author's doctoral studies. The author appreciates Dr. Grady's strong commitment toward excellence in research, education and his ideas and technical suggestions that allowed completion of this work.

The author would like to appreciate his dissertation committee members: Dr. Mircea Driga, Dr. Aristotle Arapostathis, Dr. Edward Powers, and Dr. William Guy for their suggestions and support throughout the project.

The author would like to thank his true friend Arastou Oskoui for his care and support, and his lifelong friend Javid Maghsoudi for his friendship and inspirations.

A special note of thanks to Austin Energy and the City of Austin for advocating higher education for its staff at all levels and in particular allowing its measured field data to be used by the author for verification of the methodology developed in this dissertation. The author also appreciates all the help provided by his friends and colleagues.

Finally, the author would like to thank the light of his life Ladan Vatani for her love, support and motivations and her courage in life, and his kind brother Eshragh for his devotions and care for their mother.

Mehrdad Vatani

The University of Texas at Austin

December 2006

A VOLTAGE-ONLY METHOD FOR ESTIMATING THE LOCATION OF TRANSMISSION FAULTS

Publication No._____

Mehrdad Vatani, Ph.D.
The University of Texas at Austin, 2006

Supervisor: W. Mack Grady

This dissertation develops, and illustrates with actual data, a new voltage-only based fault location procedure that incorporates the system impedance matrices into the problem so that as few as three or four voltage recording devices can estimate the fault location over a wide area. This procedure can quickly help pinpoint the fault and complement other available information normally used to manually locate the fault.

The second approach takes advantage of the capabilities of microprocessor relays on distribution feeders to reflect their voltage sag measurements back to the transmission system for use with the above algorithm.

Table of Contents

List of Tables

List of Figures

Chapter 1: Introduction

Accurately locating faults in a timely manner can expedite restoration of the faulted transmission line and reduce equipment damage that often occurs when there is a transmission line fault. Rapid equipment repairs and service restoration subsequent to a permanent fault are essential elements of electric utility operation. During peak load situations where transmission line availability is critical, a prolonged transmission line outage is detrimental to system operation and can have severe economic and reliability impacts on electric utility customers.

With today's tighter supply of generation, coupled with 1. generation being imported over long distances, 2. high demands for electricity, and 3. congested transmission lines, a sustained fault can have adverse economic impact as well as impact on system operation and reliability. Moreover, there are an increasing number of sensitive loads. In particular the high-tech industrial customers in today's market demand more reliable power, quicker response time in locating and repairing faults, and an accurate determination of the cause of faults as a preventive measure. Historically, common practices in electric utility companies were such that only sustained faults were investigated. These attitudes have changed in recent years with privatization and deregulation of the electric utility industry and competitive markets throughout the world.

The recent changes in the power industry such as open access and deregulation have an impact on the reliability and security of power systems. Regulatory agencies such as Electric Reliability Council of Texas (ERCOT) require electric utility entities to maintain higher system reliability and security by implementing better protection and control schemes in their transmission systems. Moreover, since the beginning of the year

2000, ERCOT requires the member utilities to submit their transmission line outage history to assure a reliable electric network in Texas. Since 1997, the Public Utility Commission of Texas (PUCT) requires similar fault reports on transmission and distribution system from all utilities in the state of Texas to assure reliable service to customers. Reliability statistical indices such as system average interruption frequency index (SAIFI), system average interruption duration index (SAIDI), customer average interruption duration index (CAIDI), momentary average interruption frequency index (MAIFI), and average service availability index (ASAI) data are all part of the reporting requirements. These data are directly related to transmission line faults and the fault restoration efforts by the utility companies.

The existing practiced algorithm for fault location depends on many elements in which each element can introduce a possible source of error in fault location methods. Current microprocessor-based fault recording devices, such as relays and fault recorders, have provided more accurate digitized line voltage and current data for locating a fault in transmission systems. There are several different methods in today's market which uses such data for fault location.

Accurate fault location and analysis helps to identify causes of both temporary and permanent faults, weak spots in the transmission system, and transmission tower footing resistance. This can alleviate and prevent re-occurrence of similar future faults, improve system and service reliability, reduce operation and maintenance cost, and identify system upgrade or deficiencies.

Therefore, due to the new electric utility industry environment which demands better utilization of its manpower and power system resources, recent deregulation in the electric utility industry and its consequent competitive environment in this market segment, demand for faster restoration time from the highly load-sensitive customers, and requirements from the regulatory agencies, a more accurate method for fault location which is not dependent on many system elements is needed. Moreover, other forces that make the need for a new fault location method imperative are: innovation and availability of enormous amount of data form new digital power system protection devices, of new technologies in data collection and analysis, and in communications and data signal processing. Available advanced data acquisition and data processing technique made possible by advancement in precise time receivers.

The location of a transmission system fault is often not determined as fast as it should be. In ideal situations where microprocessor-based relays are extensively used, these relays can immediately estimate fault location on the lines they protect by using their voltage and current measurements. However, they are not very useful when the fault is a few buses away or when there are false or sympathetic trips on other circuits. Those situations usually require field inspection or the use of a simulation program to locate the fault.

This dissertation develops, and illustrates with actual data, a new voltage-only based fault location procedure that incorporates the system impedance matrices into the problem so that as few as three or four voltage recording devices can estimate the fault location over a wide area. The procedure can quickly help pinpoint the fault and complement other available information. A typical application of this approach as being used in the following way: a utility that has a number of relatively expensive fault

recorders at the most critical substations (e.g., 5-10% of all substations), whose data are readily available at their central control center or engineering office, can with no additional investment use this fault location procedure independent of and supplemental to the data captured by system protection devices, including SCADA and RTU. Furthermore, sag data from one transmission voltage level (e.g., 138kV) can be used to locate faults on other levels (e.g., 345kV or 69kV).

Chapter 1 describes the current-day's methodologies of locating a fault by 1) impedance method, where the voltage and current at the faulted line terminations are measured, 2) traveling wave method where the relative time of the traveling wavefront produced by the fault is measured at both terminations of the faulted line.

Chapter 2 describes the innovative method for a better and more accurate location of a fault on a transmission line. This method of fault location is bases on voltage-only measurements in a few buses in the system. It utilizes system impedance matrices and a least-squared error minimization technique to estimate the fault location. This chapter formulates the problem for all fault types.

In chapter 3, the author applies this new methodology to several examples of actual, real-world, collected fault data to test the proposed methodology. Actual field data for 15 events were used to verify and validate the developed methodology and equations. The results of the research are described in detail followed by graphs and tables. For each case, the bus ranking and the error of actual fault bus determined by the algorithm and the error of the bus chosen by the algorithm for two, three, four, and five meter cases are shown in tabular format. An enhancement of the algorithm for locating phase-phase and

phase-phase to ground fault types and the results of the enhanced algorithm are compared to the results of the original algorithm. Moreover, the goodness of the best choice is explained by comparing the least-squared error of the chosen bus to that of the next four most likely candidates.

The next phase of this work as described in Chapter 4, takes advantage of the capabilities of microprocessor relays on distribution feeders to reflect their voltage sag measurements back to the transmission system for use with the above algorithm to estimate the fault location on transmission system.

In Chapter 5, the developed methods in the previous chapter are tested and validated using actual field measured values. First the measured voltage values are verified to be correct, then actual fault events were used for validation.

Chapter 6 gives a brief review of this dissertation and describes the significant elements. A table with comparison of the current existing methods and the new methodology with their advantages and disadvantages are presented in this conclusion chapter. Possible future research relating to this topic is also presented.

1.1 Present-day Methodologies

Historically, since the 1940's, before the invention of the solid state and microprocessor-based relays, the only method of fault location was analysis of the information from the line protection electromechanical relays. The whole principal of protection schemes is to provide sufficient and adequate redundancy to protect a line during a fault and minimize the damages to the equipment on the line. Power system protection schemes use protective relays. The main purpose of a relay is to protect the line when a fault occurs on the line due to lightning or other causes. In addition to providing protection, the relays can also provide information to locate the fault on the protecting line. The protective relay elements detect the voltage and current abnormalities during a fault in a timely manner and send signals to the transmission line breakers to open both terminations of the faulted line to clear the fault and minimize the damage to transmission line equipment. Depending on the voltage of a transmission line, a fault normally can be cleared in about 4-7 cycles; the higher the transmission lines voltage, the faster the clearing time. It would take 1-2 cycles for the relays to detect the fault and 2-5 cycles for the breakers to receive the trip signal from the relay and mechanically open and isolate the fault.

The basic objective of system protection in generation, transmission and distribution systems of a power system is to isolate a disturbance or fault as quickly as possible without interruption of power flow in the rest of the system. The key element in system protection is reliability of the protection system. Two main elements of reliability are dependability and security. Dependability means the protection system would work when it is needed, and security means that the system will not operate when it should not.

There are two independent protection techniques used in protecting a transmission line, namely Primary and Backup protections for both phase and ground faults. There are variety of schemes within each main scheme depending on the system protection engineer's protection philosophy, the application of the scheme, and the characteristics of the utility's transmission system. The main protection system for a given zone of protection is called the Primary protection system. It operates in the fastest time possible and removes the least amount of equipment from service. The main application of Primary protection is fast tripping time of the breakers to isolate the fault from the power system. The Primary scheme also provides protection for the entire transmission line (100% of the line). The Backup protection scheme is commonly used as a backup for the Primary scheme. Backup protection is essential in transmission line protection because if a fault is not cleared rapidly by the Primary, it can cause system instability as well as extensive equipment damage and hazards to personnel. The IEEE Standard Dictionary defines the Backup relaying as "protection that operates independently of specified components in the primary protective system and that is intended to operate if the primary protection fails or is temporarily out of service". The key components of the Backup protection scheme is the presence of time delay elements. The relays used in the Backup are generally slower than the Primary and remove more system elements to clear a fault. Backup may be installed locally in the same substation as the Primary protection, or remotely. In general, Backup protection includes remote backup, local backup, and breaker failure relaying. The breaker failure is a subset of local backup and is used when a transmission line breaker fails to trip when it receives a trip signal. The IEEE Standard Dictionary defines the remote backup as "backup protection in which the protection is at the station or stations other than that which has the primary protection."

There are numerous combinations of the Primary and Backup techniques used for transmission line protection by the electric utilities depending on the company's protection philosophy and economics. For example, a Primary can be protected by a Backup scheme, or by another Primary scheme. In another words, a Primary can be used as a Backup for a Primary scheme. This means that two primary schemes can be used for line protection: one designated Primary and one Primary as the Backup.

As described above, the two key elements in the Primary scheme are 1) the 100% coverage of the entire protecting circuit and 2) the instantaneous clearance of the fault without any time delay elements.

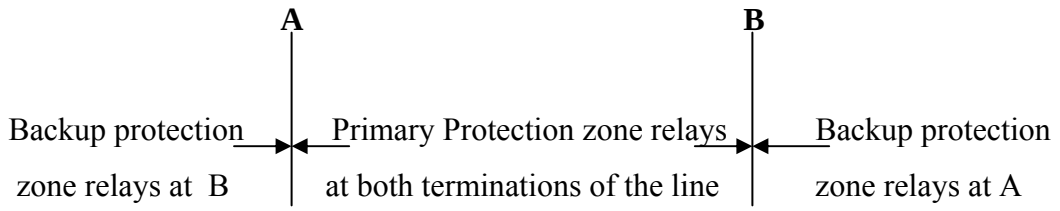

Figure 1.1: Zones protection schemes [1]

There are time delays between the operations of the Primary and the Backup systems. This time delay between the operation of each protective scheme is called CTI (Coordination Time Interval). This delay is necessary to assure proper coordination of the operations of each protection scheme and so that a minimum number of schemes operate for a fault. The first sign of the fault on a transmission line is normally detected by the Primary protection relays and if this fails, various backup systems should ensure to clear the fault. However, it is crucial to have time delays between the redundant protection

schemes. These redundancies are essential in all levels of a power system from generation to distribution levels.

Pilot protection is used for most of the Primary protection schemes. The Pilot scheme is used as a supplementary tool in the Primary protection to assure fastest and timely clearance of a fault without any time delay. Pilot refers to a communication channel between two or more ends of a transmission line to provide instantaneous clearing over 100% of the line. Pilot requires direct communications between the terminations of the protecting circuit. The information between the substations is sent over a communication channel using power line carrier (PLC), microwave, fiber optic cable or telephone circuits. Some of the commonly used schemes under the Primary protection scheme which uses Pilot include: Current Differential, Time-Overcurrent Protection, Transfer Trip, Directional Comparison Blocking, Directional Comparison Unblocking, Permissive Underreach Transfer Trip (PUTT), Permissive Overreach Transfer Trip (POTT), and Power Line Carrier (On/Off) scheme.

The Backup protection scheme uses what is called “distance phase and ground protection” with “zones of protection”. A distance relay responds to input quantities as a function of the electric circuit distance between the location of the relay to the location of the fault. There are many types of distance relays namely: impedance, reactance, offset distance, and mho relays. The way that a distance relay operates is that it compares the current and the voltage of the power system and determines if the fault is within or outside of its protection zone. The primary advantage of distance relays is that the relay’s zone of operation is a function of only the impedance of the protecting circuit which is fixed constant quantity and is independent of the current and voltage magnitudes. This makes the

distance relay to have a fixed reach, as opposed to overcurrent units which its reach varies with the source conditions. Zone distance relays are commonly used for the Backup protection. However, a Pilot scheme (with direct communication such as POTT scheme) can also be used in Backup scheme.

Zone relays normally have four zones of protection, Zone 1, Zone 2, Zone 3, and Reverse Zone 3. Depending on the type of the relay and its manufacturer, some relays include all four zones and are packaged into one relay, and some have separate relays for each zone of protection. For example, the KDAR phase-distance relays, type KD-10 and KD-11, are a three-phase, single zone package in design. Zone 1 setting of a relay normally provides protection for 90% of the protecting line for phase and 80% protection for ground faults. This means that its protection zone of reach is set to detect faults that occur within the first 90% of the line from that termination of the line where the relay is located. The Zone 2 relay is set to protect 100% of the protecting line plus 50% of the next shortest line connected to the remote termination of the protected line. Zone 2 relays are used in the Pilot scheme to initiate the needed communication. The Zone 3 relay is set to protect 100% of the protected line plus 100% of the next shortest line connecting to the other termination of the protected line. The Reverse Zone 3 relay looks in reverse (looking backwards) at its protected line and protects 80% of the line connecting to that terminal.

Figure 1.2 below shows four zones of protection to protect a line and to provide backup for the remote section with their designated coordination time interval (CTI) with "T" symbols on the Figure. The Figure uses 4 buses and 3 lines with breakers on each termination of the lines. As it was described earlier, the Zone 1 is normally set for 80%-90% of line impedance, Zone 2 for 100% of the line plus 50% of the next shortest line of

the remote bus, and Zone 3 for 100% of both lines plus 25% of the next line to the remote bus. The Zone 1 tripping is instantaneous but does not reach the remote bus, the 10%-20% reach margin is to have a safety factor for security (over-trip protection), to accommodate differences or inaccuracies in relays, CT, PT, and the transmission line impedance. This safety factor is redundantly protected by the Zone 2 relay which operates with one step of CTI (T2). Backup Zone 3 also operates with T3 timer to coordinate with the Zone 2 unit of the remote bus. Finally Reverse Zone 3 coordinates with T3 timer with the relays operating behind the protecting line rather than ahead. Zone 2 and Zone 3 relays also work with the Pilot schemes to initiate the communication. For example, Zone 3 is used to start the communication carrier used in Directional Comparison Blocking Pilot relaying scheme. The above protecting zones may change slightly if either termination of the protecting lines has infeed. Infeed is when there is more than one source of fault current feeding the fault on the transmission line. The detailed consideration of this phenomenon is beyond the scope of this dissertation.

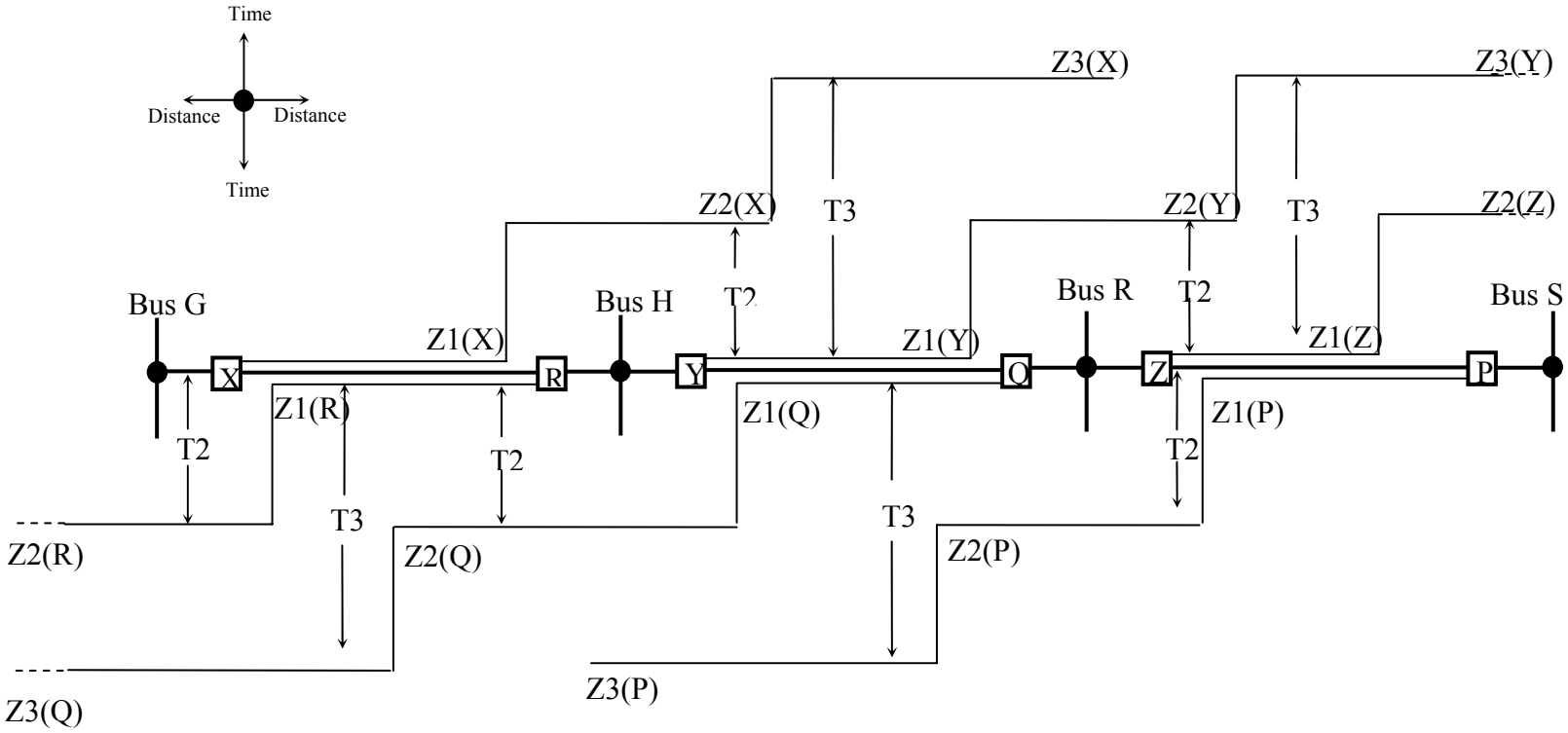

Figure 1.2: Protection zones of distance relays [1]

The solid-state types of phase and ground distance relays, such as SKD, SKDT, LDZG, and LKD, operate in a similar manner to the electromechanical relays described above. They employ the single comparator technique that involves the detection of the phase relationship between the two ac quantities. However, in today's world of microprocessor-based relays, such as MDAR by ABB (Asea Brown Bovery), and the variety of the SEL relays (Schweitzer Engineering Laboratories) such as SEL 311C, 320, or SEL 351 relays, with single or multi-processors approach in design, the logic is available for one relay to be programmed and set for any of several schemes used as either Primary, Pilot or Backup for phase and ground protections.

The crucial objective of the redundancies in protection schemes is to provide ample protection schemes so that if one scheme fails to operate, the alternative scheme will guarantee protection of the line and isolation of the fault from the system. Analysis of the relays that detect a fault can be used for fault location. Having Primary and zone relays for protection at both terminations of the protecting transmission line provide enough information to determine a fault within 15%-20% from each line termination. For example, when the Zone 1 relay operates from one termination of a faulted line and Primary relays at the other end of the faulted line, the fault location can be estimated to be within the first 20% of the line out of the Primary protection end of the line. This is because if the fault was outside the 20%, the Primary, the Zone 1 would not have operated for that fault. On the other hand, when the Zone 1 relay at both terminations of the line operates for a fault, it can indicate that the fault is within middle 60% of the faulted line. This method reduces by 40% the amount on line that line maintenance personnel should patrol, which expedites locating the actual evidences of the fault and line restoration. The faulted phase in this basic approach is determined by the relay target flag indications on certain types of the

electromechanical relays which are equipped with detected phase information. Moreover, the data collected from an analog or recently available digital fault recorders can also indicate the faulted phase. Even today, in many small and some large utilities where the old electromechanical relays are used for transmission line protection, analysis of the zone relays is the only approach to determine a fault location.

The current methodology of fault location method is to determine the apparent reactance of the line during a fault when the current is flowing, and to convert this ohmic value into distance based on the transmission line parameters. Utilizing microprocessor based relays and digital data communications, two general classes of algorithms have been used for fault location. Most algorithms are based on the calculation of the post-fault, fundamental frequency voltage and current phasors. These phasors are calculated by either filtering the transient data, or by numerical processing techniques. The second class of algorithms is based on traveling wave methods. In this method, the arrival of the high frequency pulse due to a fault at each termination of the faulted line is time tagged. Then, the fault location is determined by the information of the surge impedance of the line, the length of the line, and the difference between the times of arrival of the pulse at each termination of the faulted line. Another approach in traveling wave method has been the use of wavelets where the sampled voltage and current data are decomposed to determine the time of arrival of the high frequency fault pulse.

1.1.1 Line Impedance Method

In this method, fault location is based on voltage and current information from one termination or from both terminations of the monitored line. Although an algorithm that uses fault data from two terminals of the line provides the most accurate results in fault location, single-terminal method is desirable when the data on both terminals of the faulted line is not available due to the cost of equipping both terminations of the line with monitoring devices. The protection and monitoring devices of the line record and calculate the fault location from the impedance looking into the line from one end. Since the remote termination voltage and current information is not available, equivalent system impedance is developed for the system beyond the remote termination. The remote end equivalent voltage source is determined by the recorded local voltage and current data. Single-terminal method is the most practical since no communication channel is needed.

In the line impedance method, two approaches have been developed: one which uses frequency domain representation of the voltage and current, and the other uses the time domain of the voltage and current waveforms.

Reactance relays are used in the single-terminal method, however, accurate fault location is difficult to achieve. Fault location using reactance relays is affected by the load flow and the fault resistance. Moreover, the accuracy of the fault location with this approach can be influenced by the current flow through other phases of the transmission line by mutual impedance. T. Takagi developed a method that provides a simple calculation that considers perfect load flow to reduce the effects of fault resistance. This method is used for calculations for the single-terminal [2]. Takagi's approach uses a phasor representation for voltage and current with data sampling of every quarter of a cycle.

Although this algorithm eliminates the effect of the unknown fault resistance, it makes an assumption that the angle of the total fault current and the fault current contribution from the remote end are equal. Fault resistance and load flow is required to use the Takagi approach.

A recent improvement on Takagi approach uses iterative calculation of the difference between the total fault current and the remote end current contribution [3]. However, this algorithm assumes the phase impedances are balanced and does not consider the mutual coupling between sequence components. The other iterative procedure was proposed by Richards and Tan [4]. These techniques generally estimate the impedance to the fault as seen from the line terminal and convert this estimate to line length.

Another recent improvement of using frequency domain without iterative technique estimates the distance of a transmission line fault from the relay locations [5]. It uses the measured fundamental frequency voltages and currents at the line terminals. The measured data are collected from the digital impedance relays at both terminations of the protected line. The data do not need to be synchronized and this technique also assumes a balanced three-phase power system.

The pi model of the transmission line which includes the series impedance and shunt capacitance is shown in Figure 1.3. R_X and R_Y represent the digital impedance relays at both termination of the line. These relays detect and isolate the fault by sending signals to the circuit breakers. At the same time, they also measure the fundamental frequency of the power qualities in terms of voltage and current. These measured values are analyzed to determine the fault by either a computer or by the same relays.

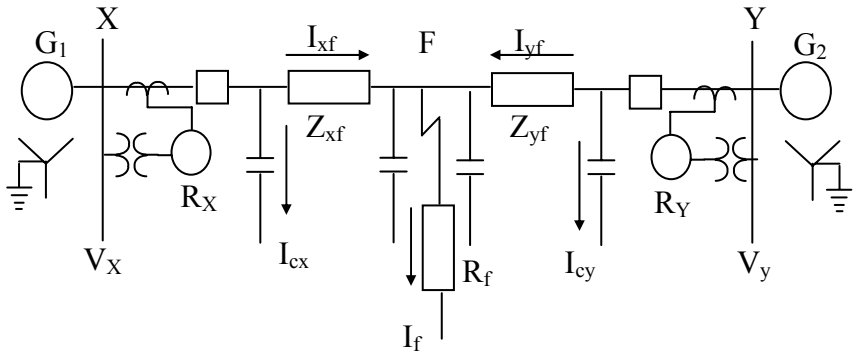

Figure 1.3: Fault at F in balanced three-phase system

For all types of faults: phase-ground, phase-phase, phase-phase-ground, and three-phase fault, this technique uses symmetrical component analysis and sequence network diagram as shown on Figure 1.4 below.

The distance of a fault from bus X, (L_x) and from bus Y, (L_y) is obtained from Z_{1xf} and Z_{1yf} using the following:

$$L_x = L\left[\frac{IM(Z_{1xf})}{IM(Z_1)}\right]$$

$$L_y = L\left[\frac{IM(Z_{1yf})}{IM(Z_1)}\right]$$

where:

- L is the length of the line from bus X to bus Y.
- $IM(Z_{1xf})$ and $IM(Z_{1yf})$ are the imaginary part of the positive-sequence line impedance from buses X and Y to the fault.
- Z_1 is the positive-sequence impedance of the transmission line from bus X to bus Y [5].

Another approach using line impedance for an a-phase-ground fault at bus K [6]:

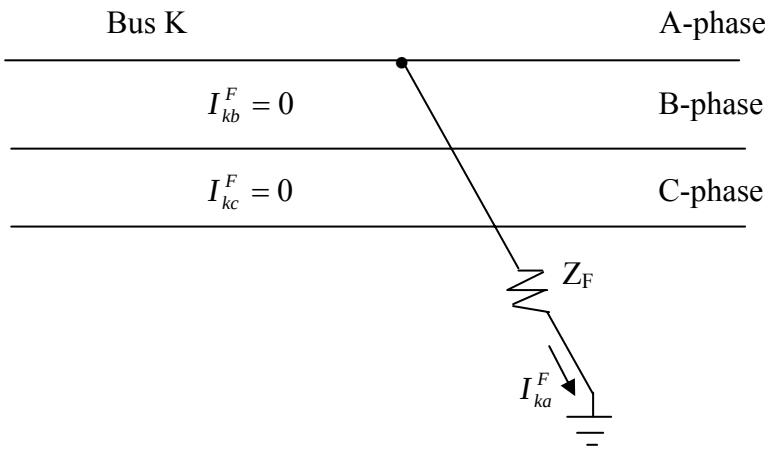

Figure 1.4: A-to-ground fault at bus K

$$V_{ka}^{F} = I_{ka}^{F} Z_{F}$$

$$I_{ka}^{F} = \frac{3V_{ka}^{Pre}}{Z_{k0,ko} + Z_{k1,k1} + Z_{k2,k2} + 3Z_{F}}$$

using

$$I_{k0}^{F} = I_{k1}^{F} = I_{k2}^{F} = \frac{I_{ka}^{F}}{3}$$

all the network voltages can be found from

$$V_{j012}^{F} = V_{j012}^{Pre} - Z_{j-k,012} I_{k012}^{F}$$

The above algorithms use the frequency domain approach, meaning phasor voltage and current quantities are used to determine fault location. The fault location is calculated based on the average 60 Hz content over several cycles.

A similar algorithm uses the time domain representation of voltage and current. A new estimate of fault location is calculated at each sample point in time. The fault location

algorithm uses the phase representation of self and mutual impedances for the transmission line and remote source equivalent. For fault location in this method, sampled fault voltage and current channels from a digital data from a fault recorder are used. This fault location algorithm is based on the Z-transform technique [7]. In this technique, the system parameters are determined from sample data system to model system response to a fault.

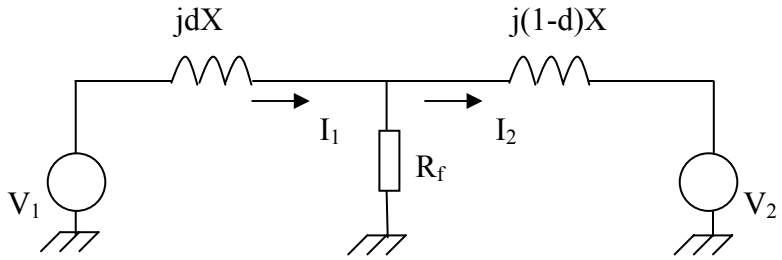

Figure 1.5: Single phase circuit for Z-transform method [7]

The single-phase model of transmission line with both line terminations during a fault is shown above in Figure 1.5. The known quantities of this model are: the total line reactance X and the V_1 and I_1 which are sampled and recorded by the fault recorders or relays at one termination of the line. The remote termination voltage, V_2, is known from the pre-fault data. The unknown quantities are the fault resistance R_f and the fractional distance to the fault. Immediately before the fault, both R and d are equal to zero. To solve for the unknown quantities, KVL can be applied to the loops as shown in Figure 1.5:

$$\begin{aligned} V_1 - jI_1 dx - (I_1 - I_2)R_f &= 0 \\ (I_1 - I_2)R_f - jI_2(1-d)x - V_2 &= 0 \end{aligned} \qquad (1.1)$$

After simplifications and cancellations, the remote termination current, I_2 is eliminated and the above equations can be used to solve for d.

More details on this algorithm are available in Reference [7].

There are also novel methods for locating phase-ground and phase-phase-ground faults on a non-direct-ground neutral system using single-termination data [8, 9]. Non-ground neutral and arc-suppression-coil-ground neutral systems are normally called non-direct ground neutral systems. The difference in fault location algorithm in this method from the other algorithms is that the faulted phase and the zero-sequence are used for its modeling. In this model, the accuracy of the fault location is not affected by the load and the fault resistance. The procedure in this algorithm is set up such that the faulted line and phase are determined automatically and do not require manual analysis of the data by an engineer for fault location. In this method, the pi-model of the transmission system and the faulted network three-sequence networks are used. It assumes [8]:

$$Z_1 = Z_2 = Z \quad and \quad Z_0 = \sigma\, Z \qquad\qquad where \quad \sigma = 3 - 5.5$$

The zero-sequence voltage and current are determined by three-phase voltages and currents using:

$$I_0 = \left(I_a + I_b + I_c\right)/3$$
$$V_0 = \left(V_a + V_b + V_c\right)/3$$

This method also uses the Z-transform theory to locate transmission line faults with sampling data of faulted power network. The general principal for this approach is that the sample fault wave of the faulted line is identified first (based on the difference of power flow direction between the faulted line and non-faulted lines). Once the faulted line and phase are determined, the Newton-Raphson method is used to determine distance to the fault.

The results of several simulations using the above method, with the assumption that the line impedance and the sampling data of the voltage and currents, are accurate. However, the sampled data shows 10% inaccuracy in the above assumptions. The results of the simulations indicate some inaccuracy with the parameters and the data, which contributes to the error in fault location.

The other impedance method of fault location is based on voltage and current information from both terminations of the monitored line. This method is a more advanced and complex theoretical approach of the impedance methods. It uses data from both terminals and requires additional system modeling, models the transmission line based on a fundamental frequency, and pi-representation of each section of the line [10]. A reduced model of the transmission system around the faulted line is developed. Then, a number of Electromagnetic Transient Program (EMTP) cases are run to establish simulated fault voltage and current. The fault location algorithm uses series impedances and shunt admittance matrices for each line sections. The EMTP results determine the transmission line constants to be used to build the matrices. An assumption of the faulted section is made by assuming its series impedance is proportional to the distance to the point of fault. This approach models an unknown resistance at the fault point, and then develops a complex equation relating sending and receiving end voltages and currents, including the unknown fractional distance to the fault and fault resistance. By taking the real and imaginary parts of the complex equations, the model sets up a system of nonlinear equation with real coefficients. And finally it solves for the fractional distance to the fault and the fault resistance using the Newton's Method for solving the nonlinear equations.

In this method, the voltage and the current are synchronized by clocks at both terminations of the line. Digital fault recorders or microprocessor bases are used as the source of voltage and current data. The field test with this method showed that one millisecond error results in plus or minus one mile depending on the timing error [10]. For this approach, less than one millisecond (equals 21.6 electrical degree) timing error is considered acceptable.

The superior advantage of this method over other methods is that the ground faults can be located with no knowledge of the zero-sequence impedance of the transmission line. However, one disadvantage of this scheme is that the data must be retrieved and then processed by a skilled technical staff, thus adding time to the fault location process.

In the simple impedance method, fault location is based on the assumption that the fault resistance at the point of fault is zero and that the transmission line model is uniform. This reduces the fault location problem to a single-termination feed problem. A small fault resistance (1Ω) can cause an appreciable arc voltage drop that produces an error in determination of the fault for remote faults.

The general principal of impedance-based fault location for the above three methods is that they all require the same signal processing steps as does protecting transmission lines. The phasor quantities are removed by using filters (digital and analog) to ensure that the transients do not affect the measurement of pharos quantities. The analog filter removes all high frequency components and the digital filter removed all the dc offset.

Fault type must be determined for accurate fault location. Depending on the fault type, to calculate the apparent positive-sequence impedance to the fault, one of the following impedance calculations will be used [11]:

Ground Faults:

$$\begin{aligned} AG: &\quad Z_1 = V_a / \left(I_a + K^* IR\right) \\ BG: &\quad Z_1 = V_b / \left(I_b + K^* IR\right) \\ CG: &\quad Z_1 = V_c / \left(I_c + K^* IR\right) \end{aligned} \tag{1.2}$$

$$where\ K = \left(Z_o - Z_1\right)/3 * Z_1$$

Phase-phase and phase-phase to ground faults:

$$\begin{aligned} AB\ or\ ABG: &\quad Z_1 = V_{ab} / I_{ab} \\ BC\ or\ BCG: &\quad Z_1 = V_{bc} / I_{bc} \\ CA\ or\ CAG: &\quad Z_1 = V_{ca} / I_{ca} \end{aligned}$$

Three-phase faults: any of the above equations.

The distance to the fault is determined by dividing the measured reactance by the total reactance of the line multiplied by the line length. An important assumption here is that the line impedance is proportional to the fault distance.

Perfect line loading conditions have some impact on fault location. The two-terminal method is the least sensitive to the effect of perfect loading. The single-terminal

method is somewhat more sensitive, and the simple impedance method is the most sensitive to perfect loading conditions.

Other main sources of errors in impedance-based fault location, which can impact on accuracy of fault location, include [11]:

Zero-sequence impedance – The zero-sequence impedance (Z_0) of a transmission line depends on the soil receptivity as well as the conductor size, configuration and height. Any uncertainty in these quantities is source for an error in locating a fault. For a 345kV line, the fault location will be 15% short if the actual Z_0 is 20% lower than the value used in the fault location.

Zero-sequence mutual coupling (Z_0M) – Mutual coupling from parallel lines has a major impact on the zero-sequence network. Z_0M is uniform along the double circuits on a parallel line. In the impedance method, fault calculations depend on the voltage at the fault and all current contributions to the fault.

Conductor size and circuit configuration – conductor size and its configurations affect Z_0 and Z_1 along the transmission line and consequently cause an error in fault location.

Current Transformer saturation – CT saturation generally can occur for close-in faults (i.e., those close to either termination of the line). CT saturation can cause a reduction in the fault current which makes the measured impedance increase above the actual value and consequently, cause the fault location to appear longer than its

actual location. If CT saturation causes 20% error in the current measurement for a short line (for example, one mile), then the distance error will be 0.2 miles.

Lines with tapped load – Load current on a tapped station on a transmission line close to short circuit current can generate an error in fault location calculations.

Series compensation – Series capacitors on the bus and the line side of the transmission line can cause transient error in fault calculations.

Infeed and three-terminal lines – Infeed causes longer distance to fault location, in particular in single-end method. Having a co-generator connected to the tap point, for example, the infeed of the current from the co-generator, will affect the fault location by representing it to be longer.

There are solutions and remedial proposals available to the above problems to reduce the error in fault location. The details are found in References [3, 7, 11].

1.1.2 Traveling Wave Method

Fault location for overhead and underground transmission line using the traveling wave method has been reported since 1931 [13]. The re-emergence of this method is partially due to the recent market demand for fast and accurate fault location and the availability of new technology in high-speed data acquisition, time synchronization using GPS, and advancement in remote control and communication systems. Two proposed methods for locating faults on transmission lines using traveling wave include:

1) Two-end traveling wave fault location – in this scheme, the relative time of arrival of the traveling wavefront produced by the fault is measured at both terminations of the faulted line. A high-speed communication channel must be available for accurate time measurement.

2) One-end traveling-wave fault location - this scheme is used for high voltage dc (HVDC) lines which do not require equipment at both terminations of the line. This method does not need a wide-bandwidth communications channel. To use this technique for an ac transmission line, more research is needed.

Fault location algorithms using traveling waves are based on measuring the energy received and reflected at either both, or one, termination of the faulted line using synchronized times. This energy is a fault generated transient. When a fault occurs, the voltage change at the point of the fault generates a high frequency electromagnetic impulse. This generated impulse is called a “traveling wave”. The traveling wave at each termination of the faulted line is time-tagged using an accurate time signal from GPS. The distance to the fault is determined by the time difference between an incident wave approaching the fault and the corresponding wave reflected at the fault.

The distance to the fault is determined by analyzing the high frequency transients rather than using the steady state components. The impulse signals propagate along the faulted transmission line in both directions at an assumed velocity close to the speed of light. The surges along overhead transmission lines consists of voltage and current waves related through the surge impedance of the line, Z_0, which can be considered purely resistive with a value 200-400 ohms.

Four types of fault location problems, based on their mode of operations, are found in the literature Reference [12]. These are:

A - does not include any pulse generating circuitry, but relies on the fault to produce one or more traveling wave transients for fault location. It is a single ended method which uses the transient recorded at only one termination of the line and depends on the multiple reflections between the location of the fault and the line terminal.

B - includes pulse or signal generating circuitry. It uses double ended method (uses the transient recorded at both terminations of the faulted line).

C - is similar to type B which includes pulse or signal generating circuitry, but is a single ended method.

D - is similar to type A, but uses double ended method and synchronized timing unit at both termination of the line and does not depend on the multiple reflections.

The principal operation of type A fault location is shown in Figure 1.6 below which is a modified form of a Bewley Lattice diagram [12].

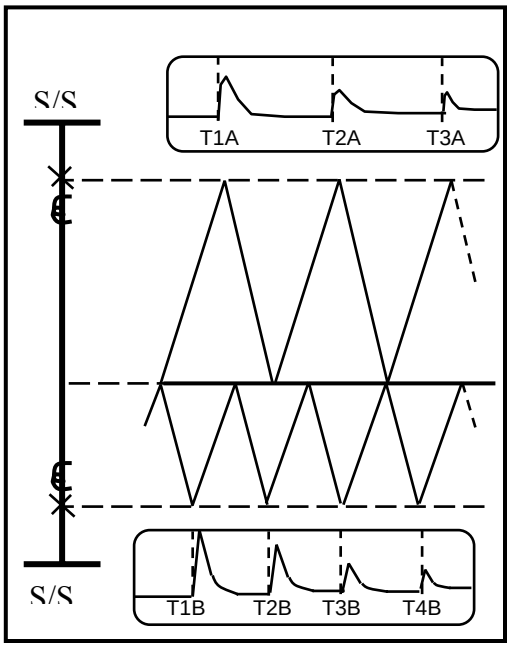

Figure 1.6: Lattice diagram for stable low resistance arc

The horizontal axes of Figure 1.6 above represent time, and the vertical shows the distance. The slope of the lines is proportional to the velocity of propagation of the signals which is assumed to be constant. The figure represents a fault that the generated traveling wave propagates in the opposite direction of the faulted line, away from the fault location. An important assumption is made that a significant part of the wave is reflected back into the faulted line. This means that the wave must have enough energy for an extended period of time so that its reflection can be detected.

The time interval between the pulses T1A and T2A are proportional to the distance of the fault from termination A using the equations below [12]:

$$Distance\ from\ A = (T2A - T1A) * V / 2 \qquad (1.3)$$
$$Distance\ from\ B = (T2B - T1B) * V / 2 \quad ,$$

where V is velocity of propagation.

However, the fault resistance, which is the non-linear resistance of the arc path plus any series linear resistance, may not cause total reflection of the pulse energy arriving at the fault, and some reflection will pass through, to appear at the opposite end of the line. This makes it difficult to determine the correct pulse to be used in Equation (1.3) above.

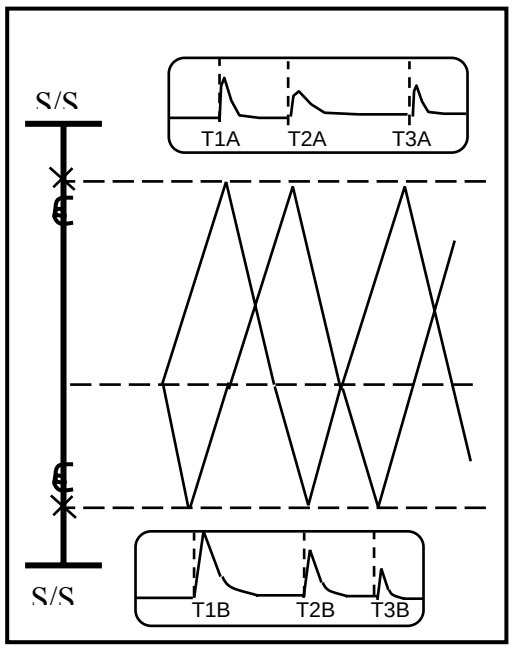

Figure 1.7: Lattice diagram for transient arc

Figure 1.7 above shows that the fault has extinguished before either of the two waves have returned from their terminals.

The distance still can be calculated at each terminal of the line by using similar to Equation (1.3):

$$Distance\ from\ A = (T3A - T2A) * V / 2 \qquad (1.4)$$
$$Distance\ from\ B = (T3B - T2B) * V / 2$$

The other main complexity with this method is that the arc at the fault point may extinguish before the reflection reaching the line terminations. One method to determine the fault location is to take the velocity of propagation out of the equation is to use the known length:

$$Distance\ from\ B = \frac{T2A - T1A}{T3A - T1A} \times Line\ Length \qquad (1.5)$$
$$Distance\ from\ A = \frac{T2B - T1B}{T3B - T1B} \times Line\ Length$$

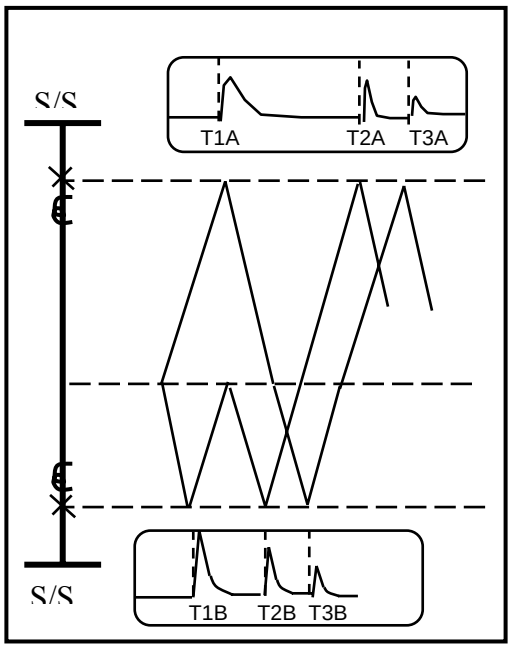

Figure 1.8: Lattice diagram for short duration and low resistance fault

Figure 1.8 shows the case where the fault extinguishes after the reflection has arrived from one end of the line, but before the reflection from the opposite termination. The fault location for this situation can also be calculated using the determined T1B and T2B in Equation (1.3) and by replacing T3B with T2B in Equation (1.4).

A similar approach is used for types B, C, and D fault location [12]. These fault location types are dependent on the modes of their operations, and all are based on voltage rather than current wave. For example, type A in a single ended mode produces two waveforms which travel in opposite directions away from the fault point.

Although the traveling wave method overcomes some of the inaccuracies of the reactance method, it has its limitations. The main source of error is the assumption of constant propagation of the wave. Other sources of error are the frequency dependence of wave propagation. And finally, this method does not work with close-in faults and the faults close to a zero crossing of voltage waveform at the fault point.

Another recent method using traveling waves, developed in 1996, is determined by accurately time tagging the arrival time of the traveling wave at both terminations of the faulted line and comparing the related time difference ΔT to the total propagation time of the line T_p. This method also makes the assumption that the waveforms generated at the fault location propagate along the faulted line in both directions away from the fault point at the speed of light.

The general determination of the distance between the fault point and the nearest terminal (L_1) is [11]: $L_1 = 0.5(T_p - \Delta T)/(L/T_p)$

Where L is total line length. The traveling time over each line is determined by dividing the length of the conductor by the velocity of propagation which is assumed to be close to the speed of light. Time of arrival measurements at different stations is highly correlated to the propagation time of the interconnecting transmission lines. This method was developed and applied to B.C. Hydro's extensive 500 kV network and was capable of locating a fault within ± one tower span (300 Meters) [13]. This corresponds to a time-tagging accuracy of about 1 μs with the assumption that the velocity of the traveling wave is close to the speed of light 300 m/μs. The time-tagging accuracy of the GPS receivers is about ± 0.3 μs of UTC (Universal Coordinated Time). This method is most applicable and practical for the faults caused by lightning due to the induced high magnitude surge on the transmission line.

A new method in fault location using traveling waves is developed which addresses some of the above problems, in particular for close-in faults, and faults that occur close to a zero crossing of the voltage signal at the fault point [14]. Having a fault close to a zero crossing of the voltage signal causes the surge to be small and the detection of the reflections very difficult. This new method is based on estimating a set of parameters from a data signal. It uses traveling wave and is based on maximum likelihood estimation of time of arrival of the reflected surge. The reflected traveling waves are expressed in terms of a set of incident wave called basic signals. The basic signals are the wavelets, which constitute the waveform. The method is based on estimating a set of parameters, namely the time of the arrival of the reflected traveling wave, from a data signal. The results of applying this method by using the signals generated by ATP shows that the accuracy of fault location is very dependent on the choice of basis signals.

A similar approach to the traveling wave method is fault location using the noise generated by the fault in the sending end current signal [15]. This noise is due to the voltage and current traveling wave. The main elements of this algorithm are a wavelet-based filter module, a Prony-based signal processing, and an ANN (artificial neural network)-based estimator. The main function of the Prony fitting is to extract modal data from the filtered signal. The fault location is determined by using the modal information. Wavelet-based filters are used to reduce the noise content in the signal. No pre-fault data or the data from the remote end is required in this method. The signal is decomposed first, the noise is removed, and finally the signal is reconstructed. The samples from the wavelet filter are processed using Pony filter. The output of the Pony filter is then passed to the ANN as input signal for fault location. Ultimately, the changes in frequency result in different fault location estimates. The main source of the error is the accuracy of the Prony fitting. Changes in fault resistance have significant impact on the damping, but not on the estimated fault location. Application of this theory on simulated networks showed about 2.8 percent error in estimating the fault location for different cases.

Chapter 2: Formulation of the Problem Using Voltage Monitors on Transmission System

Fault location has traditionally been achieved by measuring rms short-circuit current magnitudes on both ends of a faulted line, and then comparing simulations with these measurements. The new fault location procedure is based upon voltage-only measurements at a few buses in the system. This procedure utilizes system impedance matrices and a least-squared error minimization technique to estimate the fault location. The estimation algorithm has been successfully tested with 15 actual faults to verify its validity. All fault types: three-phase, phase-phase, phase-phase-ground, and phase-ground, on 69kV and 138kV systems have been verified with the field data using this methodology.

The characteristics of the a-b-c sag measurements themselves tell us whether the fault is single-phase to ground, phase-to-phase, or three-phase. The majority of transmission faults are single-phase to ground. For simplicity, we begin our analysis by formulating the problem for balanced three-phase faults.

2.1 Balanced Three-Phase Faults

In this problem, we have a set of voltage sag measurements at metered buses m1, m2, m3, ... , mn, and we wish to identify the bus at which the fault occurred. The fault current at the faulted bus is unknown, but that fault current is bounded (in per unit) by well known formulas [18], [19].

To identify the faulted bus, we evaluate the following error function at each candidate bus k, for k = 1, 2, 3, … n,

$$err_k^2 = \sum_{m=1}^{n} \left(\left| \Delta V_{m,meas}^{+} \right| - \left| \Delta V_{m,pred(k)}^{+} \right| \right)^2 , \qquad (2.1)$$

where

$\left| \Delta V_{m,meas}^{+} \right|$ is the measured positive-sequence sag magnitude (i.e., the same value as the phase a sag), in per unit, at metered bus m,

$\left| \Delta V_{m,pred(k)}^{+} \right|$ is the corresponding predicted positive-sequence sag magnitude.

Assuming a pre-fault voltage magnitude of 1.0, the magnitude of the voltage at bus m during the fault is

$$\left| \Delta V_{m,pred(k)}^{+} \right| = 1.0 - \left| Z_{m,k}^{+} I_k^{+} \right| , \qquad (2.2)$$

where I_k^{+} is the unknown positive-sequence fault current at candidate bus k, in per unit. The magnitude of I_k^{+} cannot exceed the maximum available fault current at that bus given by

$$\left|I_k^+\right|_{MAX} = \frac{1}{\left|Z_{k,k}^+\right|}. \qquad (2.3)$$

From (2.2), we obtain sag magnitude

$$\Delta V_{m,pred(k)}^+ = 1.0 - \left|\Delta V_{m,pred(k)}^+\right| = \left|Z_{m,k}^+ I_k^+\right|.$$

In a purely inductive system (i.e., the standard assumption), $Z_{m,k}^+ = j\left|Z_{m,k}^+\right|$, and $I_k^+ = -j\left|I_k^+\right|$, so that $Z_{m,k}^+ I_k^+$ is a real, positive number. Furthermore, even if the system is not purely reactive, I_k^+ tends to have the opposite phase angle of $Z_{m,k}^+$, so that it is safe to assume that $Z_{m,k}^+ I_k^+$ is indeed a positive real number and equal to $\left|Z_{m,k}^+\right|\left|I_k^+\right|$.

The impedance values in the equations are:

$Z_{k,k}^+$ is the diagonal term (i.e., self impedance) of the positive-sequence impedance matrix, in per unit, for candidate bus k,

$Z_{m,k}^+$ is the off-diagonal positive-sequence impedance matrix term, in per unit, that links the voltage change at metered bus m to the fault current at candidate bus k.

Combining (2.2) into (2.1) yields

$$err_k^2 = \sum_{m=1}^{n}\left(\left|\Delta V_{m,meas}^+\right| - \left|Z_{m,k}^+\right|\left|I_k^+\right|\right)^2 . \qquad (2.4)$$

For each candidate k, one value of $\left|I_k^+\right|$ will yield the smallest err_k^2 in (2.4). This $\left|I_k^+\right|$ can be found by taking the derivative of (2.4) with respect to $\left|I_k^+\right|$, and then setting it to zero, yielding

$$\sum_{m=1}^{n}\left(\left|\Delta V_{m,meas}^+\right| - \left|Z_{m,k}^+\right|\left|I_k^+\right|\right)\bullet\left|Z_{m,k}^+\right| = 0. \qquad (2.5)$$

Solving (2.5) for $\left|I_k^+\right|$ yields

$$\left|I_k^+\right| = \frac{\sum_{m=1}^{n}\left|\Delta V_{m,meas}^+\right|\left|Z_{m,k}^+\right|}{\sum_{m=1}^{n}\left|Z_{m,k}^+\right|^2}, \qquad (2.6)$$

subject to upper bound

$$\left|I_k^+\right| \le \left|I_{k,MAX}^+\right| = \frac{1}{\left|Z_{k,k}^+\right|}. \qquad (2.7)$$

It will be helpful later to define ratio α so that

$$\left|I_k^+\right| = \alpha\left|I_{k,MAX}^+\right|.$$

Constraint (2.7) has proven to be very useful because it quite effectively eliminates "far away" buses from the list of likely candidates.

To find the most likely fault location, a ranking process proceeds as follows: for each bus k = 1, 2, 3, … , n, the solution to (2.6), subject to constraint (2.7), is substituted into (2.4). The buses are then ranked according to their squared error in (2.4). The bus

that produces the smallest squared error is the most likely fault location, the bus that produces the highest squared error is the least likely fault location, and so on.

2.2 Single-Phase to Ground Faults

The procedure for handling single-phase to ground faults is similar, except for the complication of dealing with sequence components. Assume that a fault occurs on arbitrarily chosen phase a of bus k. The well known fault current equations from [18] and [19] are, in per unit,

$$\left|I_k^a\right| = \frac{3}{\left|Z_{k,k}^0 + Z_{k,k}^+ + Z_{k,k}^-\right|}$$

$$\approx \frac{3}{\left|Z_{k,k}^0 + 2Z_{k,k}^+\right|}, \qquad (2.8)$$

and

$$\left|I_k^0\right| = \left|I_k^+\right| = \left|I_k^-\right| = \frac{\left|I_k^a\right|}{3}, \qquad (2.9)$$

where superscripts 0, +, and – refer to zero, positive, and negative-sequence components, respectively. If there are no wye-delta transformers between buses k and m, then phase a at bus m will have the deepest sag and the voltage magnitude at phases b and c may actually rise. The squared error function for the candidate bus k becomes

$$err_k^2 = \sum_{m=1}^{n} \left(\left|\Delta V_{m,meas}^a\right| - \left|\Delta V_{m,pred(k)}^a\right|\right)^2 \quad , \qquad (2.10)$$

where, using sequence components,

$$\left|\Delta V_{m,pred(k)}^a\right| = \left|\Delta V_{m,pred(k)}^0 + \Delta V_{m,pred(k)}^+ + \Delta V_{m,pred(k)}^-\right|$$

$$= \left| Z^{0}_{m,k} I^{0}_{k} + Z^{+}_{m,k} I^{+}_{k} + Z^{-}_{m,k} I^{-}_{k} \right|$$

$$\approx \left| Z^{0}_{m,k} I^{0}_{k} + Z^{+}_{m,k} \left(I^{+}_{k} + I^{-}_{k} \right) \right|. \qquad (2.11)$$

Substituting (2.9) into (2.11) yields

$$\left| \Delta V^{a}_{m,pred(k)} \right| = \left| \frac{Z^{0}_{m,k} + 2Z^{+}_{m,k}}{3} \right| \left| I^{a}_{k} \right|. \qquad (2.12)$$

Substituting (2.12) into (2.10) yields

$$err^{2}_{k} = \sum_{m=1}^{n} \left(\left| \Delta V^{a}_{m,meas} \right| - \left| Z^{net}_{m,k} \right| \left| I^{a}_{k} \right| \right)^{2}, \qquad (2.13)$$

where

$$\left| Z^{net}_{m,k} \right| = \left| \frac{Z^{0}_{m,k} + 2Z^{+}_{m,k}}{3} \right|. \qquad (2.14)$$

The constraint on $\left| I^{a}_{k} \right|$ is

$$\left| I^{a}_{k} \right| \le \left| I^{a}_{k} \right|_{MAX} = \left| \frac{3}{Z^{0}_{k,k} + 2Z^{+}_{k,k}} \right|.$$

The procedure for solving the $\left| I^{a}_{k} \right|$ that minimizes (2.13), subject to constraint, and for ranking the fault candidate buses proceeds in exactly the same way as described for the three-phase case.

2.3 Phase-Phase Faults

The procedure for handling phase-phase faults is similar, except for the complication of dealing with sequence components. Assume that a fault occurs on arbitrarily-chosen phases b and c of bus k. The squared error function for the candidate bus k becomes

$$err_k^2 = \sum_{m=1}^{n} \left(\left| \Delta V_{m,meas}^{b} \right| - \left| \Delta V_{m,pred(k)}^{b} \right| \right)^2 . \qquad (2.15)$$

To calculate $\left| \Delta V_{m,pred(k)}^{b} \right|$ we will consider the sequence and phase current for a line-line fault between b and c [22] as follows:

Sequence currents:

$$I_k^0 = 0$$

$$I_k^+ = \frac{1}{Z_{k,k}^+ + Z_{k,k}^-} \qquad (2.16)$$

$$I_k^+ = \frac{1}{2Z_{k,k}^+} = -I_k^-$$

Phase currents:

$$I_{k,a}^F = 0$$

$$I_{k,b}^F = -I_{k,c}^F$$

Sequence voltages:

$$V_{m,pred(k)}^{0,F} = 0$$

$$V_{m,,pred(k)}^{+,F} = 1 - Z_{m,k}^{+} I_k^{+}$$

$$V_{m,,pred(k)}^{-,F} = 0 - Z_{m,k}^{-} I_k^{-} = -Z_{m,k}^{+}\left(-I_k^{+}\right)$$

Phase voltages:

$$V_{m,pred(k)}^{a,F} = V_{m,pred(k)}^{0,F} + V_{m,pred(k)}^{+,F} + V_{m,pred(k)}^{-,F} = \left(1 - Z_{m,k}^{+} I_k^{+}\right) + \left(Z_{m,k}^{+} I_k^{+}\right) = 1$$

$$V_{m,pred(k)}^{b,F} = V_{m,pred(k)}^{0,F} + a^2 V_{m,pred(k)}^{+,F} + a\ V_{m,pred(k)}^{-,F} = 0 + a^2\left(1 - Z_{m,k}^{+} I_k^{+}\right) + a\left(Z_{m,k}^{+} I_k^{+}\right)$$

$$= a^2 + \left(a - a^2\right) Z_{m,k}^{+} I_k^{+}$$

$$= a^2 + j\sqrt{3} Z_{m,k}^{+} I_k^{+} \qquad (2.17)$$

$$V_{m,pred(k)}^{c,F} = V_{m,pred(k)}^{0,F} + a V_{m,pred(k)}^{+,F} + a^2 V_{m,pred(k)}^{-,F} = 0 + a\ \left(1 - Z_{m,k}^{+} I_k^{+}\right) + a^2\left(Z_{m,k}^{+} I_k^{+}\right)$$

$$= a - j\sqrt{3} Z_{m,k}^{+} I_k^{+} \qquad (2.18)$$

Constant a is the complex number $1\angle 120^{\mathrm{O}}$, or $-\frac{1}{2} + j\frac{\sqrt{3}}{2}$; hence, $a^2 = -\frac{1}{2} - j\frac{\sqrt{3}}{2}$.

Now, the magnitudes of the voltage sags are

$$\left|\Delta V^{a}_{m,pred(k)}\right| = 1-1 = 0$$

$$\left|\Delta V^{b}_{m,pred(k)}\right| = 1-\left|V^{b,F}_{m,pred(k)}\right| = 1-\left|a^{2} + j\sqrt{3}Z^{+}_{m,k}I^{+}_{k}\right|.$$

Since the product $Z^{+}_{m,k}I^{+}_{k}$ is assumed to be a real number,

$$\left|\Delta V^{b}_{m,pred(k)}\right| = 1-\left|a^{2} + j\sqrt{3}\left|Z^{+}_{m,k}\right|\left|I^{+}_{k}\right|\right|$$

$$= 1-\left|-\frac{1}{2} - j\frac{\sqrt{3}}{2} + j\sqrt{3}\left|Z^{+}_{m,k}\right|\left|I^{+}_{k}\right|\right|$$

$$= 1-\left|-\frac{1}{2} - j\sqrt{3}\left(\frac{1}{2} - \left|Z^{+}_{m,k}\right|\left|I^{+}_{k}\right|\right)\right|$$

$$= 1-\sqrt{\left(-\frac{1}{2}\right)^{2} + \left[-\sqrt{3}\left(\frac{1}{2} - \left|Z^{+}_{m,k}\right|\left|I^{+}_{k}\right|\right)\right]^{2}}$$

$$= 1-\sqrt{\frac{1}{4} + 3\left(\frac{1}{2} - \left|Z^{+}_{m,k}\right|\left|I^{+}_{k}\right|\right)^{2}}\ . \qquad (2.19)$$

Following the same procedure for $\left|\Delta V^{c}_{m,pred(k)}\right|$,

$$\left|\Delta V^{c}_{m,pred(k)}\right| = 1-\left|V^{c,F}_{m,pred(k)}\right| = 1-\left|a\ - j\sqrt{3}\left|Z^{+}_{m,k}\right|\left|I^{+}_{k}\right|\right|$$

$$= 1-\left|-\frac{1}{2} + j\frac{\sqrt{3}}{2} - j\sqrt{3}\left|Z^{+}_{m,k}\right|\left|I^{+}_{k}\right|\right|$$

$$= 1 - \left| -\frac{1}{2} + j\sqrt{3}\,(\frac{1}{2} - \left| Z^{+}_{m,k} \right\| I^{+}_{k} \right|) \right|$$

$$= 1 - \sqrt{\frac{1}{4} + 3\left(\frac{1}{2} - \left| Z^{+}_{m,k} \right\| I^{+}_{k} \right|\right)^2} \quad . \qquad (2.20)$$

Equations (2.19) and (2.20) are identical, which means that phases b and c see the same voltage sag magnitude.

To identify the faulted bus, we evaluate the following error function at each candidate bus k, for k = 1, 2, 3, … n, as was described above in Equation (2.1),

$$err_k^2 = \sum_{m=1}^{n} \left(\left| \Delta V_{m,meas} \right| - \left| \Delta V^{b}_{m,pred(k)} \right| \right)^2 ,$$

where

$\left| \Delta V_{m,meas} \right|$ is the measured sag magnitude at either phase b or phase c, and

$\left| \Delta V^{b}_{m,pred(k)} \right|$ is the corresponding predicted sag magnitude at either phase b or phase c.

Expanding,

$$err_k^2 = \left| \Delta V_{m,meas} \right|^2 - 2\left| \Delta V_{m,meas} \right| \left| \Delta V^{b}_{m,pred(k)} \right| + \left| \Delta V^{b}_{m,pred(k)} \right|^2 \quad , \qquad (2.21)$$

where $\left| \Delta V^{b}_{m,pred(k)} \right|$ is defined in (2.19).

Unlike the three-phase and single-phase squared error expression, minimizing the corresponding Equation (2.21) is not easily solved in closed form. Thus, for each candidate fault bus k, we numerically step through values of $\left| I^{+}_{k} \right|$, using

$$\left|I_k^+\right| = \alpha \left|I_{k,MAX}^+\right| = \frac{\alpha}{2\left|Z_{k,k,}^+\right|}, \quad 0 \le \alpha \le 1.$$

There is an α for each candidate bus, and the bus with the least-squared error is the most likely candidate.

2.4 Phase-Phase to Ground Faults

The procedure for handling phase-phase to ground faults is similar to phase-to-phase. Again, assume that a fault occurs on arbitrarily chosen phase b and c to ground of bus k. The conditions at the fault location k are expressed by the following [22]:

Sequence currents:

$$I_k^0 = \frac{I_k^+ Z_{k,k}^+ - 1}{Z_{k,k}^0}$$

$$I_k^+ = \frac{1}{Z_{\mathrm{k,k}}^+ + \dfrac{Z_{k,k}^+ Z_{k,k}^0}{Z_{k,k}^+ + Z_{k,k}^0}} \qquad (2.22)$$

$$I_k^- = \frac{I_k^+ Z_{k,k}^+ - 1}{Z_{k,k}^+}$$

Phase currents:

$$I_{k,a}^F = 0$$

Sequence voltages:

$$V_{m,pred(k)}^{0,F} = 0 - Z_{m,k}^0 I_k^0 = Z_{m,k}^0 \left(\frac{1 - I_k^+ Z_{k,k}^+}{Z_{k,k}^0} \right) = \frac{Z_{m,k}^0}{Z_{k,k}^0} \left(1 - I_k^+ Z_{k,k}^+ \right)$$

$$V_{m,pred(k)}^{+,F} = 1 - Z_{m,k}^+ I_k^+$$

$$V_{m,pred(k)}^{-,F} = 0 - Z_{m,k}^+ I_k^- = Z_{m,k}^+ \left(\frac{1 - I_k^+ Z_{k,k}^+}{Z_{k,k}^+} \right) = Z_{m,k}^+ \left(\frac{1}{Z_{k,k}^+} - I_k^+ \right)$$

Phase voltages:

$$V_{m,pred(k)}^{a,F} = \frac{Z_{m,k}^{0}}{Z_{k,k}^{0}}\left(1 - I_k^{+} Z_{k,k}^{+}\right) + 1 - Z_{m,k}^{+} I_k^{+} + \frac{Z_{m,k}^{+}}{Z_{k,k}^{+}}\left(1 - I_k^{+} Z_{k,k}^{+}\right)$$

$$= \frac{Z_{m,k}^{0}}{Z_{k,k}^{0}} + 1 + \frac{Z_{m,k}^{+}}{Z_{k,k}^{+}} - I_k^{+}\left[\frac{Z_{m,k}^{0} Z_{k,k}^{+}}{Z_{k,k}^{0}} + Z_{m,k}^{+} + Z_{m,k}^{+}\right]$$

$$V_{m,pred(k)}^{b,F} = \frac{Z_{m,k}^{0}}{Z_{k,k}^{0}}\left(1 - I_k^{+} Z_{k,k}^{+}\right) + a^2\left(1 - Z_{m,k}^{+} I_k^{+}\right) + aZ_{m,k}^{+}\left(\frac{1 - I_k^{+} Z_{k,k}^{+}}{Z_{k,k}^{+}}\right)$$

$$= \frac{Z_{m,k}^{0}}{Z_{k,k}^{0}}\left(1 - I_k^{+} Z_{k,k}^{+}\right) + a^2\left(1 - Z_{m,k}^{+} I_k^{+}\right) + aZ_{m,k}^{+}\left(\frac{1}{Z_{k,k}^{+}} - I_k^{+}\right)$$

$$= \frac{Z_{m,k}^{0}}{Z_{k,k}^{0}}\left(1 - I_k^{+} Z_{k,k}^{+}\right) + a^2 - a^2 Z_{m,k}^{+} I_k^{+} + a\frac{Z_{m,k}^{+}}{Z_{k,k}^{+}} - aZ_{m,k}^{+} I_k^{+}$$

$$V_{m,pred(k)}^{b,F} = \frac{Z_{m,k}^{0}}{Z_{k,k}^{0}}\left(1 - I_k^{+} Z_{k,k}^{+}\right) + a^2 + a\frac{Z_{m,k}^{+}}{Z_{k,k}^{+}} + Z_{m,k}^{+} I_k^{+}. \qquad (2.23)$$

Similarly for c phase,

$$V_{m,pred(k)}^{c,F} = \frac{Z_{m,k}^{0}}{Z_{k,k}^{0}}\left(1 - I_k^{+} Z_{k,k}^{+}\right) + a\ \left(1 - Z_{m,k}^{+} I_k^{+}\right) + a^2 Z_{m,k}^{+}\left(\frac{1 - I_k^{+} Z_{k,k}^{+}}{Z_{k,k}^{+}}\right)$$

$$= \frac{Z_{m,k}^{0}}{Z_{k,k}^{0}}\left(1 - I_k^{+} Z_{k,k}^{+}\right) + a\ - a\ Z_{m,k}^{+} I_k^{+} + a^2\frac{Z_{m,k}^{+}}{Z_{k,k}^{+}} - a^2 Z_{m,k}^{+} I_k^{+}$$

$$= \frac{Z^0_{m,k}}{Z^0_{k,k}}\left(1 - I^+_k Z^+_{k,k}\right) + a \quad + a^2 \frac{Z^+_{m,k}}{Z^+_{k,k}} + Z^+_{m,k} I^+_k . \tag{2.24}$$

Symmetry of Equations (2.23) and (2.24) shows that phase b and c will have the same voltage sag magnitude.

Using Equation (2.23), the voltage sag magnitude at phase b (and also phase c) is

$$\left|\Delta V^b_{m,pred(k)}\right| = 1 - \left| \frac{Z^0_{m,k}}{Z^0_{k,k}} + a^2 + a \frac{Z^+_{m,k}}{Z^+_{k,k}} + I^+_k \left(Z^+_{m,k} - \frac{Z^0_{m,k} Z^+_{k,k}}{Z^0_{k,k}} \right) \right| . \tag{2.25}$$

Substituting for a^2 and a ,

$$\left|\Delta V^b_{m,pred(k)}\right| = 1 - \left| \frac{Z^0_{m,k}}{Z^0_{k,k}} + \left(-\frac{1}{2} - j\frac{\sqrt{3}}{2} \right) + \frac{Z^+_{m,k}}{Z^+_{k,k}} \left(-\frac{1}{2} + j\frac{\sqrt{3}}{2} \right) + I^+_k \left(Z^+_{m,k} - \frac{Z^0_{m,k} Z^+_{k,k}}{Z^0_{k,k}} \right) \right|$$

$$= 1 - \left| \frac{Z^0_{m,k}}{Z^0_{k,k}} - \frac{1}{2} - \frac{1}{2}\left(\frac{Z^+_{m,k}}{Z^+_{k,k}} \right) + I^+_k \left(Z^+_{m,k} - \frac{Z^0_{m,k} Z^+_{k,k}}{Z^0_{k,k}} \right) - j\frac{\sqrt{3}}{2}\left(1 - \frac{Z^+_{m,k}}{Z^+_{k,k}} \right) \right| . \tag{2.26}$$

The usual assumption about the phase angles of impedances and currents is now made. Then, the solution for the best $\left|I^+_k\right|$ and best bus k proceeds the same as in the phase-phase case, except that

$$\left|I^+_k\right| = \alpha \left|I^+_{k,MAX}\right| = \alpha \left| \frac{1}{Z^+_{k,k} + \dfrac{Z^+_{k,k} Z^0_{k,k}}{Z^+_{k,k} + Z^0_{k,k}}} \right| \text{ where } 0 \le \alpha \le 1 . \tag{2.27}$$

Chapter 3: Case Studies Using Voltage Monitors on Transmission System

The following sections describe the power system that was used for the case studies in this dissertation. The monitoring and metering devices along with their sample data, and the calculation of the voltage sag values that were used as the meter data are also shown in this chapter.

Several graphics are used to display the location of the meters and examples of an event and the captured meter data are illustrated. Fifteen actual events are described and the data from these events which were used to validate the theory described in Chapter 2 of this dissertation. The results of all the studied cases are presented in tabular format. Finally, some analysis of the results is presented at the end of this chapter.

3.1 The Austin Energy System

Austin Energy (AE) is a community-owned electric utility and a department of the City of Austin. The company's goal is to provide world-class customer service. Austin Energy is the nation's 10th largest community-owned electric utility serving 360,000 customers and a population of more than 800,000. It provides service within the City of Austin, Travis County and a small portion of Williamson County. As a publicly owned power company and a city department, Austin Energy returns profits to the community annually. Austin Energy powers the capital city of Texas through a diverse generation mix of nuclear, coal, natural gas and renewable energy sources. That's just over 2,600 megawatts (MW) of total generation. Most generation sources are in the East part of the system and there are a few ties to other utilities at North, South and the East side of the system which can provide voltage support.

Austin Energy's service statistics:

844,263 - service area population

421 spare miles of service area size

9 transmission substations

54 distribution substations

2,383 MW system peak

2,934 MW generation capacity

608 miles of transmission lines

10,308 miles of overhead and underground distribution lines

Austin Energy's transmission system contains 608 miles of transmission lines and nine transmission substations at 345 kV, 138 kV, and 69 kV voltage levels. It has ties with

LCRA through eight 345 kV lines and five 138 kV lines and with CenterPoint through one 345 kV line.

For the studies in this dissertation, short circuit data for the Electric Reliability Council of Texas (ERCOT) are read into the PSS/E program [20], full detail data for Austin Energy are retained, and an equivalence of the remainder of ERCOT at the Austin Energy tie buses is made by using an automatic feature in PSS/E. The resulting 118 bus system is then read by PCFLO [21], which in turn creates the positive/negative-sequence and zero-sequence impedance matrices needed for this analysis. This is one of the main elements in this work as acquiring a system's sequence impedance matrices is not easily achieved.

All collected fault data are telemetered back to a central control center. The procedure described in this paper can take advantage of these data at no extra cost, and supplement whatever existing fault location procedure is being utilized. The algorithm can be easily expanded to predict voltage sag levels through the entire system.

3.2 Contour Map

The purpose of creating a contour map is to help visualize an electric power system bus voltage magnitude for a fault on transmission system. The voltage sag is normally caused by a fault or a system disturbance. It is a reduction in the voltage magnitude for a short period of time, a few cycles [24]. For this study, the impact of voltage sag due to numerous system-wide faults at different geographic locations of the system was monitored and recorded. The results were displayed in numeric and contour format for better visualization. Display of the sag results in a contour map format provides a quicker and larger exposure of the sag values experienced by the system. The system used for this study is Austin Energy's transmission system which consists of 69 kV, 138 kV, and 345 kV. The result of this study may also provide best locations for monitoring devises to encompass the entire system during a fault.

Thirty-five different fault types were applied. The voltage magnitudes for each fault position have been calculated for the 118 buses in the system. The result of two events used in this work is shown below. After determining the available voltage sag values in the buses in the system, contour maps were drawn for various voltage sag levels namely: 20%, 30%, 40%, 50%, 70%, and above 90%. At the beginning stage of this study, the contours were drawn manually for each voltage sag level. As expected, the voltage sag decrease for contours away from the fault locations. The first contour map as shown in Figure 3.1 is for an event on a 138 kV bus at MC substation in the North part of the town. The location of the fault is shown by an arrow on the graph. The second example shown below is for a fault on CKT 825, a 69 kV line in downtown Austin. The propagation of the voltage sag throughout the system for this fault is shown with the contours is shown in Figure 3.2.

Table 3.1 is a sample of the recorded voltage values during the fault at MC bus. For example for the first record in the table, the voltage at Grove substation dropped to 71.8%. The table with the recorded voltage magnitude during fault for the entire 118 buses in the system was used for developing a contour map for this fault. As predicted, the resulted map indicates that buses near to a fault location experience the worse voltage sag. The severity of the voltage sag for a fault close to the bus is affected by the distance to the fault which can be seen on Figure 3.1. For this fault the customers on the north side of the town experienced a larger voltage sag impact. A similar contour map is shown in Figure 3.2 for a fault on CKT 825 in the southeast part of the system with the impacted voltage sags.

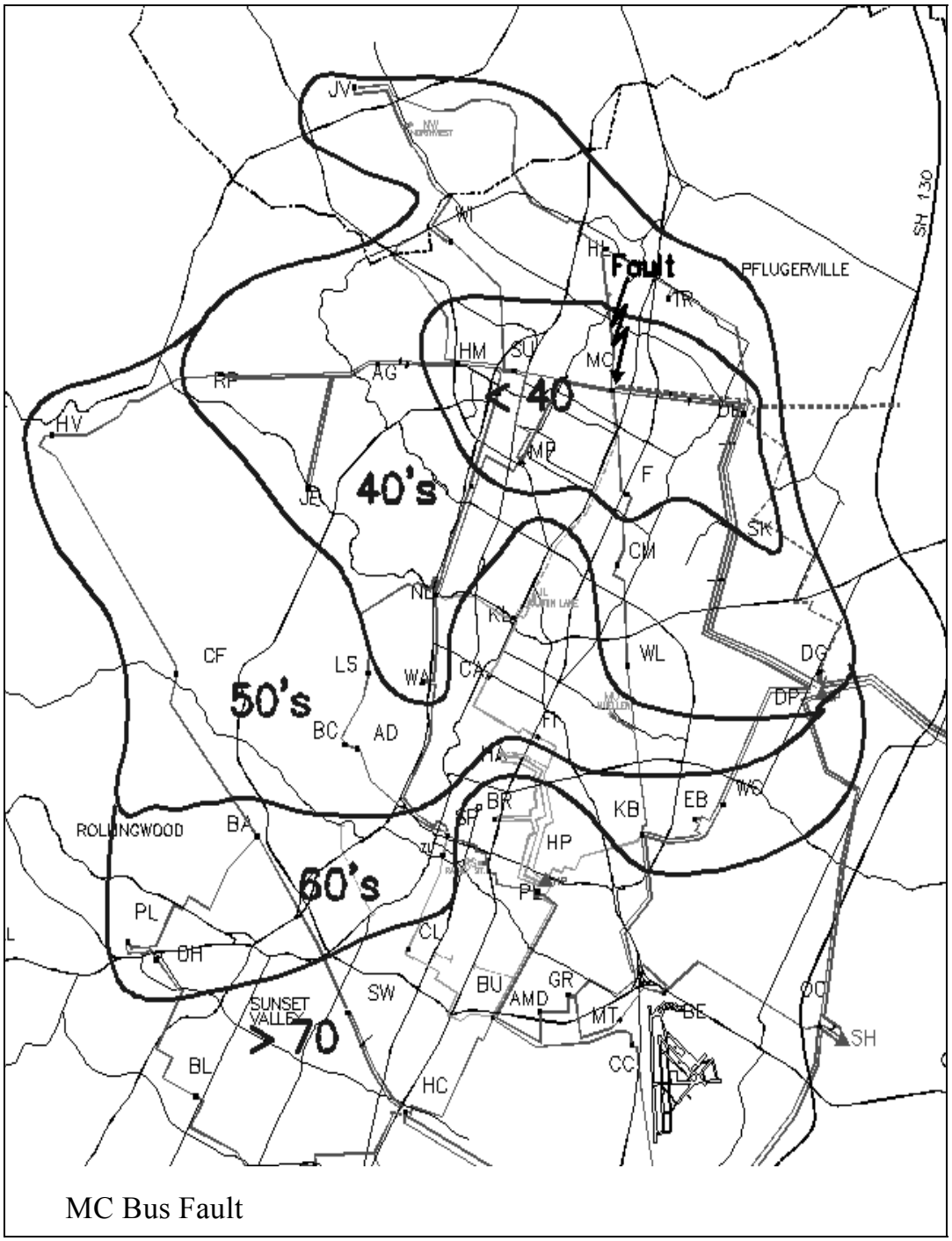

MC Bus Fault

Figure 3.1: Voltage magnitude in Austin for a fault at MC substation

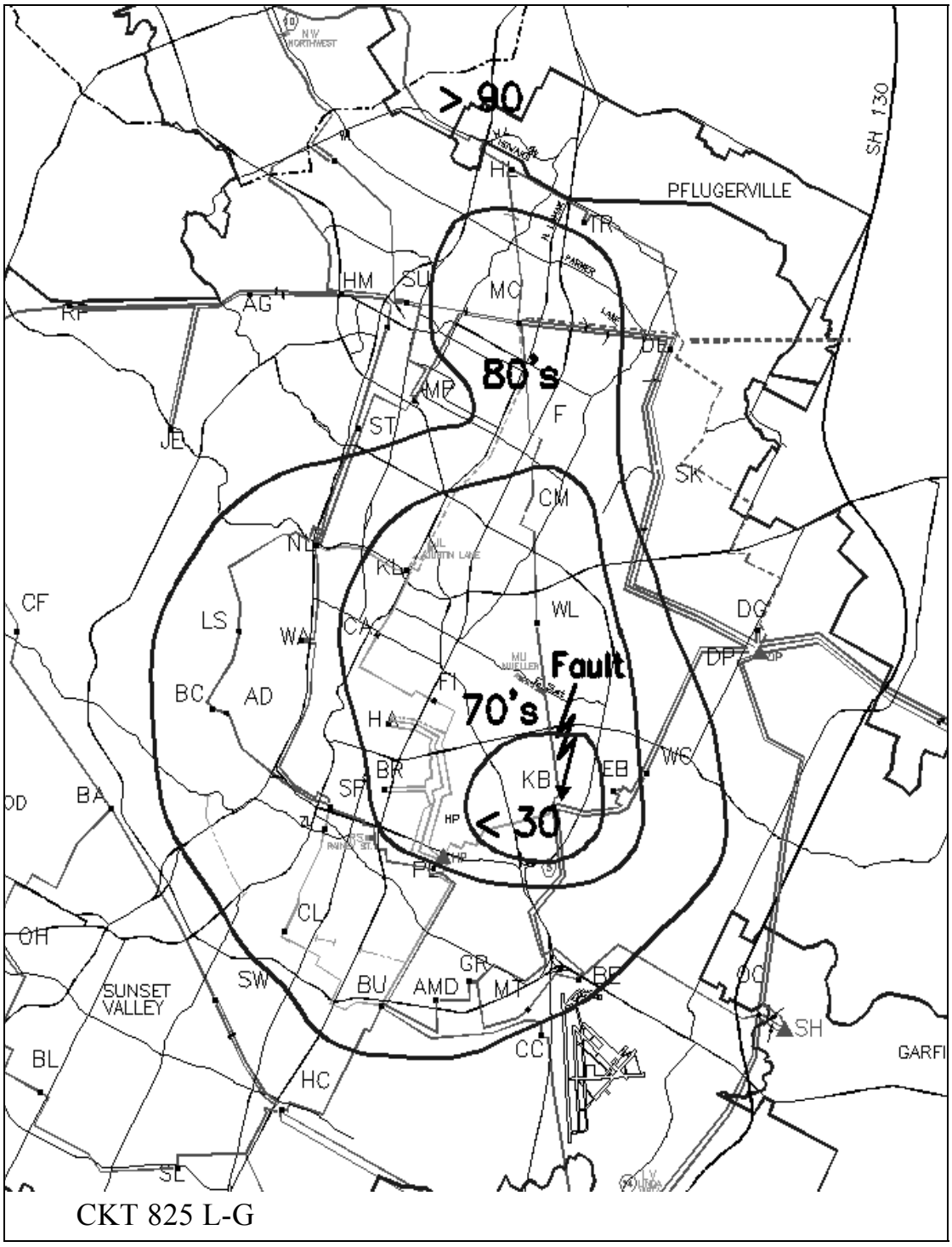

Figure 3.2: Voltage magnitude in Austin for fault on CKT 825

Bus #	Substation	Voltage (PU)		Bus #	Substation	Voltage (PU)
9200	GROVE	71.80%		9239	MAGPLANT	37.90%
9202	HAMILTON	25.70%		9243	NORTH	61.50%
9203	HAMILMB2	25.60%		9247	OAKHILL	67.60%
9204	HARRIS	75.30%		9251	ONION	78.40%
9212	HOLLYMB1	75.30%		9255	PATTON	67.20%
9213	HOLLYMB2	75.30%		9257	PEDERNAL	75.30%
9214	HOLLYMB3	75.30%		9259	PILOT	76.50%
9215	HOLLYMB4	75.30%		9260	RIVERPLS	35.40%
9216	SANDHILL	78.80%		9263	SALEMWLK	70.80%
9217	HOWARD	23.80%		9267	SLAUGHTR	72.90%
9220	JETT	30.30%		9271	SPRINKLE	29.00%
9223	JOLLYVIL	37.00%		9275	STECK	28.00%
9227	KOENIG	50.30%		9279	SUMMITN	22.10%
9228	LAKESHOR	41.90%		9280	SUMMITS	22.10%

Table 3.1: Voltage magnitude values at system buses for a severe fault at MC substation

To improve the efficiency and accuracy of plotting such contour maps, and eliminate any potential human error during the manual data input and drawing of the contour map, various methods were investigated including using a software program to automate the plotting of the contour map. First, the application of contour map option in Excel was used. But this application in Excel seemed to be for a simple application, not for drawing a contour map for voltage sag applications with a system base map. One problem was that the input data to Excel was not evenly spaced. The second approach was to download a macro in Excel such that solved the previous problem, however, there was not an easy way to put a base map on the contour map; the base map being the system service area map.

The third approach which seemed to work best for this application was using a software program called 3DField [25]. This program can plot contour maps, can take comma separated text file as input which can be obtained from Excel, and also a base map can be inserted on which to plot the contour. The system bus numbers are correlated to actual GPS coordinates for the system buses so that the voltage sag data point becomes the input to this program. As an example, the input comma (or tab) separated text files has the following format:

X	Y	Z	PointName
-97.2	30.6	50	PL

The X is the longitude, Y is the latitude, Z is the voltage sag, or actual voltage, at different system buses or substations, and PL is the abbreviated substation name.

To represent a sample contour map using 3DField software program, three actual fault cases that will be used for the studies in this work are illustrated. These cases were selected because of the location of these faults such that the contour map would have a complete representation of the voltage sag propagation throughout the entire system. These cases are actual faults, which will be used later in this chapter as test cases to validate the methodology described above.

The first map, Figure 3.3, is the contour map for Case 1, a b phase to ground fault on CKT 809 on 69 kV system caused by a car hitting a pole. Substation abbreviations are shown on the base map and selected percentages of voltage magnitude are shown on each contour. For example, 50.00 percent for the most inner contour, followed by 40.00, 30.00, and others as indicated on each contour.

The second map shown below, Figure 3.4, is the contour for Case 8, an a-c phase to ground fault on CKT 834 on 69 kV system caused by lightning which burned the bottom phase's insulator stack.

The third map, Figure 3.5, is the contour for Case 15, a c phase to ground fault on CKT 979 on 138 kV system caused by a buzzard contacting a phase conductor.

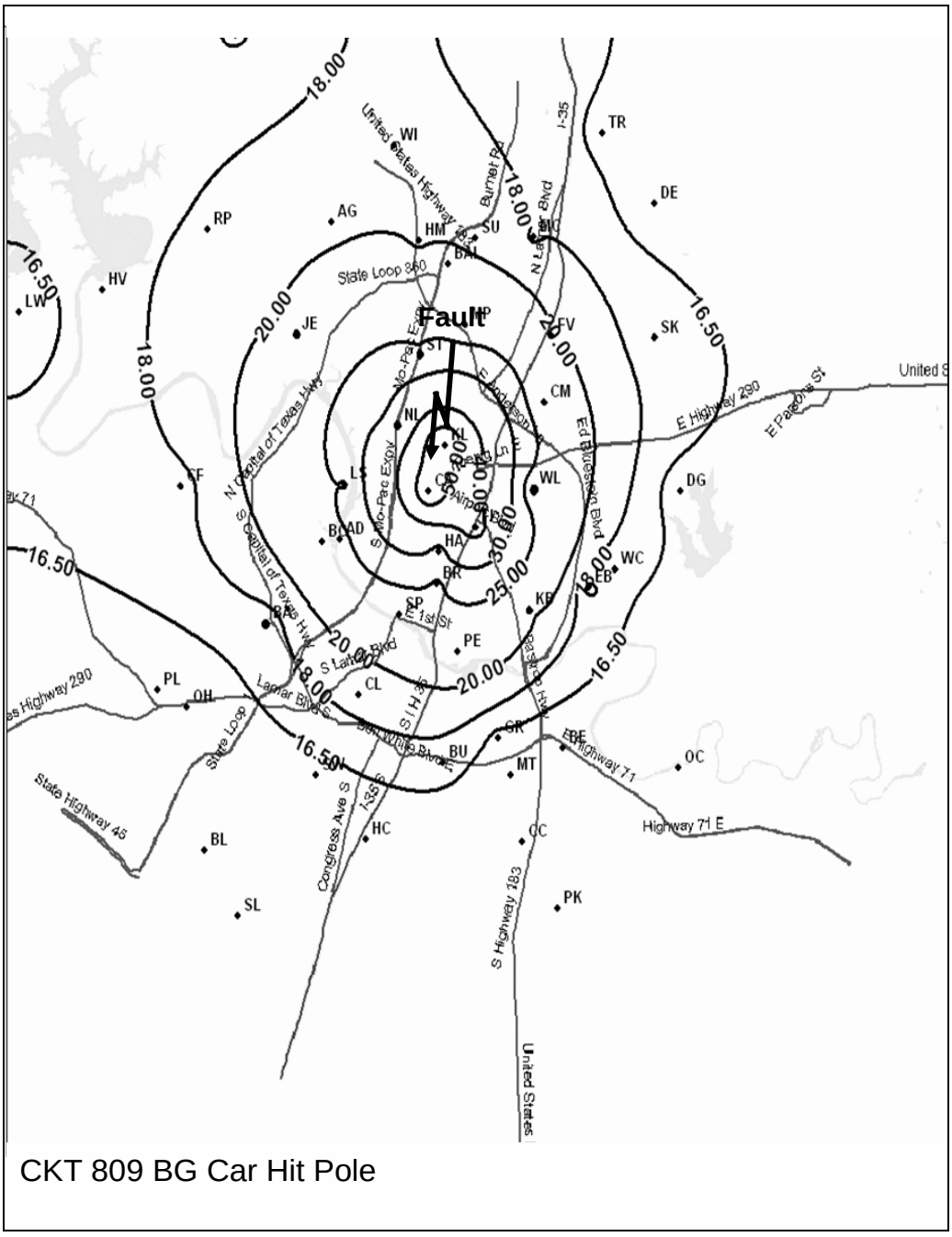

Figure 3.3: Voltage magnitude in Austin for fault on CKT 809

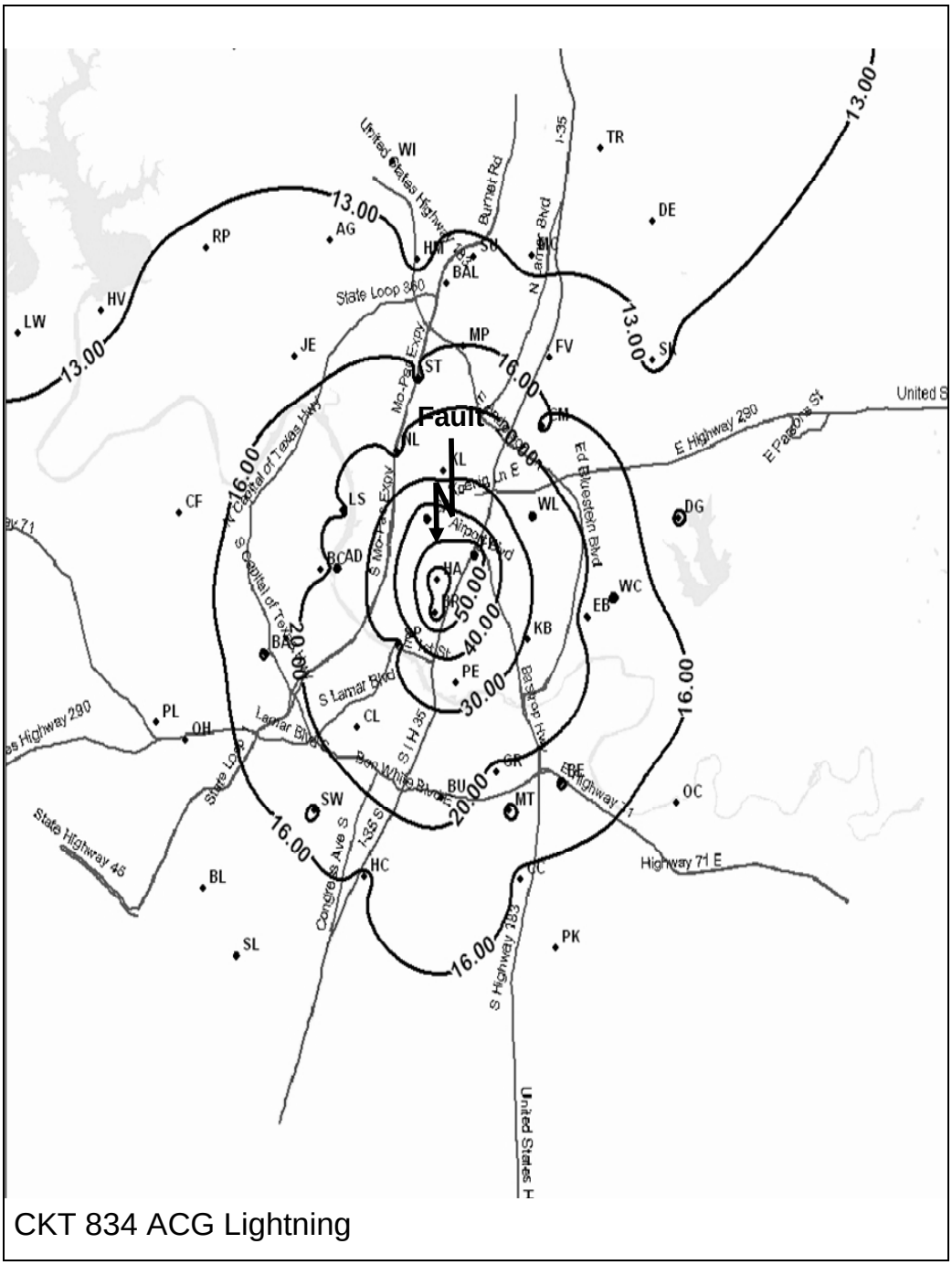

Figure 3.4: Voltage magnitude in Austin for fault on CKT 834

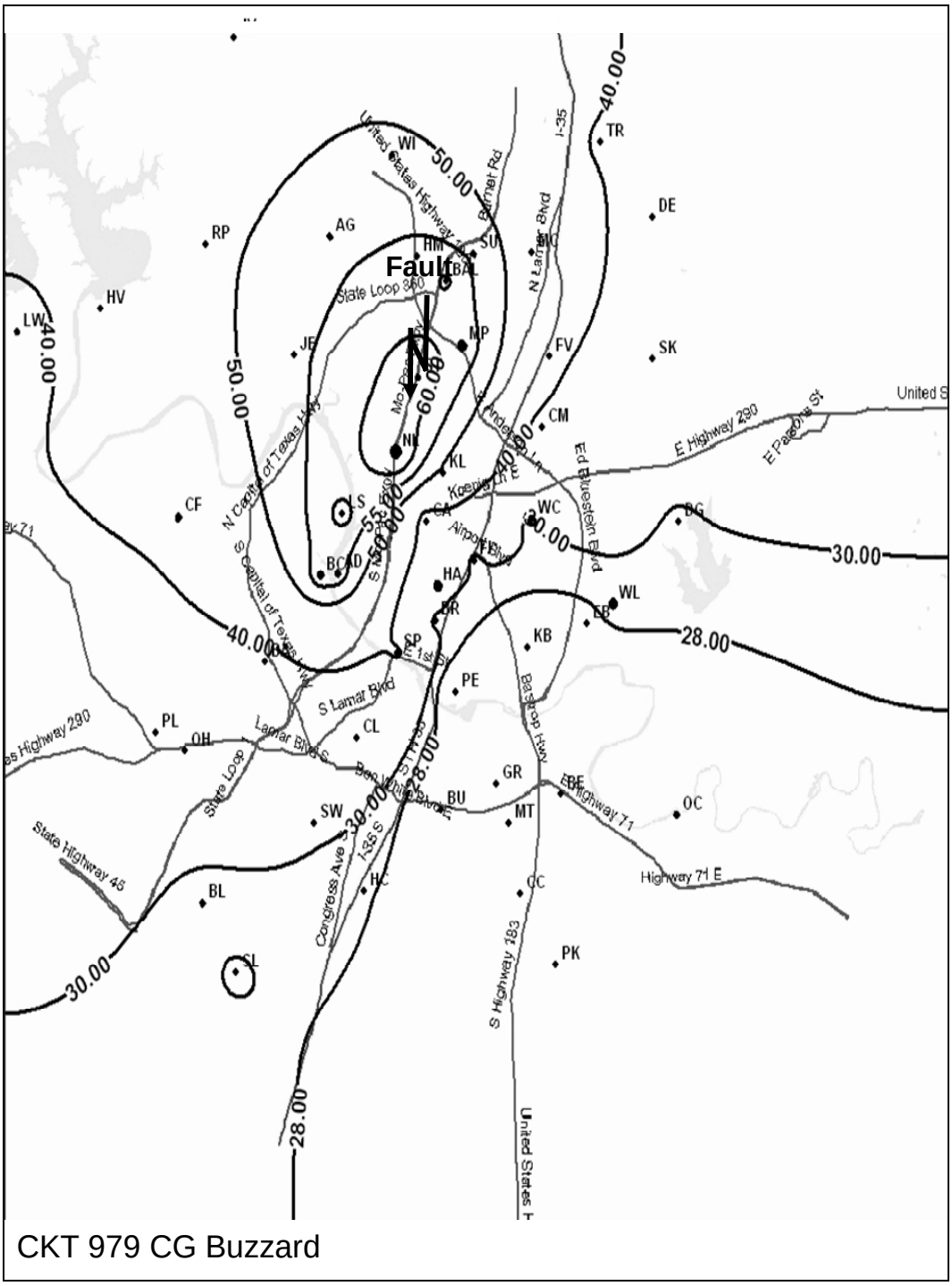

Figure 3.5: Voltage magnitude in Austin for fault on CKT 979

3.3 Examples

AE investigates all disturbance events in its transmission system. A formal report is issued for each event. The report contains the operation of the relay protection schemes for the event, field data, analysis of the data, and corrective recommendation to prevent recurrence of a similar event. A database containing the main information of each event in terms of date and time of the event, faulted phase, location and the cause of the fault are kept on the network drive and webpage. It has a collection of transmission fault data since 1975. The information from the database is used for reliability and system performance improvements as well as by the system equipment maintenance and planning.

To verify and validate the described theory in this dissertation, data from actual faults were used. The line fault data in terms of voltage signal is recorded and collected by digital fault recorders and microprocessor-based protective relays at various locations in the system as meter locations. Balanced three-phase, phase-ground, phase-phase, and phase-phase-ground transmission line fault types at voltage level of 69 kV and 138 kV were selected for this study. Fifteen actual events were tested to validate the methodology described in this chapter. Eight of the 15 cases are single-phase to ground faults due to the common occurrence of this type of faults. Two are phase-phase to ground, two are phase-phase, and three are three-phase faults. The meters were either fault recorders or microprocessor relays at different locations in the system.

3.4 Meter Data Calculations

Two types of meters were used in the study of the cases as the measured voltage values: 1) DFR - digital fault recorder, 2) microprocessor based relay. For the purpose of this work, only the recorded event data of these two devices are used. Each device triggers and captures fault data for an event; however, their applications and their functions in a power system are different. DFRs are transmission system monitoring and recording devices with numerous recording analog and digital points (also called channels) for monitoring and recording voltage and current quantities of multiple lines in a transmission system. They have adjustable triggering level for each channel. The sample rates for these devices range from 11.5 kHz to 195 kHz. Therefore they can capture any transient in the system. Each recorder is equipped with a GPS for time synchronization. The recorder has adjustable recording period of typically 4-6 cycles of pre-fault and 80-120 during and post fault.

Microprocessor relays are not only are monitoring devices, but are also equipped with control functions. They have intelligence and logic with programming capabilities for certain conditions of a power system to make decisions and perform system control functions. Within a couple of cycles of detecting an abnormal system condition, they can send a trip signal to a transmission line breaker in order to isolate a fault during a power system event. They can also detect and record abnormal conditions in a power system in terms of voltage, current, and frequency. Such relays are critical parts of power system protection schemes as was described in Chapter 1.

Although both devices provide sufficient and necessary event data for the studies in this dissertation, there are many differences between the application and event data

collection methodology of these two devices. The microprocessor relays only capture events for particular terminations of the line that they protect and there can be one or more such relays for every termination of the lines in a transmission system. However, when a fault occurs in a transmission system, only a few of these distribution systems relays initiate and generate event data. The relays on the line that they protect and sometimes the relays at the adjacent buses to the faulted lines will pick up. On the other hand, although there are only a few DFRs that monitor an entire power system, almost all of the DFRs in the system can pick up for every fault occurs in the system depending on the size of the system. In other words, for event data collection purposes, one difference between the two recording devices is that a DFR can be set to trigger within five percent of the system voltage deviation and it will record for a fault in almost any bus in the system. The relays are set to trigger mainly for the line that they are assigned to protect and in some cases, they may be set to trigger at locations with a couple of buses away form the actual faulted bus. For example, in Austin Energy's system there are only nine DFRs located at six various substations which detect events for the entire system. There are well above 1000 microprocessor relays in the transmission system which detect and record fault data only on certain transmission lines in the system.

One other main difference between the devices is their sampling rates. As DFRs are installed in key system locations to monitor entire transmission system, they have very high sampling rate (up to 195 kHz) to capture not only voltage sags, but also transients in the system. For the microprocessor relays and their applications, however, the sampling rates are much smaller than the DRFs, only 16 or 4 samples per cycle.

3.4.1 Digital Fault Recorders (DFR)

The format of a DFR recorded data is a waveform graphic, although the data can be exported as COMTRADE. The percentage of the measured voltage sag is calculated by putting the cursor at the highest pre-fault portion of the captured waveform and setting the second cursor at the lowest point of the during-fault part of the faulted phase. Then, the difference in the two measured points is divided by the highest point of the pre-fault to calculate the percentage of the voltage sag.

A sample of the recorded voltage and current quantities by a DFR is shown in Figure 3.6. This DFR data was used for Case 5 (described below is Section 3.6 Events) for a fault on CKT 985 as the meter location of Northland substation. The measured pre-fault and during fault values are shown on the left corner of the faulted c-phase which is the third waveform (shown as MB1 Vc). The measured pre and during fault values are shown to be 77977 Vrms and 38798 Vrms respectively. The calculated difference between the two values indicated to be 39179 Vrms. These measured values are used to determine the percentage of the sag value for this meter by:

$$\%Sag = \frac{39179}{77977} \bullet 100 = 50.2\%$$

For the same event, the voltage sag value for the second meter is calculated by using a DFR at Decker Plant as shown below. The measured pre-fault and during fault values are shown on the left corner of the faulted c phase which is the waveform before last (shown as DP-MB1 V PH). In this example:

$$\%Sag = \frac{9721.4}{81072} \bullet 100 = 11.99\%$$

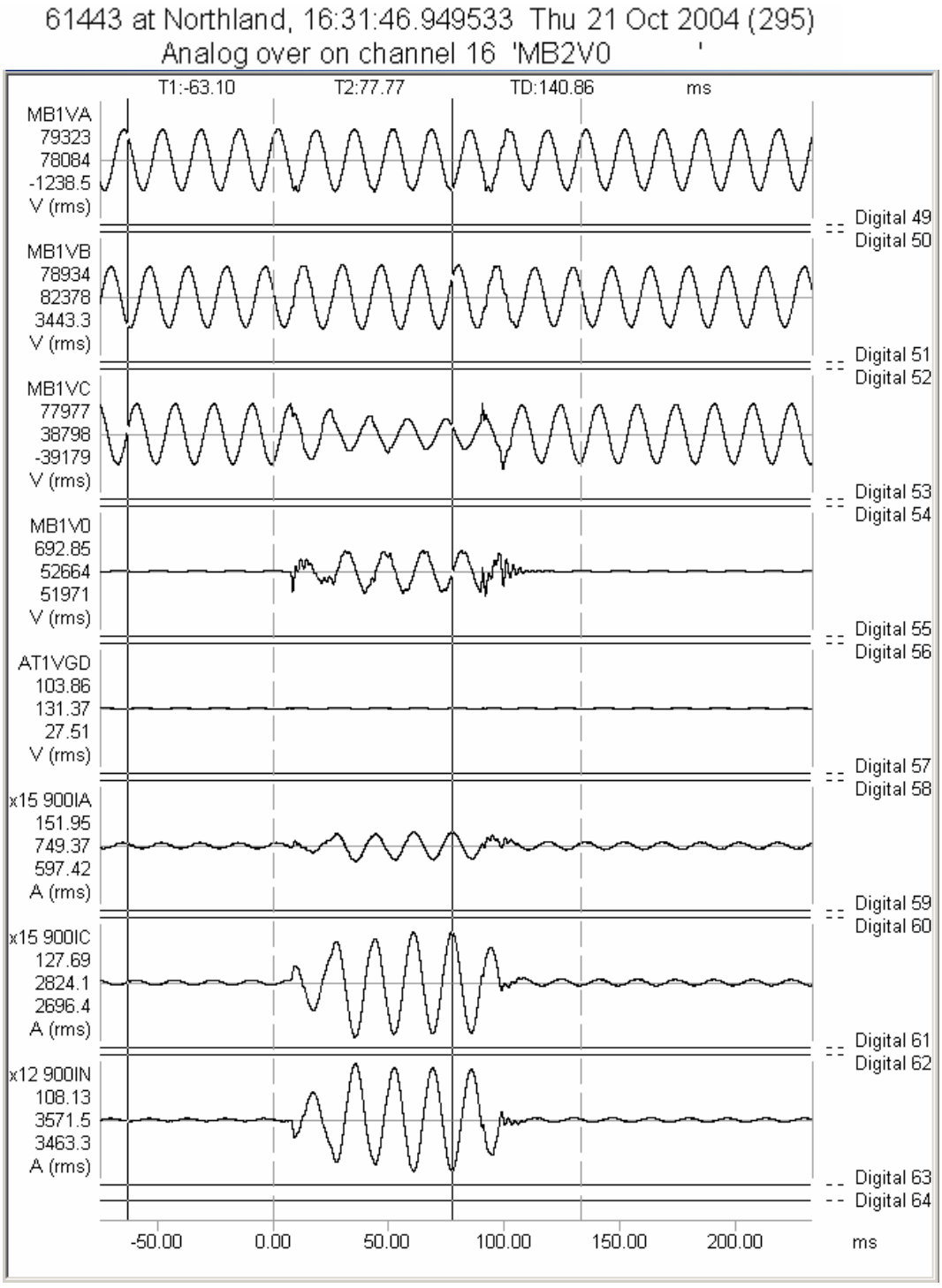

Figure 3.6: DFR recorder voltage and current quantities for Case 5 at NL

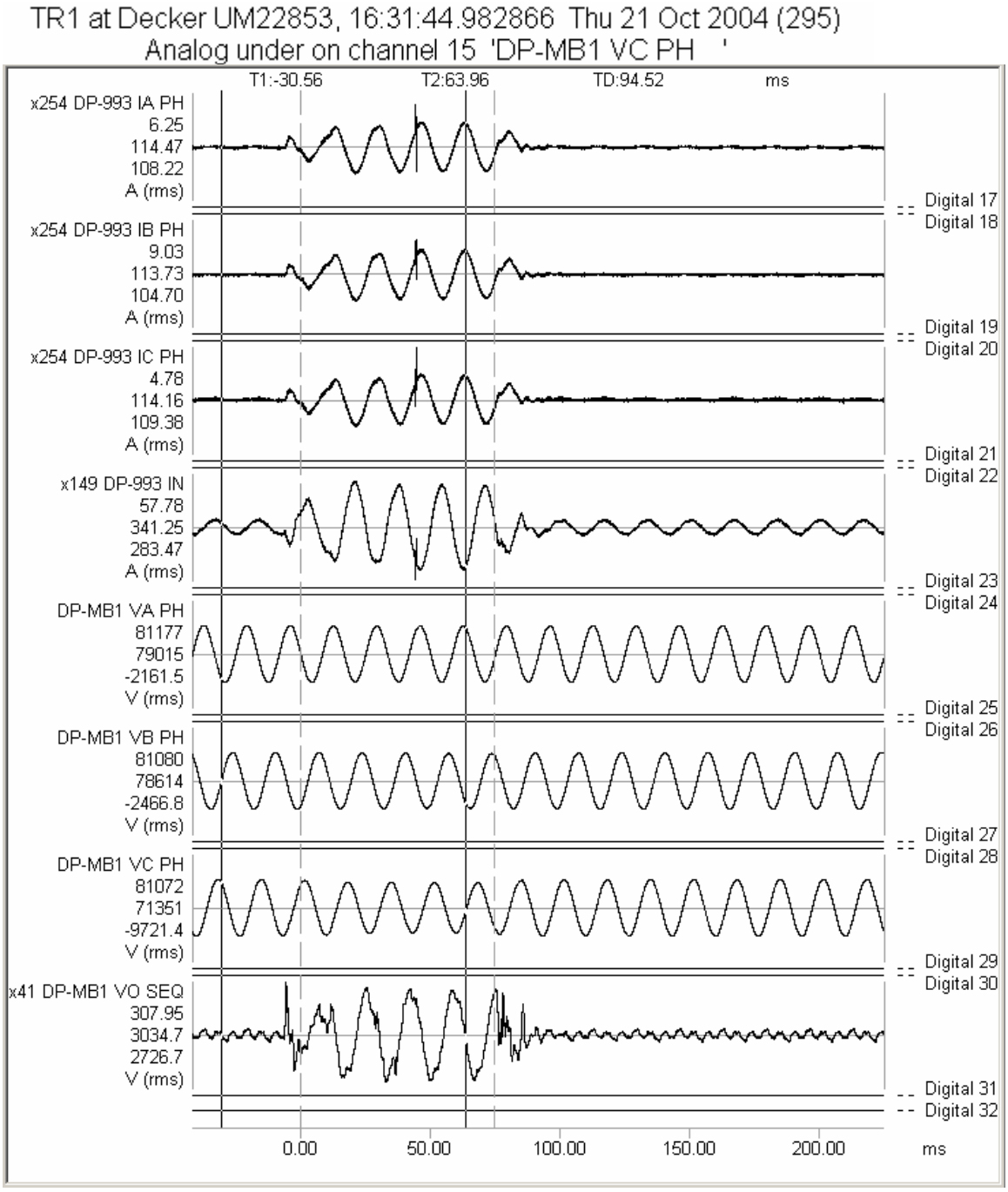

Figure 3.7: DFR recorder voltage and current quantities for Case 5 at DP

3.4.2 Microprocessor Relays

Microprocessor relays are monitoring, recording, and controlling devices which are used in a power system protection schemes. The recorded data during a fault have been used for the study of the test cases.

The format of event data from these relays can be displayed in text and waveform graph as shown in Figure 3.8 and 3.9 below. Using this format, the percentage of the measured voltage sag is calculated by finding two lowest consecutive voltage values during fault, then taking the square root of the squared sum of the two values [26]. The same process can be followed for the pre-fault portion of the fault data. Then, similar to the calculations with the DFR's pre and during-fault data, take the difference between the two values and divide the difference by the pre-fault value to fine the percentage of the sag for that event.

A sample of the recorded voltage and current quantities by a microprocessor relay is shown in Figure 3.8:

SEL-311C 21/79 BKUP GR-1010 Date: 10/21/04 Time: 15:31:11.796

GROVE GR-1010 MT

FID=SEL-311C-R107-V0-Z004003-D20020703 CID=15C5

Currents (Amps Pri)					Voltages (kV Pri)				V1		
IA	IB	IC	IP	IG	VA	VB	VC	VS	Mem	FREQ	Vdc
[1]											
-278	702	-438	-2	-14	21.0	-77.2	56.2	-0.0	21.0	59.99	132
672	-94	-554	0	24	-77.3	20.6	56.5	0.0	-77.1	59.99	132
276	-704	436	0	8	-21.0	77.2	-56.3	0.0	-21.0	59.99	132
-674	92	550	-2	-32	77.3	-20.7	-56.5	-0.0	77.2	59.99	132
[2]											
-278	702	-438	-2	-14	20.9	-77.2	56.3	-0.0	20.9	59.99	132
672	-94	-554	0	24	-77.3	20.7	56.5	0.0	-77.2	59.99	132
276	-702	436	0	10	-20.9	77.2	-56.3	0.0	-20.9	59.99	132
-676	90	578	0	-8	77.5	-20.6	-55.4	-0.0	77.1	59.99	132
[3]											
-286	694	-414	-2	-6	20.8	-77.2	54.6	-0.0	20.8	59.99	132
700	-60	-786	-2	-146	-77.3	20.7	54.8	0.0	-77.0	59.99	132
296	-702	456	0	50	-20.8	77.2	-51.1	0.0	-20.9	59.99	132
-748	14	1020	0	286	76.7	-20.8	-55.5	-0.0	76.5	59.99	132
[4]											
-326	694	-390	-2	-22	21.0	-77.2	49.3	-0.0	21.1	59.99	132
790	20	-1252	-2	-442	-76.4	20.5	52.2	0.0	-75.9	59.98	132
382	-664	154	0	-128	-21.3	77.0	-46.9	0.0	-21.1	59.98	132
-828	-54	1466	0	584	75.9	-20.3	-49.1	-0.0	75.1	59.98	132>
[5]											
-422	654	-50	-2	182	21.7	-76.7	44.3	-0.0	21.1	59.98	132
844	56	-1484	-2	-584	-75.5	20.0	49.0	0.0	-74.2	59.92	132
438	-662	20	0	-204	-21.9	76.6	-44.2	0.0	-21.1	59.92	132*
-854	-62	1492	0	576	75.2	-19.9	-47.9	-0.0	73.5	59.92	132
[6]											
-460	654	24	-2	218	21.9	-76.4	43.7	-0.0	21.0	59.92	132
852	72	-1532	-2	-608	-74.9	19.9	47.4	0.0	-72.8	59.92	132
472	-654	-54	0	-236	-21.9	76.2	-43.3	0.0	-21.0	59.92	132
-850	-82	1532	0	600	74.7	-19.9	-47.3	-0.0	72.3	59.92	132
[7]											
-482	654	54	-2	226	21.8	-76.0	43.3	-0.0	20.9	59.92	132
844	88	-1534	-2	-602	-74.5	19.9	47.2	0.0	-71.8	59.94	132
484	-660	-54	0	-230	-21.6	75.8	-43.2	0.0	-20.8	59.94	132
-830	-78	1428	0	520	74.6	-19.7	-49.2	-0.0	71.5	59.94	132
[8]											
-456	686	-76	-2	154	21.7	-75.6	45.3	-0.0	20.8	59.94	132
780	26	-1098	-2	-292	-74.6	19.8	52.8	0.0	-71.6	59.99	132
398	-734	294	0	-42	-21.9	75.5	-49.6	0.0	-20.9	59.99	132
-738	20	768	0	50	75.0	-19.9	-55.0	-0.0	72.1	59.99	132

Figure 3.8: Microprocessor relay event data for Case 5 at GR

The above data, from a relay at Grove substation, were used for Case 5, for a fault on CKT 985. The event's heading in Figure 3.8 defines the measured values of the voltage and current quantities for each column. Such relay has a sampling rate of four samples per cycle, or 240 Hz. The numbers in the brackets on the left side of the start of each sample indicate the recorded cycle number. The recording lengths of these relays are set such that the first few cycles are normally to record the pre-fault and the remaining to record during and the post fault values.

The percentage of the sag value for this meter is calculated by first finding the highest fault current value on the faulted phase column. In this event, that value is 1534 amps at the seventh cycle (underlined). Then, move across the table on that row and find the fault voltage value on the faulted c-phase column which is 47.2 kV. To find the percentage of the voltage sag, we first must find the RMS voltage values for during fault and the pre-fault periods. This is accomplished by taking the square root of the sum of the squared values of two consecutive voltage values for the identified maximum fault current. Using this procedure, the RMS value for both the pre-fault and during fault can be calculated [26]. Then similar to the DFR voltage sag calculations explained above, the difference between during fault and pre-fault values is divided by the pre-fault multiplied by 100.

For this example the percentage of the sag value is calculated by:

During fault:

$$V_{rms} = \sqrt{(47.2)^2 + (-43.2)^2} = 64$$

pre-fault:

$$V_{rms} = \sqrt{(56.5)^2 + (-56.3)^2} = 79.76$$

The sag value is calculated:

$$\%Sag = \frac{15.76}{79.76} \approx 20\%$$

This value was used as the measured meter value at GR substation for Case 5.

Another form of relay event data used to determine measured values by a meter is shown below:

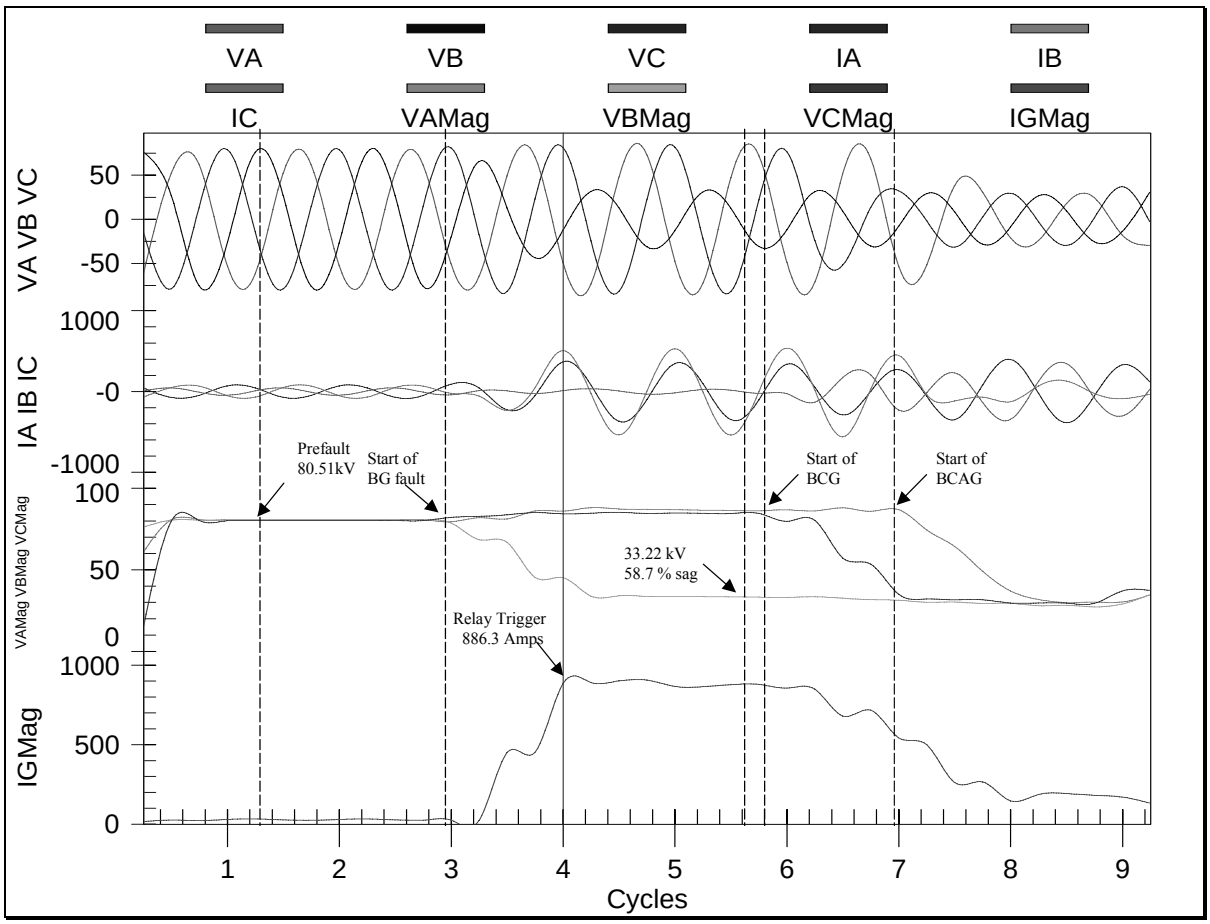

Figure 3.9: Microprocessor relay event data with voltage sag value in graphic form for Case 12 at SU

The above is the actual measured data from a meter location at the Summit substation for Case 12. The graph shows the calculated voltage values for this single-phase to ground fault at the pre and during fault points. On this graph, important measured values of this event are indicated by arrows. The calculated voltage sag for this case, as indicated on the above graph is 58.7%.

The data below was used in a similar way to determine the voltage sag value for a meter at Summit substation for Case 13 which was a three-phase fault. As it is shown on the graph, the sag value used for this case is 66.1% at SU.

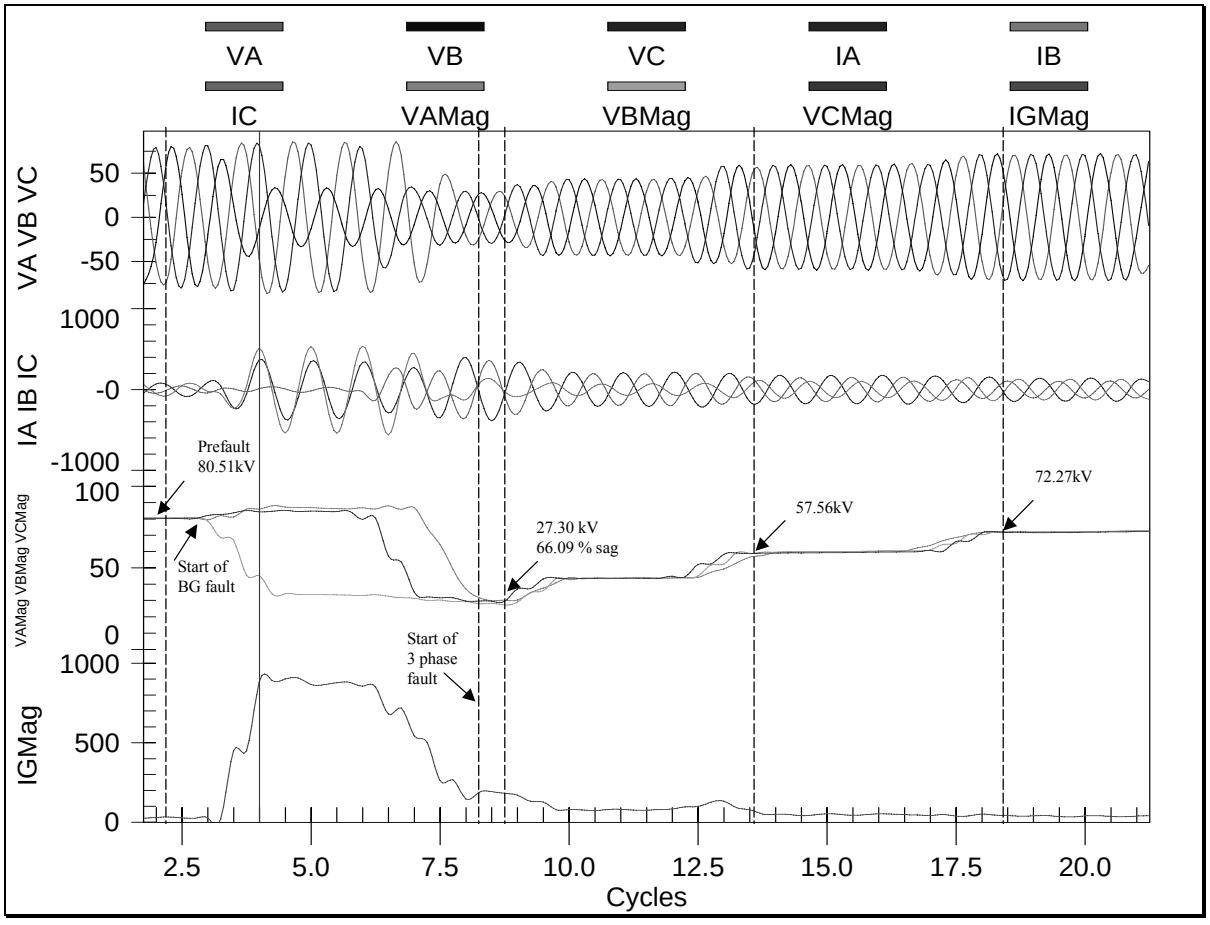

Figure 3.10: Microprocessor relay event data with voltage sag value in graphic form for Case 13 at SU

3.5 Meter Location

Meter locations were selected from the set of meters that captured the events. Locations at different voltage levels were selected for these events. However, for the study of all events, the meter values used as input to our study were chosen in order of highest to the lowest recorded voltage sag. For better estimation of fault location by the program, the meters with larger differences in their measured voltage sag percentages were chosen.

Figure 3.11 below shows the location of all meters used for study of the cases in this work; meters are indicated with circles. These include DFRs and the microprocessor relays.

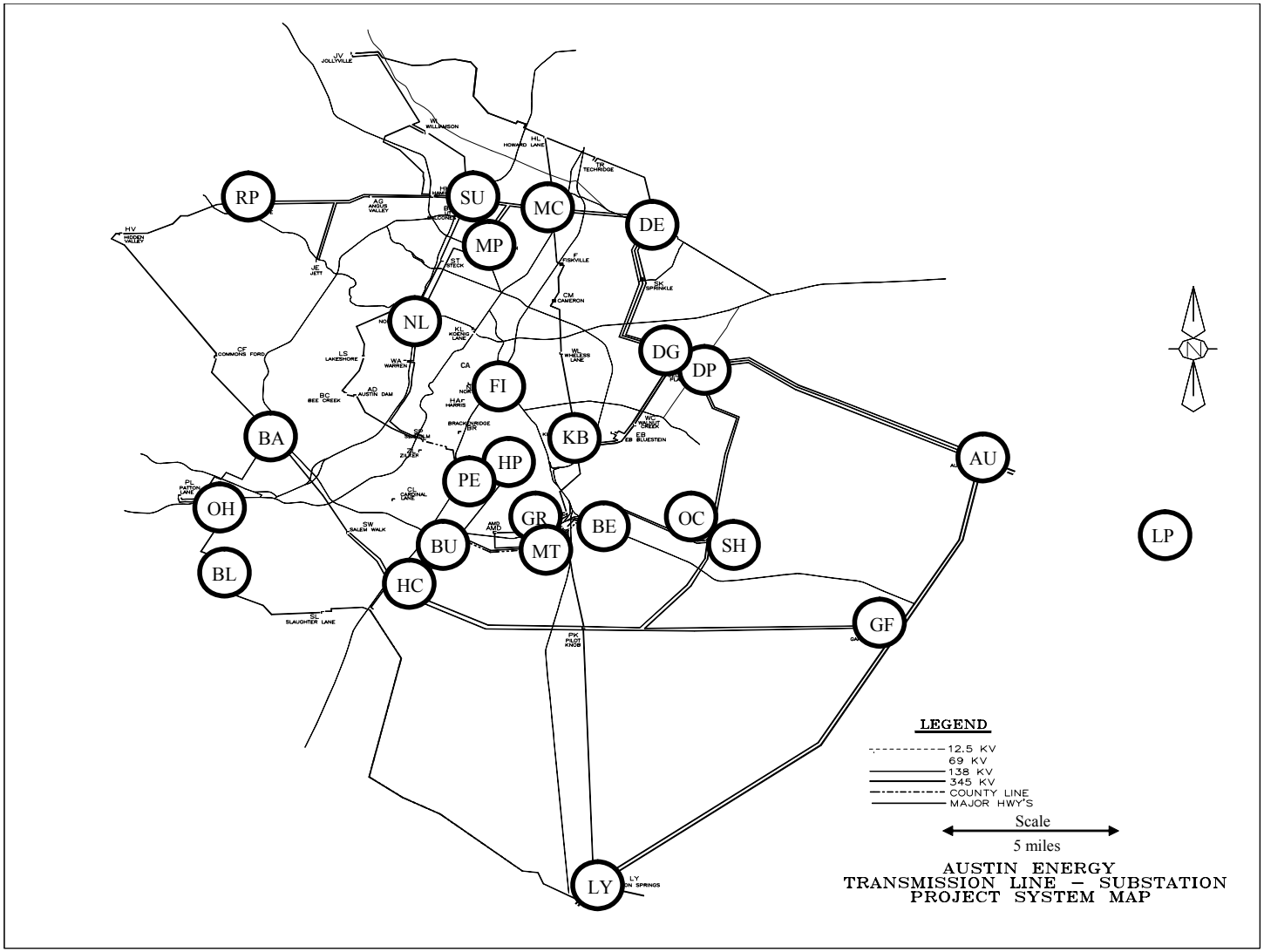

Figure 3.11: Meter locations

Table 3.2 lists the substation and meter locations' name with their abbreviations used in this paper. Substation abbreviations are mostly used throughout this work.

SUB ABR	NAME	BUS KV	SUB ABR	NAME	BUS KV	SUB ABR	NAME	BUS KV
AD	AUSTNDAM	138	HM	HAMILMB1	138	MC	MCNEILW	138
AMD	AMD	138	HM	HAMILMB2	138	MT	METCENTR	138
AV	ANGUSVAL	138	HA	HARRIS	69	MF	MARSHALD	138
AU	AUSTROP	138	HC	HICROSS	138	NL	NORTHLND	69
AU	AUSTROP	345	HC	HICRSMB1	138	NL	NORTHWES	138
AU	AUSTROP	138	HC	HICRSMB2	138	OH	OAKHILL	138
AU	AUSTROP	345	HV	HIDDENVL	138	OC	ONIONCK	138
BA	BARTON	138	HL	HOWARDLN	138	PL	PATTON	138
BC	BEECREEK	138	HP	HOLLYMB1	69	PE	PEDERNALS	69
BE	BERGSTRM	138	HP	HOLLYMB2	69	PE	PEDERNALS	138
BR	BRACK	69	HP	HOLLYMB3	69	PK	PILOTKB	138
BL	BRODIE	138	HP	HOLLYMB4	69	SW	RIVERPLS	138
BU	BURLESON	138	HO	HOLMAN	345	SW	SALEMWLK	138
BU	BURLESON	69	HL	HOWARD	138	SH	SANDHSYD	138
CM	CAMERON	138	JE	JETT	138	SP	SEAHM8	138
CL	CARDINAL	69	JV	JOLLYVIL	138	SP	SEAHMDB	69
CC	CARSON	138	KB	KINGSBRY	69	SL	SLAUGHTR	138
CA	CENTAUS	69	KB	KINGSDB	138	SK	SPRINKLE	138
CF	COMMONFD	138	KB	KINGSMB1	138	ST	STECK	138
DG	DAFFING	138	KL	KOENIG	69	STP	SOUTH TX	345
DP	DECKER	138	LS	LAKESHOR	138	SU	SUMMITN	138
DP	DECKMB2	138	LW	LAKEWAY	138	SU	SUMMITS	138
DE	DESSAU	138	LP	LOSTPINT	345	TR	TECHRIDG	138
EB	EDBLUE	138	LY	LYTTON	345	TP	TRADPOST	138
FI	FIESTA	69	LY	LYTTON	138	UT	UTBALC	138
FV	FISKVILL	138	MP	MAGPLANT	138	WC	WALNUTCK	138
FPP	FAYETT PP	345	MC	MCNEIL	138	WA	WARREN	138
GF	GARFIELD	138	MC	MCNEIL	69	WL	WHELESS	138
GF	GARFIELD	345	MC	MCNEILN	138	WI	WILIAMSN	138
GR	GROVE	138	MC	MCNEILS	138	ZL	ZILKER	69

Table 3.2: Meter location and substation names with their abbreviations

3.6 Events

AE investigates all disturbance events in its transmission system. A formal report is issued for each event. The report contains a list of the relays that operated for the event, field data, analysis of the data, and corrective recommendation as action items to prevent recurrence of a similar event. A database containing the main information of each event in terms of date and time of the event, faulted phase, location and the cause of the fault is kept on the network drive and posted on internet for external customer information and access.

The database has a collection of transmission fault data since 1975. The information from the database is used for reliability and system performance improvements as well as the Planning workgroup for transmission line performance evaluations. Since the beginning of the year 2000, all 345 kV system faults are required to be reported to Electric Reliability Council of Texas (ERCOT).

Each of the 15 study cases for the work in this dissertation is explained in the following section. This includes the meter locations and the measured voltage sag percentage for each case, the actual location of the fault, and the estimated fault locations by the new methodology developed in this dissertation. The actual fault locations are indicated by unshaded arrows, and estimated locations are indicated by shaded arrows.

Event 1. CKT 809 Faults on 02/08/05 at 16:22:46

A fault occurred on CKT 809, Koenig Lane (KL) to Northland (NL) substation, at 16:22:46 on 02/08/05 when a car hit a streetlight pole. This caused the streetlight wire to snap and make contact with both the transmission circuit and the underbuilt span of primary overhead distribution conductor. This is a 69 kV transmission line located in the north-central part of the City of Austin. All the digital fault recorders (DFR) in the system initiated and recorded events for this fault and showed a b phase to ground fault. Additionally, a microprocessor relay at FI substation picked up for this event with similar information. Other electromechanical relays in the system indicated the correct faulted phase. The protective relays operations indicated that the fault occurred at the Zone 1 portion of the line protection from KL substation and the Primary protection zone from NL termination of the line. This indicates that the fault was close to (within 20%) from KL termination.

The data from five meter locations for this case included: FI relay showed a 57.2% voltage sag, a DFR at HP showed a 25.0%, MP relay showed 17.8%, DFR at MC showed a 13.5%, and DFR at DP indicated a 9.4% sag for this fault. The fault was estimated accurately at the actual location with data from the first two meters.

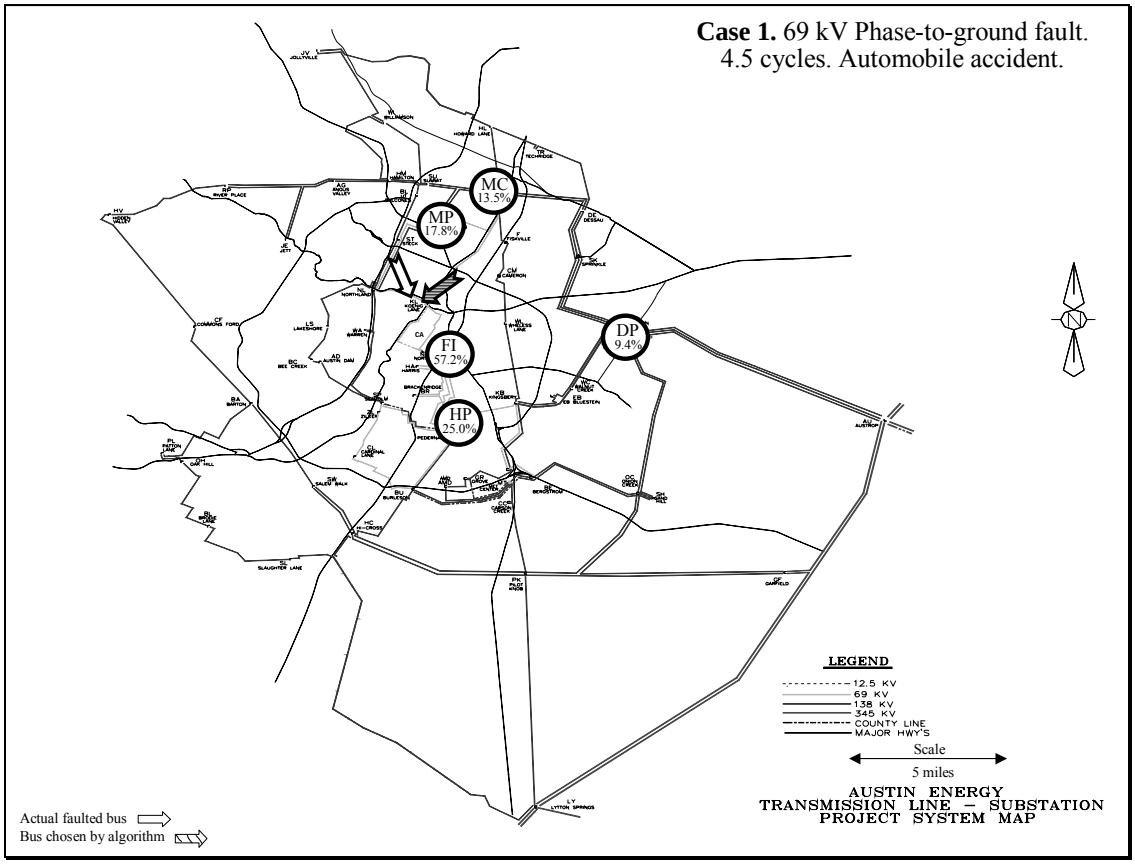

Figure 3.12: Meter locations with actual and estimated fault location for Event 1

Event 2. CKT 975 Fault on 03/25/05 at 21:34:23

A fault occurred on CKT 975, Dessau (DE) to Tech Ridge (TR) substation, during a thunderstorm that passed through the Austin area on 03/25/05. This is a 138 kV transmission line located about north part of the City of Austin. All the digital fault recorders in the system initiated and recorded events for this fault and showed a c phase to ground fault. Additionally, microprocessor relay at Kingsbury substation picked up for this event with a similar information. Other electromechanical relays in the system indicated the correct faulted phase. The protective relays operations indicated that the fault occurred at the Zone 1 portion of the line protection from DE substation and the Primary protection zone from TR termination of the line. This indicates that the fault was close to (within 20% of) the DE termination.

The data from five meter locations for this case included: a DFR at MC substation showed a 59.6% voltage sag, a DFR at NL showed a 48.0%, DP relay showed 40.0%, DFR at AU indicated a 26.1% sag and KB relay showed 25.2% sag. The fault was estimated accurately at the actual location of DE substation with data from the first three meters when alpha was 1.08. However, with alpha equal 1.00, the algorithm located the fault at HL substation, one bus away from DE.

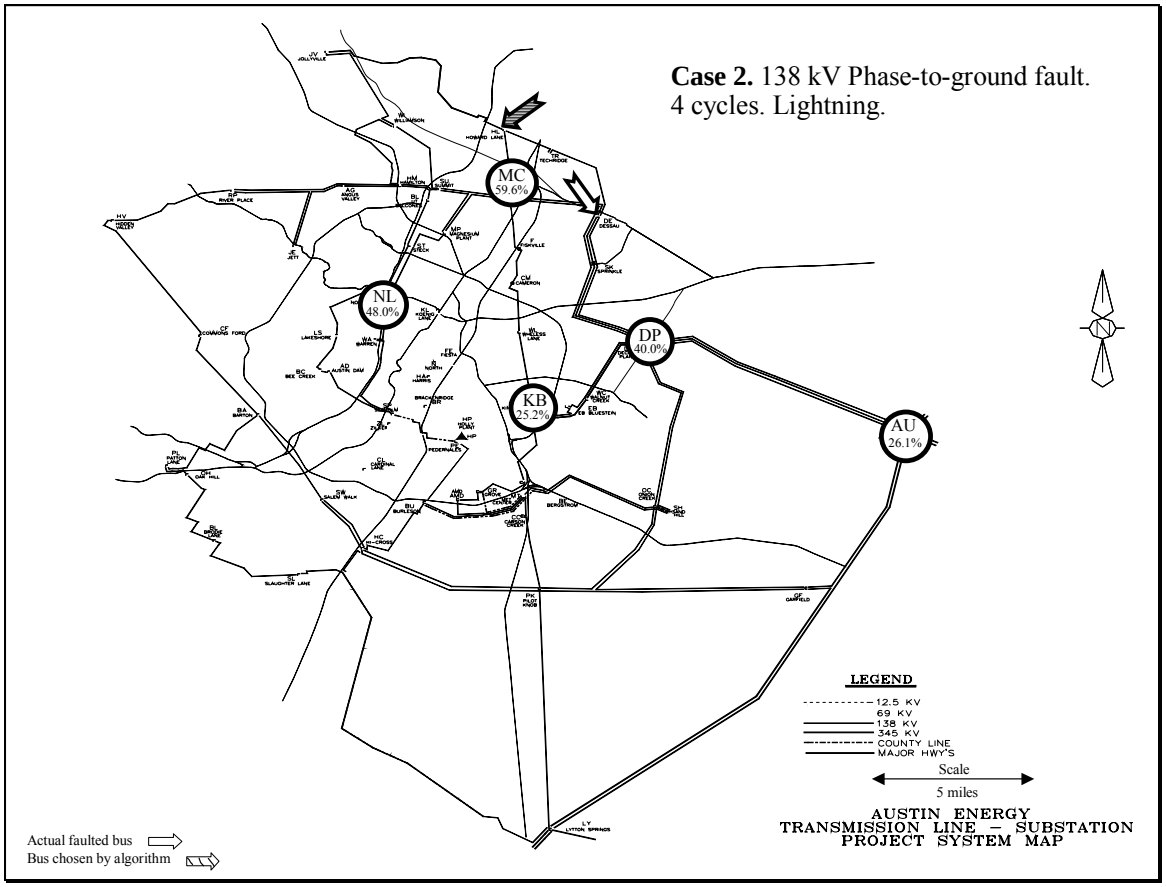

Figure 3.13: Meter locations with actual and estimated fault location for Event 2

Event 3. FV 5 Fault on 01/22/05 at 07:24:07

An insulator on a metering CT failed and blew up at Fiskville substation (FV) on 01/22/05 at 07:24:07. The substation is a 138 kV substation located in the northeast part of the City of Austin. All the digital fault recorders in the system initiated and recorded events for this fault and showed a three-phase fault. Additionally, microprocessor relay at various substations picked up for this event with a similar information. Other electromechanical relays in the system indicated the correct faulted phase. The protective relays operations made the breakers at FV substation to trip and clear this fault.

The data from five meter locations for this case included: a microprocessor relay at RP substation showed 43.8% sag, at BU a 34.3%, at OH substation 31.4%. A DFR at AU indicated a 25.7% and at LY a 21.5% voltage sag. The fault was estimated at the actual location with data from the first two meters.

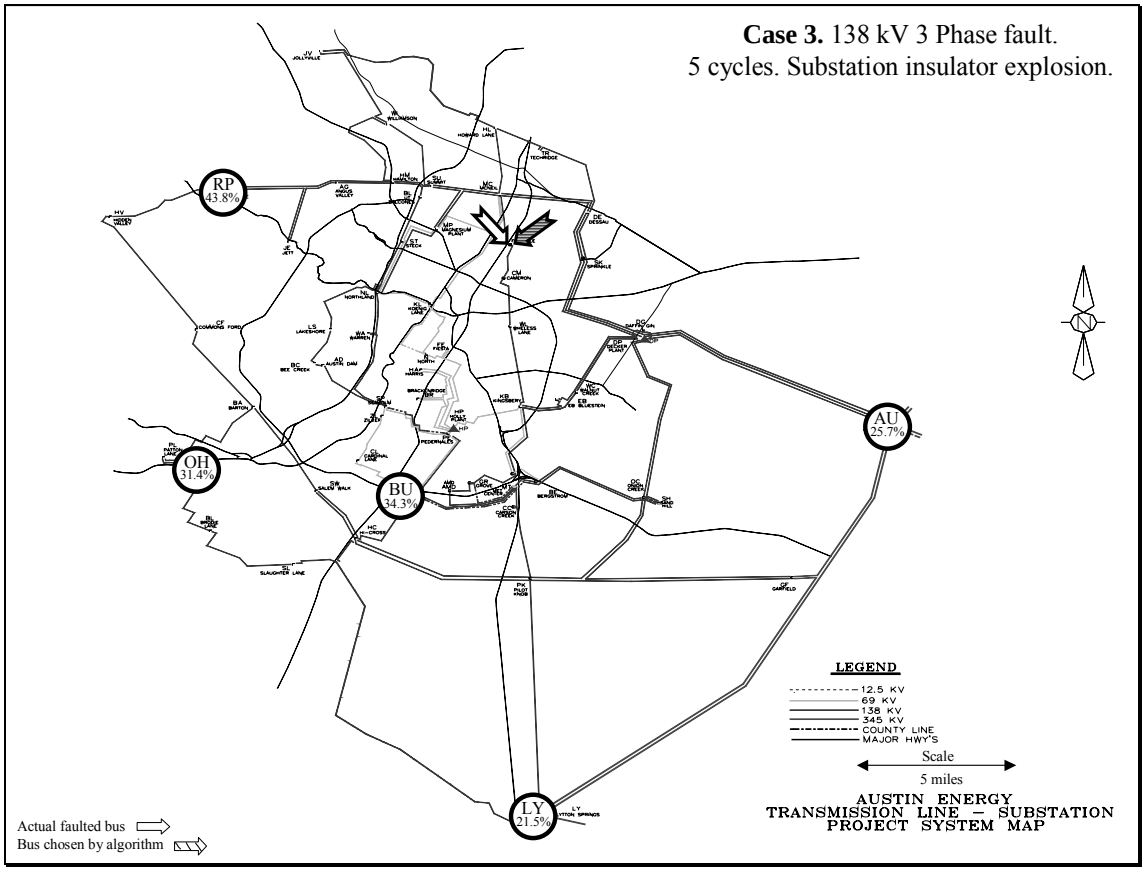

Figure 3.14: Meter locations with actual and estimated fault location for Event 3

Event 4. CKT 929 Fault on 9/11/2005 at 6:58:25

A fault occurred on CKT 929, Salem Walk (SW) to Barton (BA), on 9/11/2005 at 6:58:25 when a buzzard contacted the a phase of the circuit. This is a 138 kV transmission line located in the southwest part of the City of Austin. All the digital fault recorders in the system initiated and recorded events for this fault and showed an a phase to ground fault. Additionally, the microprocessor relays at BA and SL substations picked up for this event with similar information. Other electromechanical relays in the system indicated the correct faulted phase. The protective relays operations indicated that the fault occurred at the Zone 1 portion of the line protection from SW substation and the Primary protection zone from BA termination of the line. This indicates that the fault was close to (within 20% of) the SW termination.

The data from five meter locations for this case included: microprocessor relay at BA showed a 79.8% voltage sag, OH relay showed a 68.4% voltage sag, HC relay showed a 65.0%, BL indicated a 59.9%, at AU a 40.2% sag, and OC showed a 24.5% voltage sag. The fault was estimated accurately at the actual location with data from the first two meters.

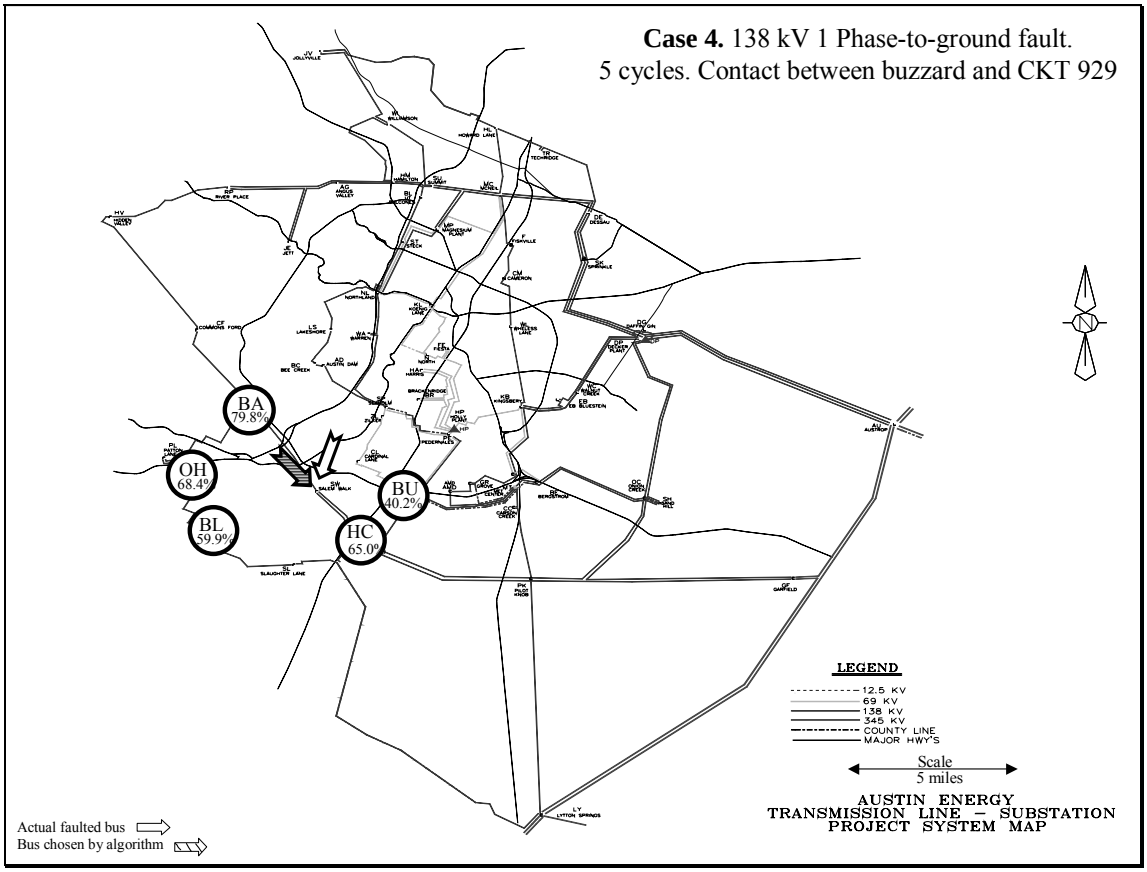

Figure 3.15: Meter locations with actual and estimated fault location for Event 4

Event 5. CKT 985 Fault on 10/21/04 at 16:31:46

A fault occurred on CKT 985, Austin Dam (AD) to Bee Creek (BC) substation, on 10/21/04 at 16:31:46 when a crane contacted the c phase of the circuit. The crane was removed and the circuit was reenergized. This is a 138kV transmission line located in the west-central part of the City of Austin. All the digital fault recorders in the system initiated and recorded events for this fault and showed a c phase to ground fault. Additionally, a microprocessor relay at FI substation picked up for this event with similar information. Other electromechanical relays in the system indicated the correct faulted phase. The protective relays operations indicated that the fault occurred at the Zone 1 portion of the line protection from BC substation and the Primary protection zone from AD termination of the line. This indicates that the fault was close to (within 20% of) BC termination.

The data from five meter locations for this case included: a DFR at NL showed a 50.2% voltage sag, an FI relay showed a 23.6% voltage sag, a GR relay showed a 20.0%, a DFR at DP indicated a 11.9%, and a DFR at AU a 7.6% sag. The fault was estimated accurately at the actual location with data from the first three meters when alpha was 1.04. With alpha equal to 1.00, the fault was estimated to be located at LS substation which is one bus away from the actual fault location. This could be due to equivalency as the faulted bus is on the border of AE's electric system located at a jointly owned substation with the neighboring utility.

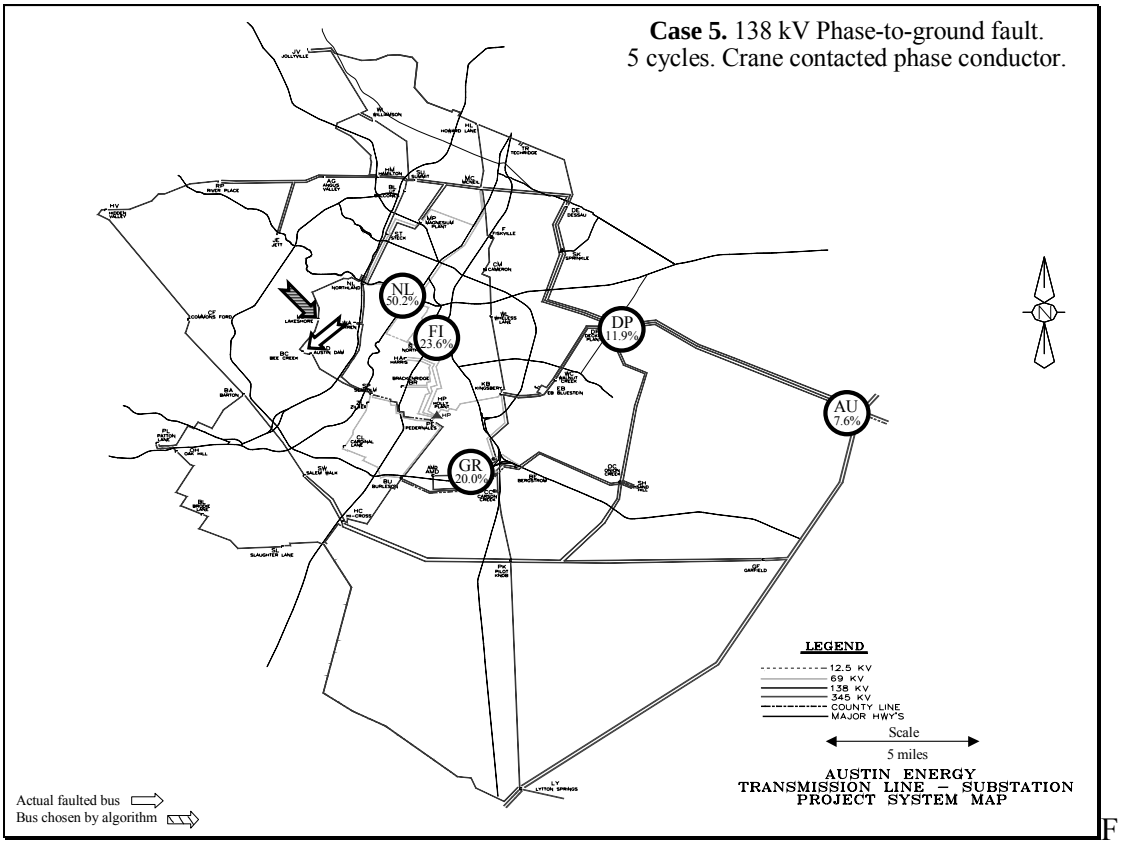

Figure 3.16: Meter locations with actual and estimated fault location for Event 5

Event 6. CKT 925 Fault on 12/17/05 at 22:23:32

A fault occurred on CKT 925, Hi Cross (HC) to Pilot Knob (PK) substation, on 12/7/05 at 22:23:32 during an ice storm that passed through the city. The storm caused several phase-to-phase circuit faults due to galloping phase conductors when the wind blew and caused the circuit conductors to collapse and cause a fault. This is a 138 kV transmission line located in the southeast part of the City of Austin. All the digital fault recorders in the system initiated and recorded events for this fault and showed an a phase to b phase fault. Other electromechanical relays in the system indicated the correct operations of the system protection schemes and the faulted phases.

The data from five meter locations for this case included: a microprocessor relay at BU showed a 42.7% voltage sag, at MT a 40.3% voltage sag, a DFR at LY recorded a 35.6%, at MC a 30.0%, and at AU showed a 24.6% voltage sag. The fault was estimated accurately at the actual location with data from the first three meters.

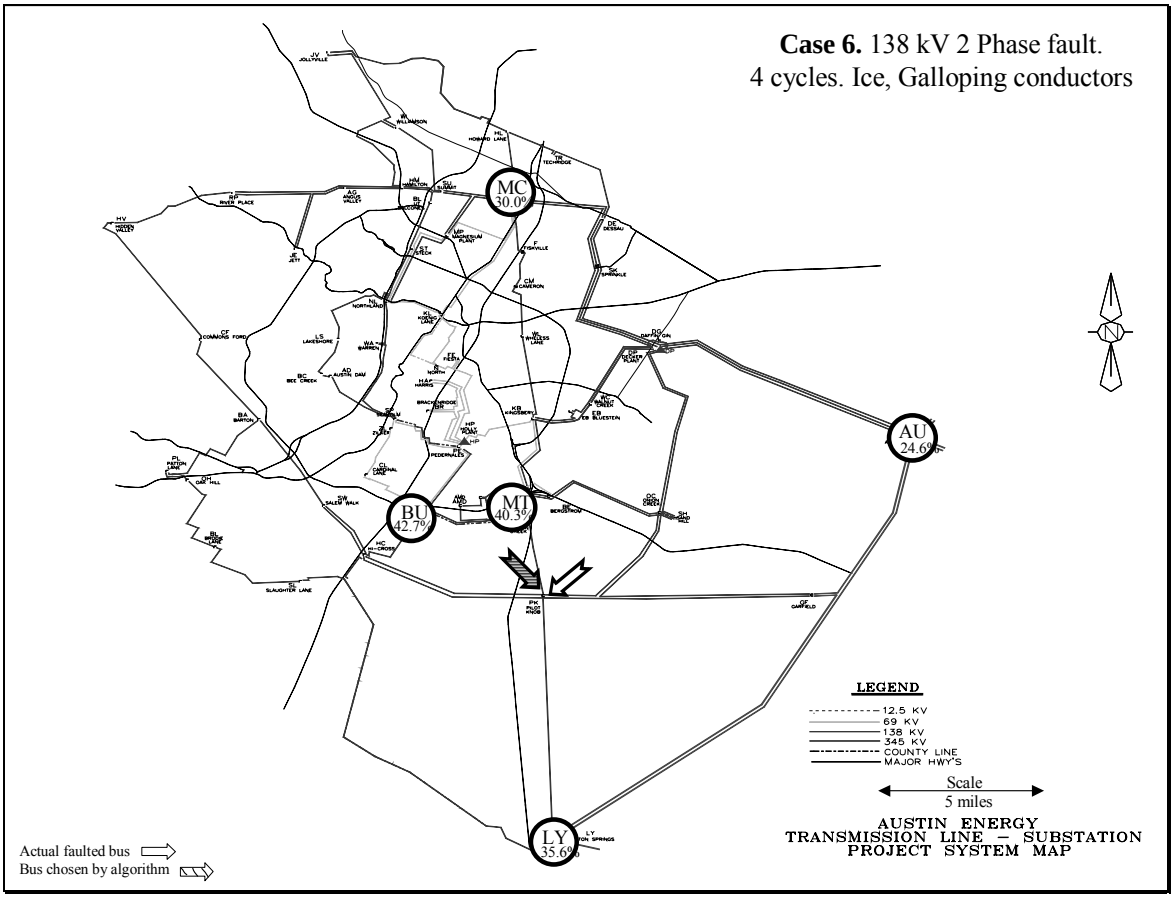

Figure 3.17: Meter locations with actual and estimated fault location for Event 6

Event 7. CKT 962 Fault on 12/7/05 at 22:19:52

A fault occurred on CKT 962, Onion Creek (OC) to Garfield (GF) substation, on 12/7/05 at 22:19:52 during an ice storm that passed through the city. This is another similar fault to the previous fault due to the storm. The fault on this circuit was also due to galloping phase conductors when the wind blew and caused the circuit conductors to collapse and cause a fault. This is a 138 kV transmission line located in southeast part of the City of Austin. All the digital fault recorders in the system initiated and recorded events for this fault and showed an a phase to b phase fault. Other electromechanical relays in the system indicated the correct operations of the system protection schemes and the faulted phases.

The data from five meter locations for this case included: a digital relay at BU showed a 31.3% voltage sag, at KB a 25.0% voltage sag, a DFR at NL recorded a 22.9%, a digital relay at HP showed a 20.6%, and a DFR at MC showed a 18.6% voltage sag. The fault was estimated accurately at the actual location with data from the first three meters.

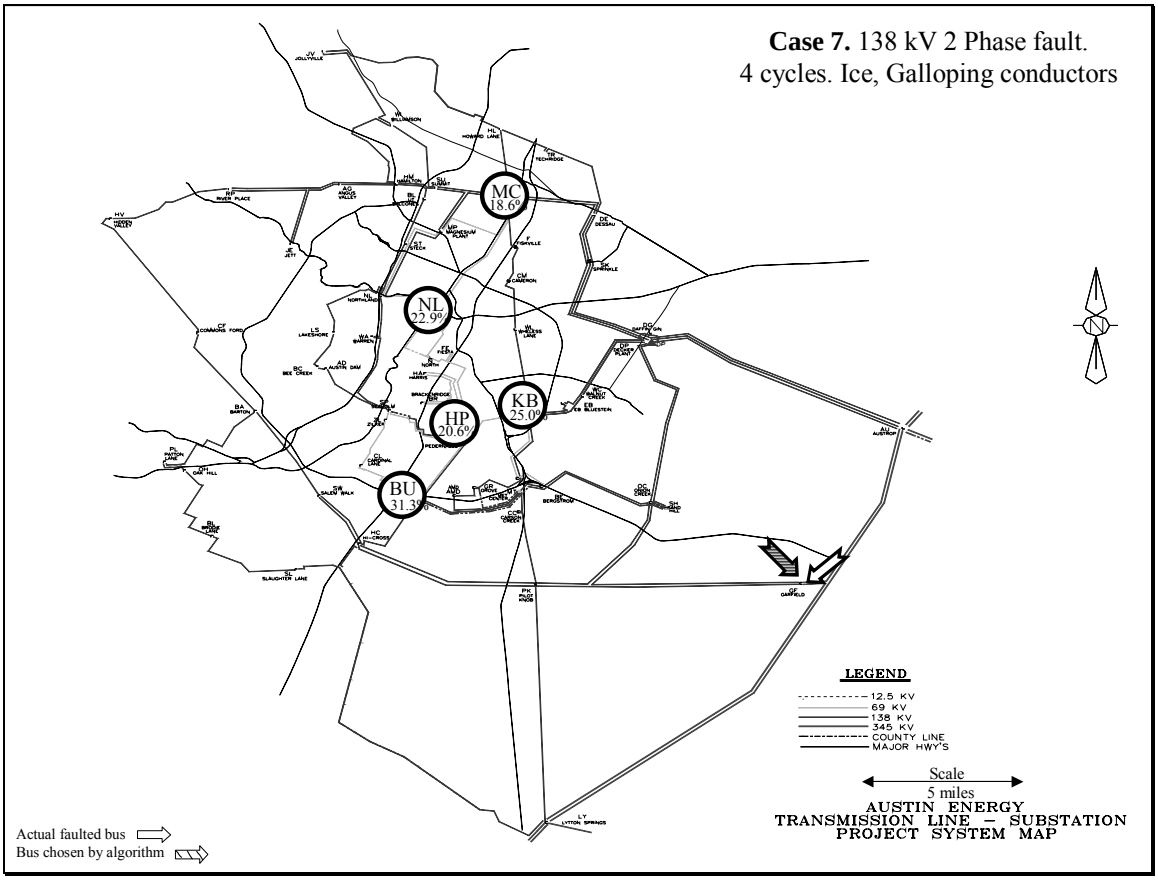

Figure 3.18: Meter locations with actual and estimated fault location for Event 7

Event 8. CKT 834 Fault on 07/25/04 at 18:41:30

A fault occurred on CKT 834, Harris (HA) to Brackenridge (BR) substation, on 07/25/04 at 18:41:30 during a thunderstorm. This is a 69 kV transmission line located in downtown Austin. All the digital fault recorders in the system initiated and recorded events for this fault and showed an a phase to c phase to ground fault. Additionally, microprocessor relays at KB and BU substations picked up for this event with a similar information. Other electromechanical relays in the system indicated the correct faulted phase.

The data from five meter locations for this case included: DFR at HP showed a 43.0% voltage sag, a digital relay at KB indicated a 29.7% voltage sag, BU showed a 25.8%, a DFR at NL showed a 13.5%, and at DP a 7.2% sag. The fault was estimated accurately at the actual location with data from the first three meters.

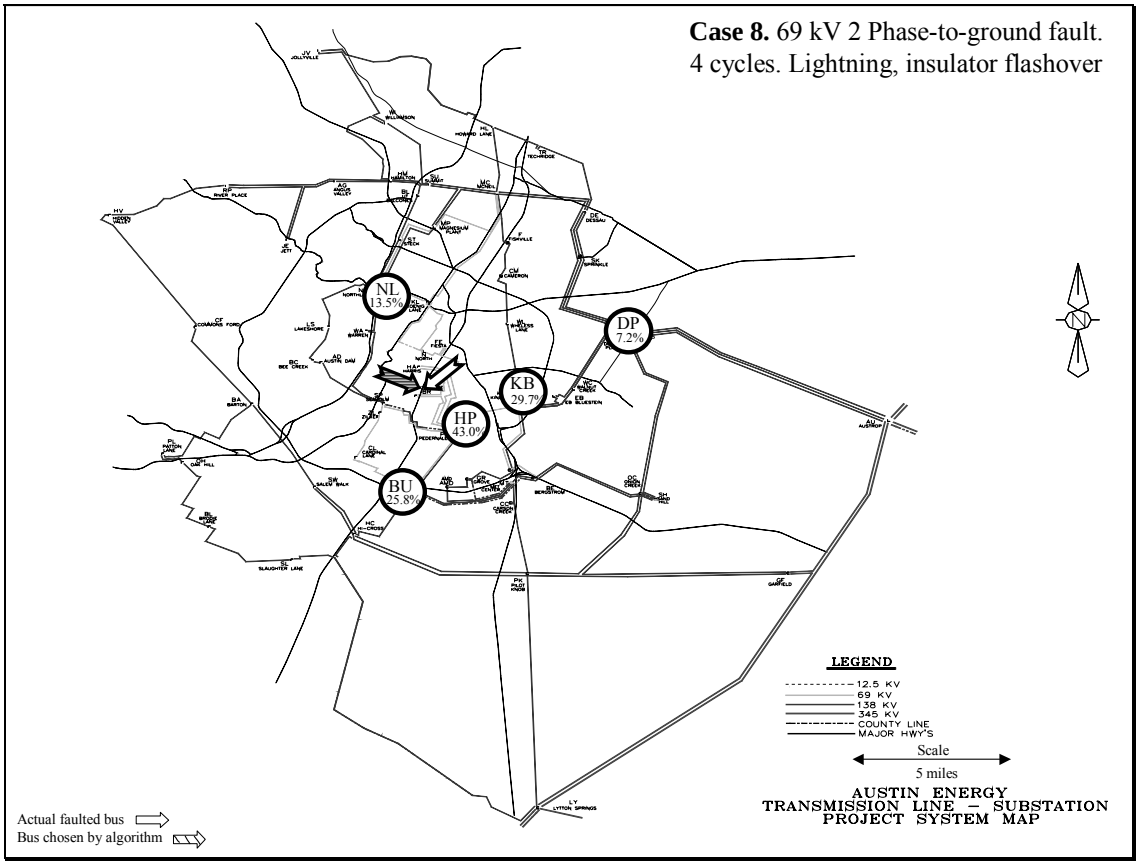

Figure 3.19: Meter locations with actual and estimated fault location for Event 8

Event 9. CKT 975 Fault on 10/02/04 at 04:40:53

A fault occurred on CKT 975, Dessau (DE) to Tech Ridge (TR) substation, on 10/02/04 at 04:40:53 during a thunderstorm. This is a 138 kV transmission line located in the north part of the City. All the digital fault recorders in the system initiated and recorded events for this fault and showed an a phase to b phase to ground fault. Additionally, microprocessor relays at BU and OC substations picked up for this event with similar information. Other electromechanical relays in the system indicated the correct faulted phase.

The data from five meter locations for this case included: DFR at MC showed a 62.4% voltage sag, at NL a 52.2% voltage sag, DP showed a 46.8%, at AU a 38.2%, and at LY a 26.9% sag. The fault was estimated accurately at the actual location with data from the first two meters.

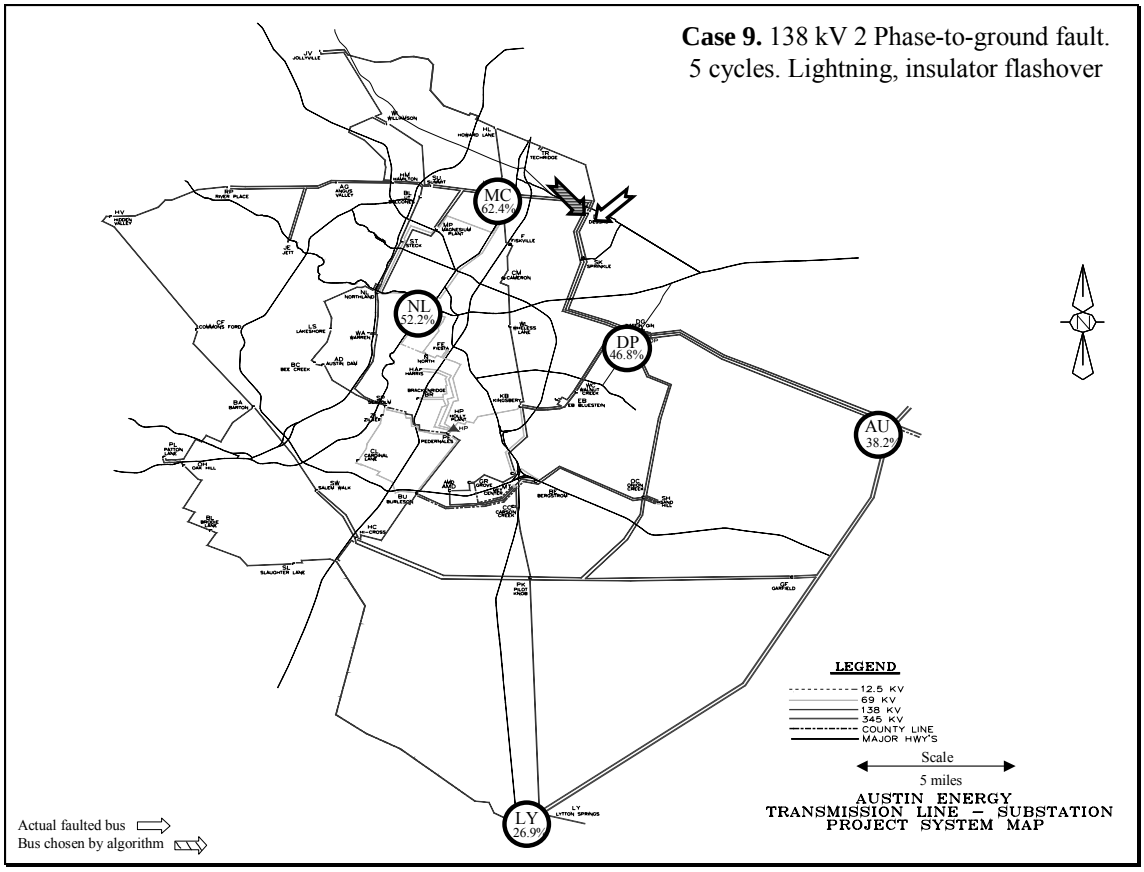

Figure 3.20: Meter locations with actual and estimated fault location for Event 9

Event 10. CKT 924 Fault on 07/07/05 at 20:30:31

A fault occurred on CKT 924, Onion Creek (OC) to Decker Plant (DP), on 07/07/05 at 20:30:31 during a thunderstorm. This is a 138 kV transmission line located in the east central part of the City of Austin. All the digital fault recorders in the system initiated and recorded events for this fault and showed a c phase to ground fault. The lightning strike broke the top insulator (c phase) into half, dropping the phase conductor onto the other two phases (a and the b phases) leading to a three-phase fault which will be described in the next event, Event 11. The DFRs on the system and the digital relays provided sufficient and clear fault data for the single-phase to ground and the three-phase fault portions of this event to be used for this case and the following case. Other electromechanical relays in the system indicated the correct faulted phase.

The data from five meter locations for this case included: a digital relay at SH showed a 48.9% voltage sag, at GR a 33.7% voltage sag, KB a 25.2%, a DFR at LY indicated a 16.3% and a digital relay at LP showed a 8.0% sag. The fault was estimated accurately at the actual location with data from the first two meters.

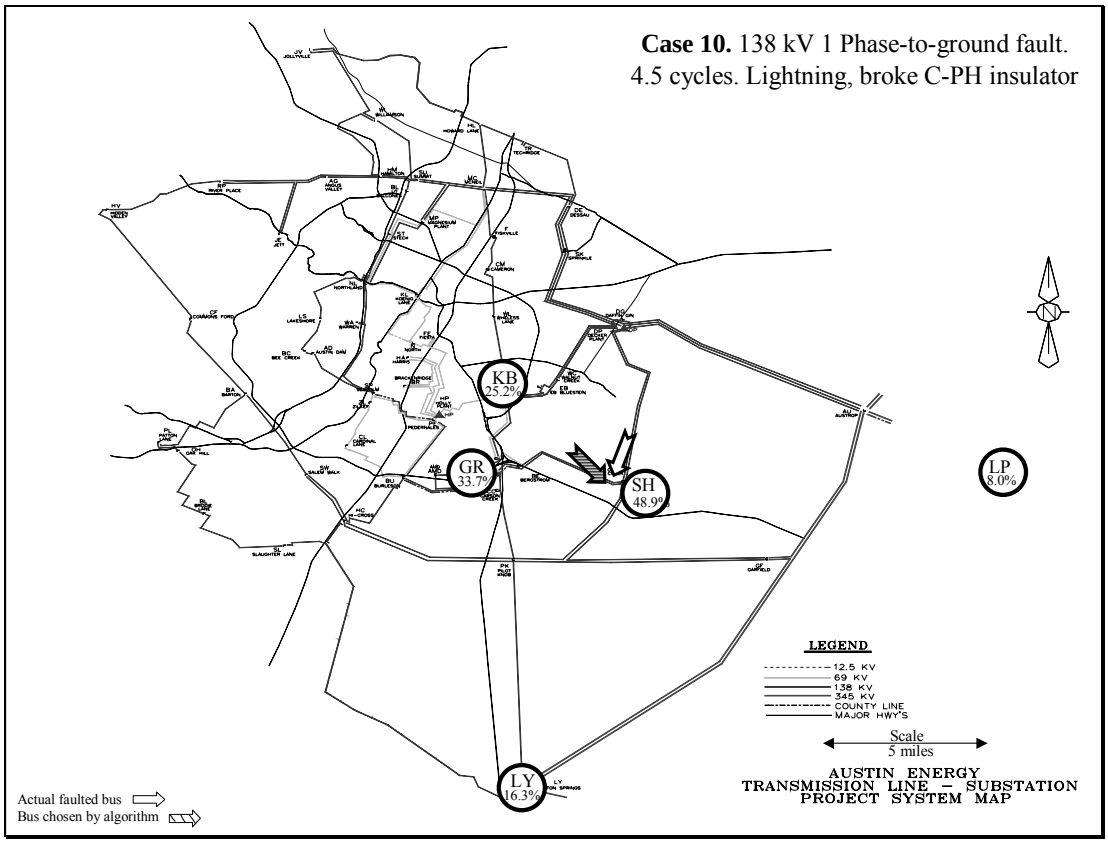

Figure 3.21: Meter locations with actual and estimated fault location for Event 10

Event 11. CKT 924 Fault on 07/07/04 at 20:30:32 (3-phase fault part of Event 10)

The continuation of the c phase to ground operation in Event 10, led to a three-phase fault. All the digital fault recorders in the system initiated and recorded events for this three-phase fault part of the event. Other electromechanical relays in the system indicated the correct faulted phase.

The data from five meter locations for this case included: a digital relay at BE showed a 48.5% voltage sag, at BU a 40.9% voltage sag, GF a 34.9%, at DE a 27.1% and a DFR at AU recorded a 22.0% voltage sag. The fault was estimated accurately at the actual location with data from the first three meters.

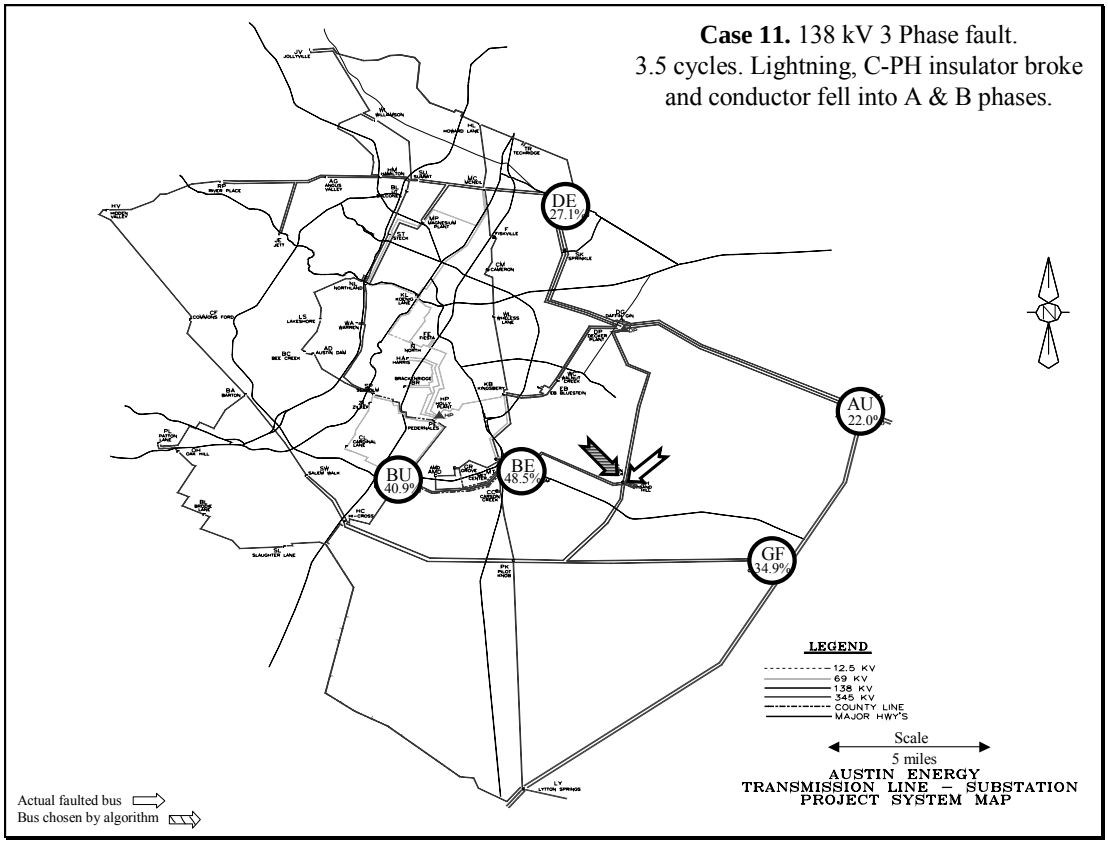

Figure 3.22: Meter locations with actual and estimated fault location for Event 11

Event 12: HL-456 Fault on 09/27/05 at 02:16:39

A fault occurred in HL-456 unit transformer at Howard Lane substation on 09/27/05 at 02:16:39 which caused the unit to catch on fire. This is a 138 kV substation located in north part of the City of Austin. All the digital fault recorders in the system initiated and recorded events for this fault and showed a b phase to ground fault. The fault evolved into a three-phase fault which will be described in the next event, Event 13. The DFRs on the system and the digital relays provided sufficient and clear fault data for the single-phase to ground and the three-phase fault portion of this even to be used for this case. Other electromechanical relays in the system indicated the correct faulted phase.

The data from five meter locations for this case included: a digital relay at SU showed a 58.7% voltage sag, at DG a 37.7% voltage sag, DFR at NL recorded a 35.8%, a digital relay at OC a 21.6%, and a DFR at AU showed a 18.5% voltage sag. The fault was estimated accurately at the actual location with data from the first three meters.

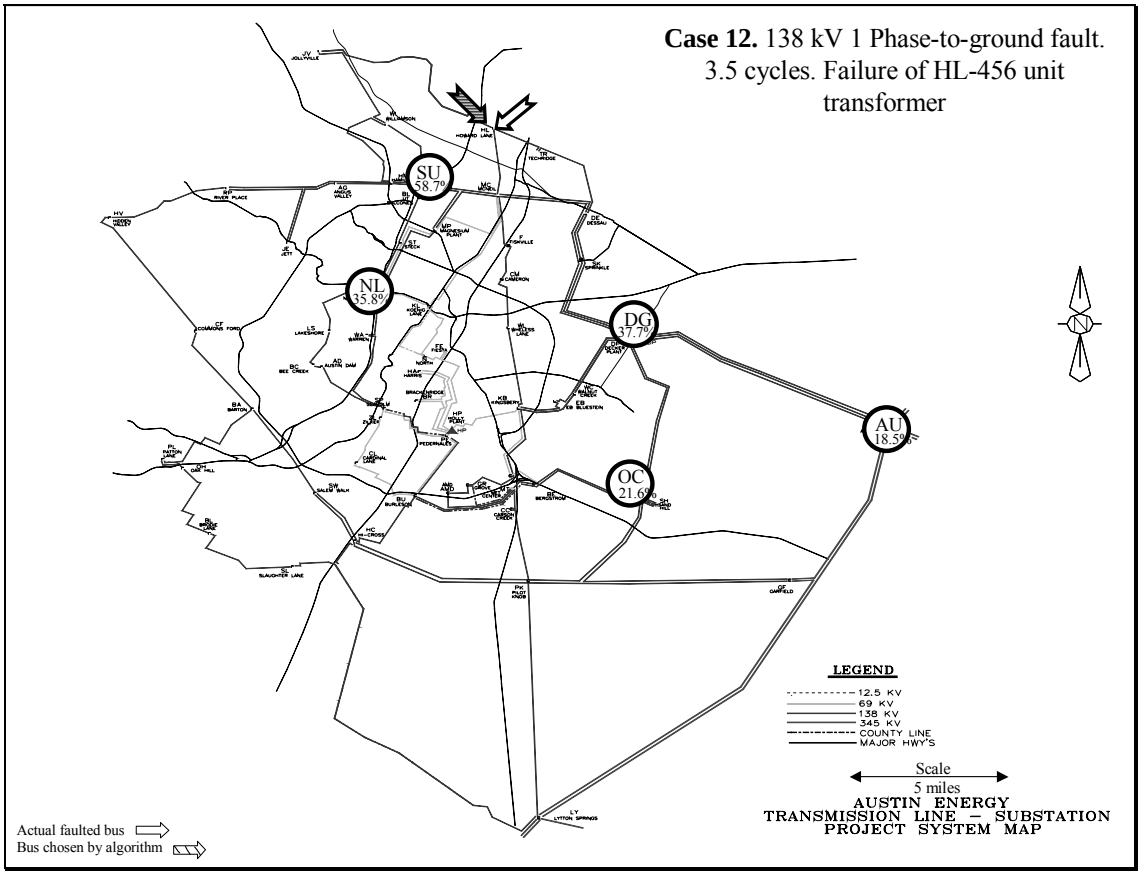

Figure 3.23: Meter locations with actual and estimated fault location for Event 12

Event 13. HL-456 Fault on 09/27/05 at 02:16:39 (3-phase fault part of Event 12)

The continuation of the a phase to ground operation in Event 12, led to a three-phase fault. All the digital fault recorders in the system initiated and recorded events for this three-phase fault part of this event. Other electromechanical relays in the system indicated the correct faulted phase.

The data from five meter locations for this case included: a digital relay at SU showed a 66.1% voltage sag, at DG a 57.6% sag, a DFR at NL recorded a 54.4%, a digital relay at OC recorded a 42.9% and a DFR at AU recorded a 36.2% voltage sag. The fault was estimated accurately at the actual location with data from the first two meters.

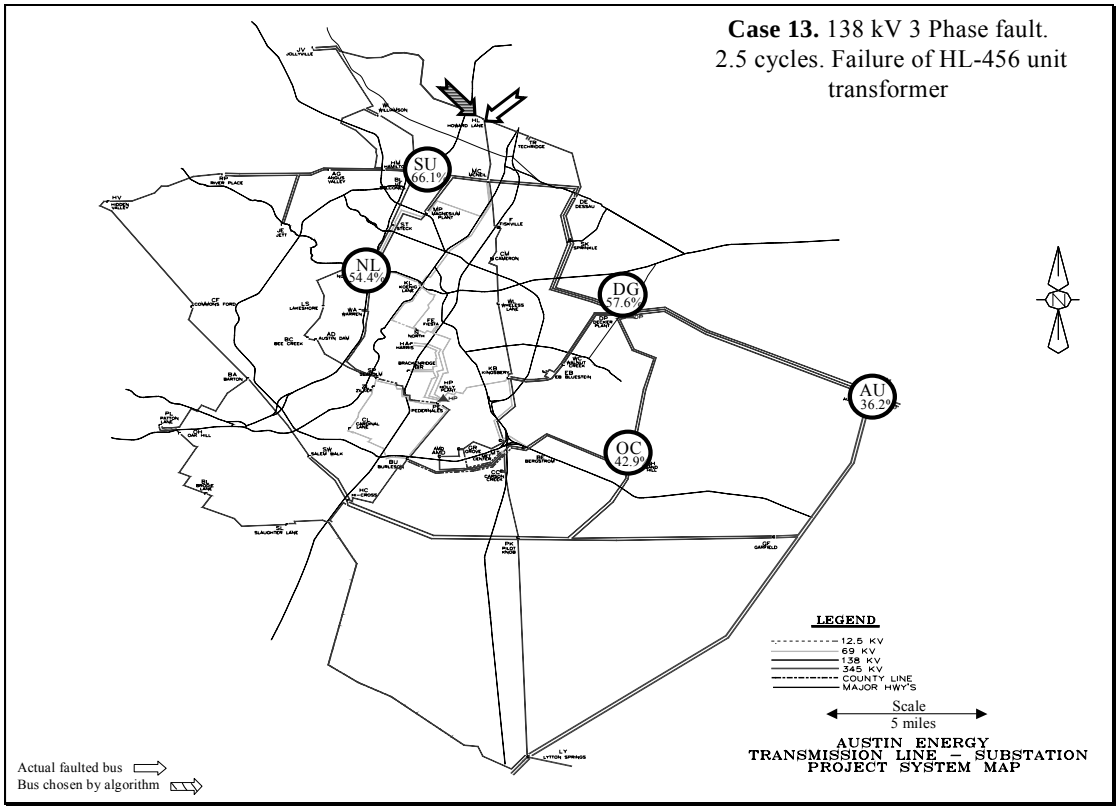

Figure 3.24: Meter locations with actual and estimated fault location for Event 13

Event 14. CKT 974 Fault on 10/27/2005 at 10:22:46

A fault occurred on CKT 974, Daffin Gin (DG) to Austrop (AU) substation, on 10/27/2005 at 10:22:46 when a buzzard contacted the a-phase of the circuit. This is a 138 kV transmission line located about northeast part of the City. All the digital fault recorders in the system initiated and recorded events for this fault and showed an a phase to ground fault. Additionally, the microprocessor relays at MP and OC substations picked up for this event with similar information. Other electromechanical relays in the system indicated the correct faulted phase.

The data from five meter locations for this case included: DFR at DP showed a 34.5% voltage sag, MC showed a 33.6% voltage sag, digital relay at MP recorded a 29.1%, BU indicated a 19.5%, and DFR data at LY indicated a 11.8% voltage sag. The fault was estimated accurately at the actual location with data from the first four meters when alpha was 1.00 and with data from the first three meters when the alpha was equal 0.99.

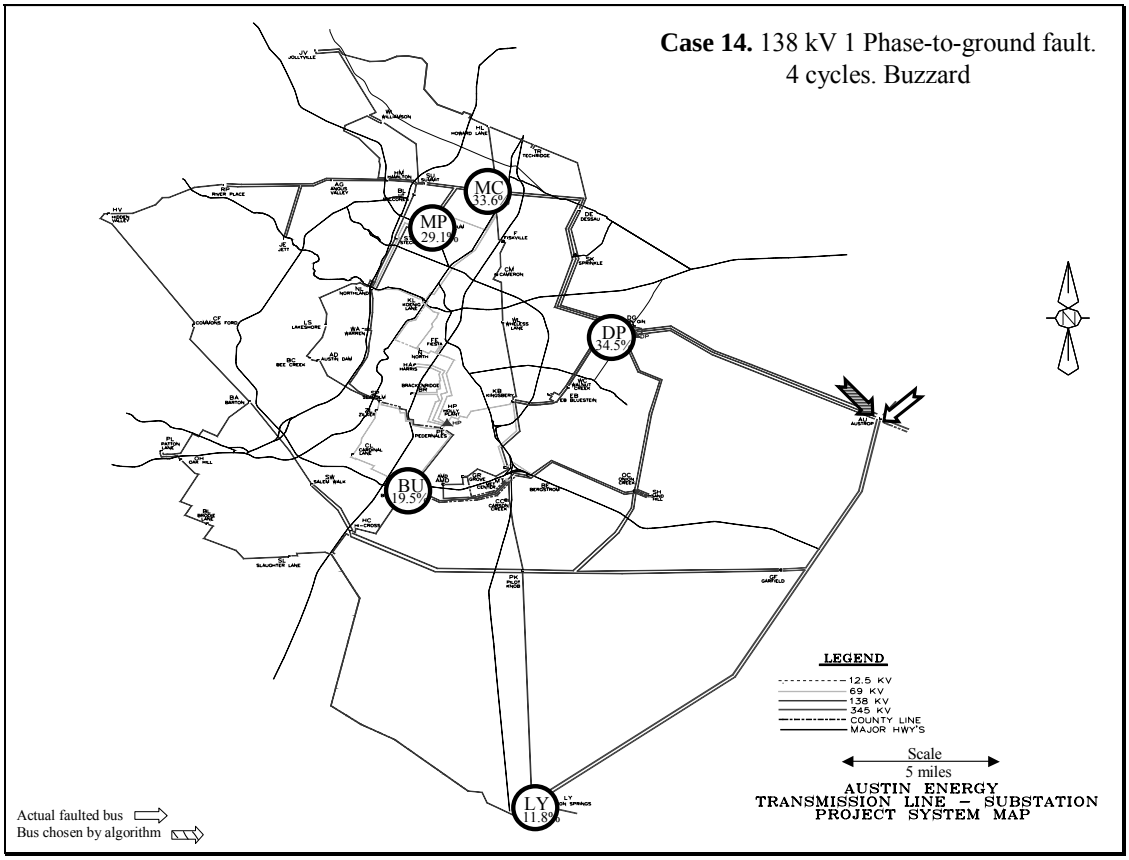

Figure 3.25: Meter locations with actual and estimated fault location for Event 14

Event 15. CKT 979 Fault on 03/25/2005 at 23:19:03

A fault occurred on CKT 979, Magnesium Plant (MP) to Northland (NL) substation, on 03/25/2005 at 23:19:03 when a buzzard contacted the c phase of the circuit. This is a 138 kV transmission line located about north-central part of the city. All the digital fault recorders in the system initiated and recorded events for this fault and showed a c-phase to ground fault. Additionally, microprocessor relays at RP and BU substations picked up for this event with similar information. Other electromechanical relays in the system indicated the correct faulted phase.

The data from five meter locations for this case included: Digital relay at RP showed a 50.2% voltage sag, DFR at MC showed a 46.9% voltage sag, digital relay at DG showed a 27.6%, KB indicated a 18.7%, and at PE a 16.8% voltage sag. The fault was estimated accurately at the actual location with data from the first two meters.

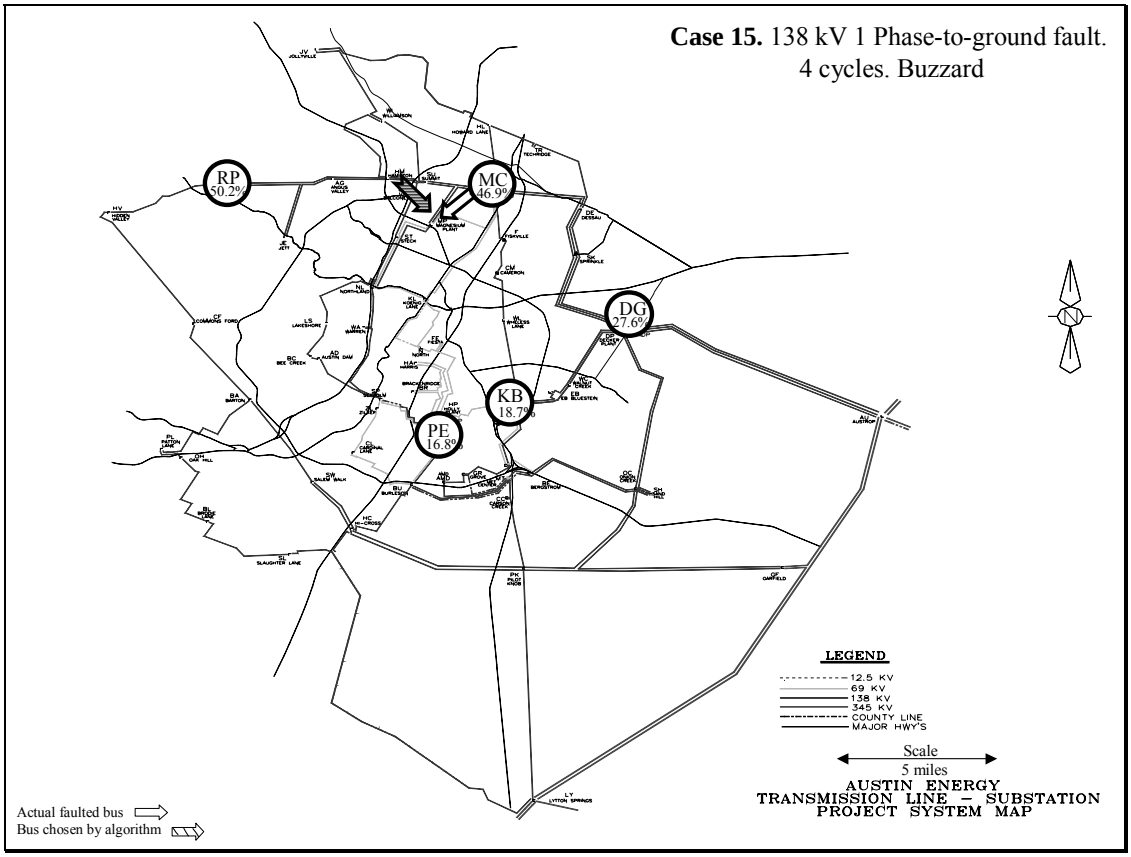

Figure 3.26: Meter locations with actual and estimated fault location for Event 15

3.7 Results

We have tested our procedure using 15 actual fault cases where the fault locations are known. For each case we have five meters. Not all cases have the same five meters because the faults occurred in different parts of the city. Depending on their threshold setting, remote meters may not respond to a fault. The meters and the voltage sag values which were used for each case are given in Table 3.3. All the voltage sag values shown in the table are in per unit.

Eight of the cases are single-phase to ground faults, three cases are three-phase faults, two cases are phase-phase faults, and two cases are phase-phase to ground faults. The meters were either fault recorders or microprocessor relays.

For each case we tested the algorithm's performance using two, three, four, and five meters. The meters are chosen in order of the depth of sag seen at their locations, so that the "Two Meters" test contains the meter with the deepest sag, and the meter with the next deepest sag measurement, and so on.

All of the results in Table 3.4 were computed by assuming that the fault current at each candidate bus was the maximum predicted available fault current at that bus ($\alpha = 1$). This assumption can actually be viewed as the product of two separate assumptions. First, we assume that our impedance matrix is correct; that is, the maximum predicted available fault current is actually the true maximum available fault current. Secondly, we assume that the fault impedance is zero, or conversely that the fault current was equal to the maximum available fault current. Any non-zero values of fault impedance in reality will

result in lower fault currents. In later chapters we will explore the effects of relaxing these two assumptions by allowing the fault current to deviate from the predicted maximum.

Case	Fault Type	Meter 1	Meter 2	Meter 3	Meter 4	Meter 5
1	1PH	FI – 0.572	HP – 0.250	MP – 0.178	MC – 0.135	DP – 0.094
2	1PH	MC – 0.596	NL – 0.480	DP – 0.400	AU – 0.261	KB – 0.252
3	3PH	RP – 0.438	BU – 0.343	OH – 0.314	AU – 0.257	LY – 0.215
4	1PH	BA – 0.798	HC – 0.650	BL – 0.599	BU – 0.402	OC – 0.245
5	1PH	NL – 0.502	FI – 0.235	GR – 0.200	DP – 0.119	AU – 0.076
6	2PH	BU – 0.427	MT – 0.403	LY – 0.356	MC – 0.300	AU – 0.246
7	2PH	BU – 0.313	KB – 0.250	NL – 0.229	HP – 0.206	MC – 0.186
8	2PHG	HP – 0.430	KB – 0.297	BU – 0.258	NL – 0.135	DP – 0.072
9	2PHG	MC – 0.624	NL – 0.522	DP – 0.468	AU – 0.382	LY – 0.269
10	1PH	SH – 0.489	GR – 0.337	KB – 0.252	LY – 0.163	LP – 0.080
11	3PH	BE – 0.485	BU – 0.409	GF – 0.349	DE – 0.271	AU – 0.220
12	1PH	SU – 0.587	DG – 0.377	NL – 0.358	OC – 0.216	AU – 0.185
13	3PH	SU – 0.661	DG – 0.576	NL – 0.544	OC – 0.429	AU – 0.362
14	1PH	DP – 0.345	MC – 0.336	MP – 0.291	BU – 0.195	LY – 0.118
15	1PH	RP – 0.502	MC – 0.469	DG – 0.276	KB – 0.187	PE – 0.168

Table 3.3: The meters and voltage sag values (in per unit)

The least-squared errors and bus candidate rankings are shown in Table 3.4. The values in this table can be interpreted as follows: for example, in Case 6, with two meters, the "winning" bus chosen by the algorithm had a least-squared error of 22.41, and the "actual" faulted bus was the 1st choice with squared error 20.06. With two meters, the method did not choose the "actual" faulted bus as the most likely candidate, but rather as the third most likely. With the third through the fifth meters, the "actual" bus was the first choice.

In application of this methodology, seven of the 15 studied cases estimated the fault at the exact actual location with the second meter data, five additional with the third meter data, one with fourth meter data, and two cases estimated the fault at one bus away from the actual fault location. It is possible that the error here, though insignificant, is due to the fact that the fault was near the system boundary where the remainder of the ERCOT system is equivalenced as discussed later. Overall performance indicates that in most situations, two voltage monitors can accurately locate a fault in a system the size of Austin Energy. Three monitors gave almost perfect results.

In Cases 2 and 5 the actual fault location was one bus away from the location chosen by the algorithm with data from five meters. Analysis indicates that this is most likely due to inaccuracies in the impedance/admittance matrices introduced by equivalencing the non-Austin Energy parts of the system. Equivalencing is a process of cutting away the non-studied portions of the 5000 bus ERCOT grid so that the impedance matrix for the study area is not prohibitively large. Errors are introduced during equivalencing, especially at the boundary of the retained area. In our case, there were 118

retained buses out of 5000 ERCOT buses. The equivalencing procedure was performed on the static fault study base case provided to ERCOT independently by the various utilities in the ERCOT grid. Hence, it is unable to capture all the changes in the ERCOT grid. Many of these changes would modify the impedance matrix of the grid, such as whether lines were switched in or out, or whether a generator was on or off line. It is virtually certain that the conditions at any given time will differ to some degree from the static ERCOT base case.

While we can adjust the impedance matrix for changes inside the Austin Energy system, of which we have complete knowledge, it is impractical to make changes in the model of the surrounding utilities, particularly after they have been equivalenced. Hence, the system model near the edges of the Austin Energy system will have some inaccuracies, and will cause difficulties for the algorithm, as seen in the results of Cases 2 and 5.

In spite of errors brought about by uncertainties in the non-Austin Energy data and by equivalencing, the fault location procedure is proven through actual test cases to work extremely well. Only at the equivalence boundaries are there any errors, and they are not very significant.

	Two Meters		Three Meters		Four Meters		Five Meters	
Case	Rank and Error of Actual Faulted Bus	Error of Bus Chosen by Algorithm	Rank and Error of Actual Faulted Bus	Error of Bus Chosen by Algorithm	Rank and Error of Actual Faulted Bus	Error of Bus Chosen by Algorithm	Rank and Error of Actual Faulted Bus	Error of Bus Chosen by Algorithm
1	1/107.77	107.77	1/107.77	107.77	1/109.80	109.80	1/119.45	119.45
2*	12/116.06	20.34	10/256.70	132.56	7/260.93	167.00	7/267.52	170.01
3	1/0.123	0.123	1/0.68	0.684	1/1.029	1.029	1/4.84	4.84
4	1/174.66	174.66	1/242.42	242.42	1/310.58	310.58	1/364.61	364.61
5*	6/7.90	0.0844	4/8.47	4.21	2/8.50	4.80	2/9.76	5.51
6	3/22.41	20.06	1/28.21	28.21	1/39.17	39.17	1/36.71	36.71
7	10/26.58	2.90	1/27.45	27.45	1/39.65	39.65	1/63.92	63.92
8	5/153.81	54.68	1/175.72	175.72	1/194.49	194.49	1/195.68	195.68
9	1/5.12	5.12	1/37.68	37.68	1/49.61	49.61	1/88.29	88.29
10	1/4.98	4.98	1/18.61	18.61	1/19.62	19.62	1/24.39	24.39
11	8/14.25	0.00	1/48.16	48.16	1/50.55	50.55	1/51.25	51.25
12	5/22.16	0.01	1/51.24	51.24	1/73.04	73.04	1/73.05	73.05
13	1/9.18	9.18	1/9.60	9.60	1/64.18	64.18	1/74.72	74.72
14	4/93.30	63.34	2/113.89	104.26	1/114.57	114.57	1/151.86	151.86
15	1/4.77	4.77	1/4.89	4.89	1/4.90	4.90	1/5.41	5.41

Table 3.4: The bus rankings and least-squared errors for all events with $\alpha = 1$

* The estimated fault location was one bus away from the actual fault location. This is due to equivalencing as the faulted bus is on the boundary of AE's system located at a jointly owned substation with the neighbouring utility.

3.8 Enhancements to Consider Fault Impedance and Impedance Matrix Uncertainties in Phase-Phase and Phase-Phase to Ground Faults

In the methodology, thus far, the fault impedance Z_f has been assumed to be zero. However in a real system fault condition, there is always some fault impedance depending on the cause of the fault. The assumption of $Z_f = 0$ causes the simulated fault current to be larger than the actual fault current. The application of a scaling factor, alpha, to compensate for uncertainly in the Z_f value and also in system impedance is therefore prudent.

The optimal alpha is found by sweeping alpha through a range of 0.5 to 2.00 and identifying the alpha value that gives the minimum error. When the best alpha is smaller than one, this means that the actual fault had a larger impedance value than the previously assumed zero. When the best alpha is greater than one, this means that there is uncertainty in the impedance matrix elements, for example if the fault is close to a generation plant, or near the border of the system close to an equivalenced bus.

Table 3.5 below summarizes the least-squared error values when the algorithm estimates the fault location by using only first three meters of data. As it is shown for alpha fixed at 1, the exact fault location was estimated in 12 cases. With least-squared error value when alpha is modified for each case, the exact fault location was estimated in 13 cases.

For the least value of the error squared value, the alpha for all cases are close to the desired 1, however, Case 8 showed almost twice as this value of 1.95. One possible reason is that the fault was next to a generation bus at Holly power plant. Another possible reason

for this is that the available meter data were far away from the actual fault location and the closest meter location data was 42.3%.

Case	Fault Type	Estimated fault location from actual with Alpha ≤1	Best Alpha	Estimated fault location using best Alpha	Least-squared error using best Alpha
1	1PH	Exact	0.98	Exact	105.98
2	1PH	One bus away	1.22	One bus away	42.77
3	3PH	Exact	0.99	Exact	0.44
4	1PH	Exact	1.17	Exact	101.65
5	1PH	One bus away	1.01	One bus away	4.01
6	2PH	Exact	1.02	Exact	4.48
7	2PH	Exact	1.00	Exact	27.45
8	2PHG	Exact	1.95	Exact	8.51
9	2PHG	Exact	1.28	Exact	19.47
10	1PH	Exact	1.00	Exact	18.61
11	3PH	Exact	1.01	Exact	48.10
12	1PH	Exact	1.09	Exact	25.82
13	3PH	Exact	0.97	Exact	4.89
14	1PH	One bus away	0.83	Exact	65.64
15	1PH	Exact	1.03	Exact	2.25

Table 3.5: Fault location found with and without modifying alpha with data from the first three meters

3.9 Goodness of the Best Choice

To analyze and evaluate the strength of the first choice selected by the algorithm described in this chapter, we compare the least-squared value of the first choice with the least-squared value of the second best choice. Another comparison is made by comparing the least-squared value of the first choice with the average of the second through the fifth choices of the algorithm. The logical conclusion is that large error gaps between the "winner" and the others indicates a stronger "winner".

To demonstrate this hypothesis, Table 3.6 below shows the error-squared values of the top five selections by the algorithm for 3, 4, and 5 meters for one of the studied cases (Section 3.6, Case 3). By looking at the least-squared values and the ratios for each meter in this case, the strongest winner is the first selection of the fault location with the 4th meter. This ratio of 0.063 indicates the first estimated location of Fiskville bus to be a winner and the strongest case amongst all five selections.

Estimated Location		**3 meters**		**4 meters**		**5 meters**
		Err^2		**Err^2**		**Err^2**
1	FISKVILL	0.683	FISKVILL	1.029	FISKVILL	4.836
2	DESSAU	1.368	HOWARD	16.263	TECHRID	23.207
3	SPRINKLE	1.612	HL 138	16.272	HOWARD	23.821
4	NORTHLN	6.082	TECHRID	16.708	HL 138	23.838
5	TECHRID	9.696	MCNEIL	17.965	MCNEIL	26.715
Ratio rows 1:2 selection		0.499		0.063		0.208
Ratio row 1:Avg. of 4		0.145		0.061		0.198

Table 3.6: Evaluation of the best choice by the algorithm for Case 3

Table 3.7 shows the ratio of the least-squared values of the first selection to the second and to the average of the next four selections for all of the 15 cases. The analysis below is for 3-meter case which provided the best estimation of the fault location for all 15 case studies in this work.

Most cases indicate a close ratio of the least-squared values between the first and the second selections. There are three principal reasons for a ratio of close to one of these two numbers. First, many of the studied fault cases were towards the middle of the line rather than on the bus and the algorithm selected both terminations of the faulted line as possible fault locations. Also, in some cases, the first and second buses were electrically identical, separated by only a breaker. Finally, in some cases the first and second buses chosen by the algorithm were electrically very close to each other. For example, in Cases 10 and 11 the two buses chosen as first and second are separated by a 0.22 mile long 138kV double circuit. In all three of these cases, a ratio of close to one should be seen as a validation of the technique. A low ratio indicates that none of the previous three situations exist, and the algorithm was easily able to choose the faulted bus. Amongst all cases, the results of the ratio in Case 3 with four meters showed the selection to be a solid bus fault and the algorithm indicated the strong evidence of the first choice to the second and the other four selections. The low ratio of 0.063 in Table 3.6 indicates a large gap between the first and the second selection by the algorithm. This is concluded from the ratio of the first to second and the first to the average of four other selections. The actual fault location was on a bus inside the Fiskville substation caused by a blown insulator.

In most cases the results and the conclusions drawn from the ratio of the least-squared value of the first location to the second is consistent with the ratio of the first to

the average of the other four selections. However, the latter ratio can also be analyzed separately to evaluate the relationship between the first selection by the algorithm compared to the other four selections. In most cases, the ratio showed that the algorithm selected the buses electrically close to the actual fault location.

The low ratio of the least-squared values of the first to the average of the other four selections in Case 10 also indicate a strong selection of the first choice by the algorithm compared to other four selections. However, this ratio for Case 2 and Case 12 indicates that the algorithm had difficulties in making distinction and separation between the first and the other four selections in these two cases. This is most likely due to the actual fault location being close to the boundaries of the system at the equivalence point.

Case Number, Ratio	Fault Type	Error^2 3 meters	Error^2 4 meters	Error^2 5 meters	Comments
Case 1 Ratio rows 1:2	1PH	0.580	0.561	0.548	A
Ratio 1:Avg. of 4		0.386	0.351	0.364	
Case 2 Ratio rows 1:2	1PH	0.993	0.989	0.987	OBA - 1st and 2nd were Howard Lane buses
Ratio 1:Avg. of 4		0.869	0.820	0.819	
Case 3 Ratio rows 1:2	3PH	0.499	0.063	0.208	BF
Ratio 1:Avg. of 4		0.145	0.061	0.198	
Case 4 Ratio rows 1:2	1PH	0.396	0.500	0.585	A
Ratio 1:Avg. of 4		0.324	0.363	0.405	
Case 5 Ratio rows 1:2	1PH	0.503	0.565	0.564	OBA
Ratio 1:Avg. of 4		0.503	0.493	0.491	
Case 6 Ratio rows 1:2	2PH	0.447	0.621	0.824	A
Ratio 1:Avg. of 4		0.366	0.498	0.705	
Case 7 Ratio rows 1:2	2PH	0.791	0.931	0.663	B
Ratio 1:Avg. of 4		0.566	0.703	0.618	
Case 8 Ratio rows 1:2	2PHG	0.841	0.531	0.529	A
Ratio 1:Avg. of 4		0.632	0.350	0.256	
Case 9 Ratio rows 1:2	2PHG	0.192	0.169	0.243	A
Ratio 1:Avg. of 4		0.147	0.152	0.232	
Case 10 Ratio rows 1:2	1PH	0.861	0.829	0.845	B
Ratio 1:Avg. of 4		0.060	0.050	0.062	
Case 11 Ratio rows 1:2	3PH	0.997	0.988	0.991	B
Ratio 1:Avg. of 4		0.596	0.450	0.430	
Case 12 Ratio rows 1:2	1PH	0.995	0.978	0.996	BF
Ratio 1:Avg. of 4		0.978	0.944	0.939	
Case 13 Ratio rows 1:2	3PH	0.971	0.994	0.994	BF
Ratio 1:Avg. of 4		0.232	0.597	0.587	
Case 14 Ratio rows 1:2	1PH	0.915	0.841	0.914	OBA – Worked fine with 4-meter case
Ratio 1:Avg. of 4		0.816	0.650	0.705	
Case 15 Ratio rows 1:2	1PH	0.829	0.615	0.441	A
Ratio 1:Avg. of 4		0.188	0.148	0.116	

Table 3.7: Evaluation of the best choices by the algorithm

OBA : One Bus Away. Equivalencing near boundary
BF: Bus Fault
Comments:
A: Between #1 and #2, closer to #1
B: Between #1 and #2, in the middle

Table 3.8 provides a summary of the evaluation of the ratio of the first to the second choice found by the algorithm in Table 3.7 above.

Ratio	Likely Interpretation
~1	Fault near middle of line Two identical buses Two buses electrically close
<0.2	Fault on/very near bus, bus far from other buses.

Table 3.8: Explanation of ratio significance in Table 3.7

Chapter 4: Extension of the Problem Formulation Using Voltage Monitors on Distribution System

The methodology described in the first phase of this dissertation utilizes system impedance matrices and a least-squared error minimization technique to estimate the fault location. This methodology would require measured voltage values at a few buses in the transmission system. The second phase of work in this chapter takes advantage of the capabilities of microprocessor relays on distribution feeders to reflect their voltage sag measurements back to the transmission system for use with the algorithm developed in phase one to estimate the fault location on transmission system.

In today's digital technology applications in the electric utility industry, in particular the application of microprocessor devices such as protection devices and relays at the distribution feeder levels, one can use the captured voltage quantities on the low side of a substation transformer for a fault on a transmission system, and transform the low side voltage to the high side, the transmission system. One popular microprocessor relay is Schweitzer Engineering Laboratory (SEL), which was mainly used as one of the meter data sources in this work. The transformed calculated high side voltage data then can be used as the measured voltage on the transmission level and used with the above algorithm described in the first phase to estimate the fault location on a transmission system. In essence, this chapter describes a method which utilizes the voltage data from the low side of the transformer on the distribution system to estimate a fault location on the transmission system.

Symmetrical components and the transformation matrix, as shown below, were applied to transform the voltage from the low to the high side of the substation transformers:

$$\tilde{V}_{abc} = T \bullet \tilde{V}_{012}, \quad and \quad \tilde{V}_{012} = T^{-1} \bullet \tilde{V}_{abc} \ ,$$

where transformation matrix T is

$$T = \begin{bmatrix} 1 & 1 & 1 \\ 1 & a^2 & a \\ 1 & a & a^2 \end{bmatrix}, \text{ and } T^{-1} = \frac{1}{3}\begin{bmatrix} 1 & 1 & 1 \\ 1 & a & a^2 \\ 1 & a^2 & a \end{bmatrix}.$$

If $\tilde{V}_{abc}$ represents a balanced set (that is, $\tilde{V}_b = \tilde{V}_a \bullet 1\angle -120^{\circ} = a^2\tilde{V}_a$, $\tilde{V}_c = \tilde{V}_a \bullet 1\angle +120^{\circ} = a\tilde{V}_a$), then substituting into $\tilde{V}_{012} = T^{-1} \bullet \tilde{V}_{abc}$ yields

$$\begin{bmatrix} \tilde{V}_{a0} \\ \tilde{V}_{a1} \\ \tilde{V}_{a2} \end{bmatrix} = \frac{1}{3}\begin{bmatrix} 1 & 1 & 1 \\ 1 & a & a^2 \\ 1 & a^2 & a \end{bmatrix}\begin{bmatrix} \tilde{V}_a \\ a^2\tilde{V}_a \\ a\tilde{V}_a \end{bmatrix} = \begin{bmatrix} 0 \\ \tilde{V}_a \\ 0 \end{bmatrix}.$$

Transforming a voltage sag from low side to high side depends on fault type. For a three-phase fault only the positive-sequence quantity needs to be transferred to the high side. Positive and negative-sequence values are calculated by the same methods for all fault types, but the zero-sequence calculations will be different. For a line-to-line fault type, only positive and the negative-sequence will be transferred. For line to ground and line to line to ground faults, all three, positive, negative, and zero-sequence quantities, must be transformed.

In this chapter, measured low and high side phasor and sequence elements relationships were verified. Then, mathematical worksheets for voltage transformation from the low side to high side for each fault type were developed. Finally actual events from the field were used to validate the developed theory.

4.1 Validation of the Measured Phasor and Sequence Elements

The template shown in Figure 4.1 was developed to calculate the high side voltage magnitude and angle when the low side voltage values are available. The measured phasor and the sequence elements on the low and high side for an event were separately tested to ensure that the transformation matrix was correctly used in the relay's internal logic and algorithm. The data for all fault types were tested using transformation matrix equations and the ABC012 program [27].

The template below was used to implement the arithmetic calculations for all fault types. The fundamental principals of transformer phase shift listed below were applied in the calculation of the low to high side voltage transformation.

- YY and Δ Δ transformers have no phase shift
- Three-wire connections (i.e., Δ and Ungrounded Y) have no zero-sequence currents
- Zero-sequence currents **can** flow on the Y side of a grounded-Y: Δ transformer
- High voltage side **positive-sequence** voltages and currents in Y:Δ (and Δ:Y) transformers **lead** those on the low-voltage side by 30º
- High voltage side **negative-sequence** voltages and currents in Y:Δ (and Δ:Y) transformers **lag** those on the low-voltage side by 30º

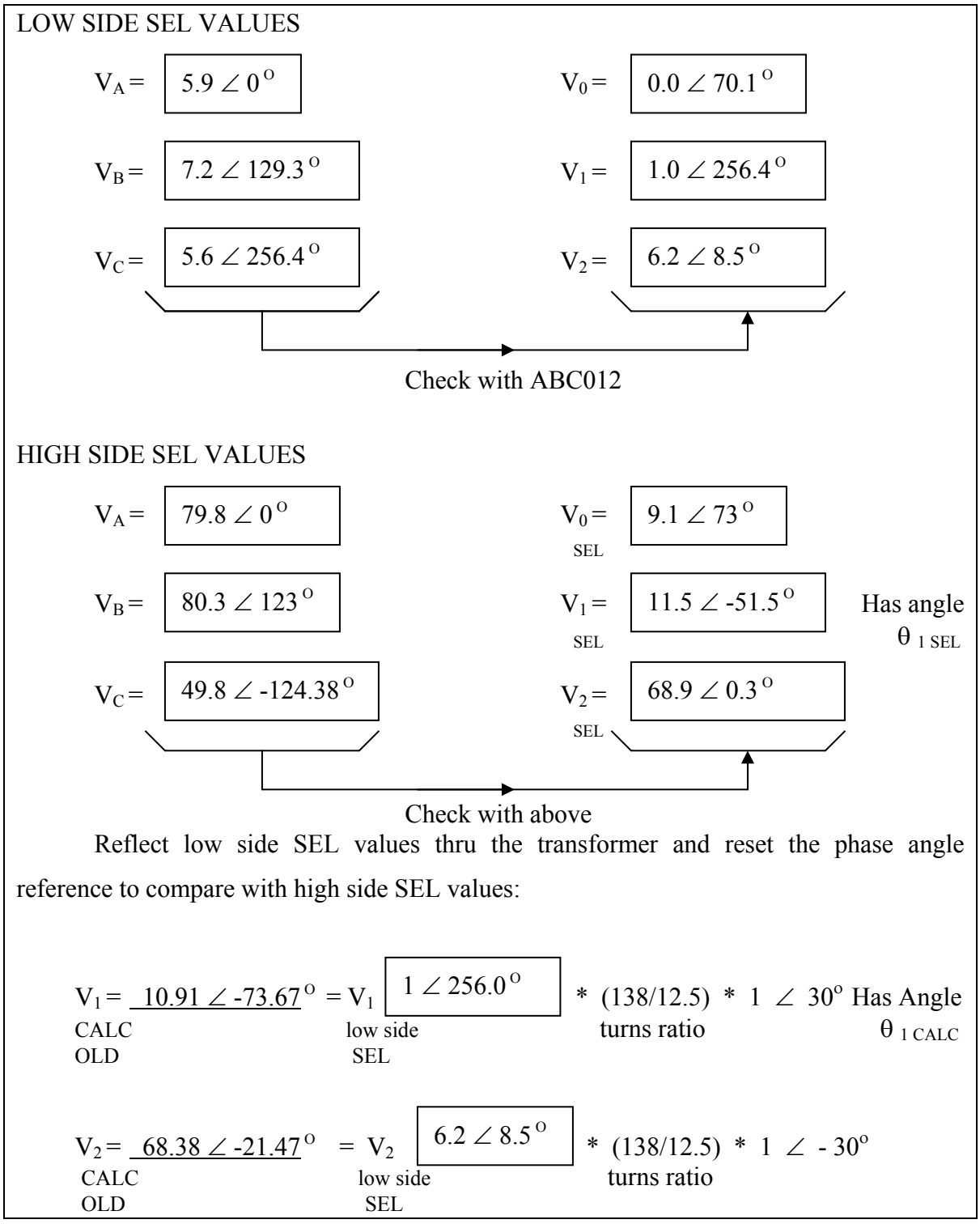

Figure 4.1: Template to calculate the high side voltage from the low side data

Correct the above for phase angle reference:

$$V_{1\,CALC\,NEW} = V_{1\,CALC\,OLD} \angle \theta_1 * 1 \angle (\theta_{1\,SEL} - \theta_{1\,CALC}) \quad (4.1)$$

$V_1 = 10.91 \angle -52^{O}$

Compare to $V_{1\,SEL}$ and $V_{2\,SEL}$

$$V_{2\,CALC\,NEW} = V_{2\,CALC\,OLD} \angle \theta_2 * 1 \angle (\theta_{1\,SEL} - \theta_{1\,CALC}) \quad (4.2)$$

$V_2 = 68.4 \angle 0.66^{O}$

Comparing the above results to SEL's measured V_1 and V_2 on the high side:

$V_1 = 11.5 \angle -51.5^{O}$

$V_2 = 68.9 \angle -0.30^{O}$

Figure 4.1: Continued, template to calculate the high side voltage from the low side data

4.2 Computing the Unobserved High Side Zero-Sequence Voltages

Once the positive and negative-sequence data on the high side are calculated from the low side data by using the above template, the following steps show the calculations for the V_0 component on the high side which is not observed on the low side of a delta-to-wye grounded transformer. The derivations for calculating V_0 depend on the fault type.

4.2.1 Balanced Three-Phase Faults

For a three-phase fault, there are no zero-sequence or negative-sequence components. The positive-sequence magnitude in per unit is the same on both sides of the transformer.

4.2.2 Single-Phase to Ground Faults

For phase a to ground fault at bus k and the meter location at bus j, we want to find $V_{j,a}^{0}$. From [6], the sequence components of phase a are:

$$V_{j,a}^{0} = -Z_{j,k}^{0} \frac{I_{k,a}^{F}}{3}$$

$$V_{j,a}^{+} = 1 - Z_{j,k}^{+} \frac{I_{k,a}^{F}}{3}$$

$$V_{j,a}^{-} = -Z_{j,k}^{+} \frac{I_{k,a}^{F}}{3}.$$

Taking a ratio of $V_{j,a}^{0}$ to $V_{j,a}^{-}$ yields

$$\frac{V_{J,a}^{0}}{V_{J,a}^{-}} = -\frac{Z_{J,k}^{0}}{Z_{J,k}^{+}},$$

so,

$$V_{j,a}^{0} = -V_{j,a}^{-}\frac{Z_{j,k}^{0}}{Z_{j,k}^{+}} \qquad (4.3)$$

A similar approach for phase c to ground fault:

$$V_{j,c}^{0} = -Z_{j,k}^{0}\frac{I_{k,c}^{F}}{3}$$
$$V_{j,c}^{+} = 1 - Z_{j,k}^{+}\frac{I_{k,c}^{F}}{3}$$
$$V_{j,c}^{-} = -Z_{j,k}^{+}\frac{I_{k,c}^{F}}{3},$$

yielding

$$V_{j,c}^{0} = +V_{j,c}^{-}\frac{Z_{j,k}^{0}}{Z_{j,k}^{+}}$$

Converting the above to phase a sequence components:

$$V_{j,a}^{0} = V_{j,b}^{0} = V_{j,c}^{0}$$

$$V_{j,b}^{+} = a^{2}V_{j,a}^{+}, \quad V_{j,b}^{-} = aV_{j,a}^{-}$$

$$V_{j,c}^{+} = aV_{j,a}^{+}, \quad V_{j,c}^{-} = a^{2}V_{j,a}^{-}.$$

So, when the sequence components for phase a are reported by an instrument (the usual case), the c phase zero-sequence component is calculated by:

$$\frac{Z_{j,k}^{0}}{Z_{j,k}^{+}} = \frac{V_{j,c}^{0}}{V_{j,c}^{-}} = \frac{V_{j,a}^{0}}{a^{2}V_{j,a}^{-}} = \frac{V_{j,a}^{0}}{V_{j,a}^{-}}a ,$$

yielding

$$V_{j,c}^{0} = aV_{j,c}^{-}\frac{V_{j,a}^{0}}{V_{j,a}^{-}} .$$

Similarly, if the fault is on phase b,

$$\frac{Z_{j,k}^{0}}{Z_{j,k}^{+}} = \frac{V_{j,b}^{0}}{V_{j,b}^{-}} = \frac{V_{j,a}^{0}}{a\,V_{j,a}^{-}} = a^{2}\frac{V_{j,a}^{0}}{V_{j,a}^{-}} ,$$

yielding

$$V_{j,b}^{0} = a^{2}V_{j,b}^{-}\frac{V_{j,a}^{0}}{V_{j,a}^{-}} . \qquad (4.4)$$

For the previous example using the template above, since the fault is a c phase to ground fault, by using (4.3) the magnitude and the phase angle for zero-sequence voltage is calculated by:

$$V_0\angle\theta_0 = V_{1new}\bullet\frac{Z_{j,k}^{0}}{Z_{j,k}^{-}}\angle\theta_{1new} + 120^{\mathrm{O}} = 10.9\bullet 0.96\angle(-51.54+120)^{o}$$

$$V_0\angle\theta = 10.47\angle 68.46^{\mathrm{O}}.$$

This result is close to the SEL's measured high side zero-sequence voltage of 9.1 $\angle$ 73.0^{o}.

4.2.3 Phase-Phase Faults

This fault type has no zero-sequence component. Therefore, no calculation is needed.

4.2.4 Phase-Phase to Ground Faults

For phase-phase to ground fault type, using Equation (2.21) in Chapter 2 for a fault at bus k and meter location at bus j, the sequence component currents are:

$$I_{k,a}^{+} = \frac{1}{Z_{\mathrm{k,k}}^{+} + \dfrac{Z_{k,k}^{-} Z_{k,k}^{0}}{Z_{k,k}^{-} + Z_{k,k}^{0}}}$$

$$I_{k,a}^{-} = -\left[\frac{1 - I_{k,a}^{+} Z_{k,k}^{+}}{Z_{k,k}^{-}}\right]$$

$$I_{k,a}^{0} = -\left[\frac{1 - I_{k,a}^{+} Z_{k,k}^{+}}{Z_{k,k}^{0}}\right].$$

Sequence voltages:

$$V_{j,a}^{0} = -Z_{j,k}^{0} I_{k,a}^{0}.$$
$$V_{j,a}^{+} = 1 - Z_{j,k}^{+} I_{k,a}^{+}.$$
$$V_{j,a}^{-} = -Z_{jk}^{-} I_{k,a}^{-}.$$

$$\frac{V_{j,a}^{0}}{V_{j,a}^{-}} = \frac{Z_{j,k}^{0} I_{k,a}^{0}}{Z_{j,k}^{-} I_{k,a}^{-}} = \frac{Z_{j,k}^{0}}{Z_{j,k}^{-}} \bullet \left[\frac{1 - I_{k,a}^{+} Z_{k,k}^{+}}{Z_{k,k}^{0}} \right] \left[\frac{1 - I_{k,a}^{+} Z_{k,k}^{+}}{Z_{k,k}^{-}} \right]$$

$$= \left(\frac{Z_{j,k}^{0}}{Z_{j,k}^{-}} \right) \bullet \left(\frac{Z_{k,k}^{-}}{Z_{k,k}^{0}} \right) \quad ,$$

yielding

$$V_{j,a}^{0} = V_{j,a}^{-} \left(\frac{Z_{j,k}^{0}}{Z_{j,k}^{-}} \right) \bullet \left(\frac{Z_{k,k}^{-}}{Z_{k,k}^{0}} \right) \quad . \qquad (4.5)$$

Chapter 5: Case Studies Using Voltage Monitors on Distribution System

Austin Energy's distribution system includes over 10,308 miles of overhead and underground distribution lines at 12.47 kV voltage level. Most of the protective relays are designed for protecting distribution circuits against faults on downstream of the feeder from the substation's distribution transformer. Presently, all relays are set with an overcurrent protection scheme, and almost none are set to initiate for voltage deviations. This is because there could be numerous voltage deviation conditions on the feeder or on the transmission system, and initiating events on distribution relays due to voltage deviations could easily fill the microprocessor relays' memory storage. However, in the future, widely applied microprocessor relays could be set to report voltage sags and provide many additional voltage monitoring points for the fault location problem. The difficulty of using them is that they are separated from the transmission system by a delta-wye transformer. The transformer modifies voltage waveforms and a correction procedure based on sequence components is needed.

To test the theoretical methodology described in Chapter 4, we use the fault data captured by the distribution feeders for an event on the transmission system, transform this low side voltage data to the high side of a substation transformer, and finally use the transformed voltage data on the high side to estimate a fault on the transmission system. To collect sufficient data on the low side of a transformer for a fault on the transmission system, we had to modify the settings of the distribution relays such that they would initiate voltage events for faults on the high side of the transformers. Relays on the distribution feeders at 17 various substations in Austin Energy's system were modified to initiate for 10% voltage deviations caused by a fault on transmission system.

5.1 Meter Data Verification and Calculations

Most microprocessor relays on distribution feeders have capability of generating phasor and sequence elements. Such data includes the magnitude and angle for all current and voltage values in phase and sequence formats. The data used for the low side is from SEL-351S-7 and for the high side from SEL-311C relays. Sample data for both types of relays are shown later in this chapter.

For validating the developed mathematical model and equations, we used actual captured voltage data where we had data from both sides of the transformer. First, the measured phasor and the sequence elements on the high and the low side of the substation transformer for an event (as shown below) were separately tested to ensure the transformation matrix was correctly used in the microprocessor relay's algorithm. This is necessary to ensure that the data from the relays used in this chapter is accurate. By using transformation matrix equations and the ABC012 program [27], the data for all fault types were tested. The result of the studies of these cases verified the accuracy of the relay's event data and its algorithm.

A sample of the recorded data on the high and the low side of substation transformer used in one of the events, (Case 3 described in Section 5.2) are shown below. The recorded data shows the phasor and sequence values with their magnitude and phase angle of the voltage and current displayed in text. These quantities can also be displayed in a graphic format.

Phasor and Sequence Elements

Relay/Terminal ID: SEL-351

Event date/time: Thursday, October 27, 2005 10:22:46.282000

Printed: 5/31/2006 2:59:40 PM

Event Report File= G:\Mehrdad 6-8-05\SEL5040 DATA\Archive\BU-456-351-LS 2005 10 27 10 2 2 46.282.eve

Cycles: 6.000

Reference Phase: A; Using Pre-fault Reference Angle

Channel	Mag	Angle	Scale	Show	Ref
IA	365.7	74.3	1	1	
IB	257.1	175.8	1	1	
IC	374.5	294.4	1	1	
IN	2.0	91.1	1	0	
IG	30.1	94.9	1	0	
VA	6.6	75.2	1	1	
VB	6.5	188.2	1	1	
VC	7.3	312.2	1	1	
VS	0.0	91.1	1	0	
Vdc	132.0	N/A	1	0	
Freq	59.9	N/A	1	0	
I0	10.0	94.9	1	1	
I1	75.1	135.9	1	1	
I2	328.0	62.0	1	1	
V0	0.0	0.0	1	1	1
V1	0.5	194.4	1	1	
V2	6.8	71.9	1	1	

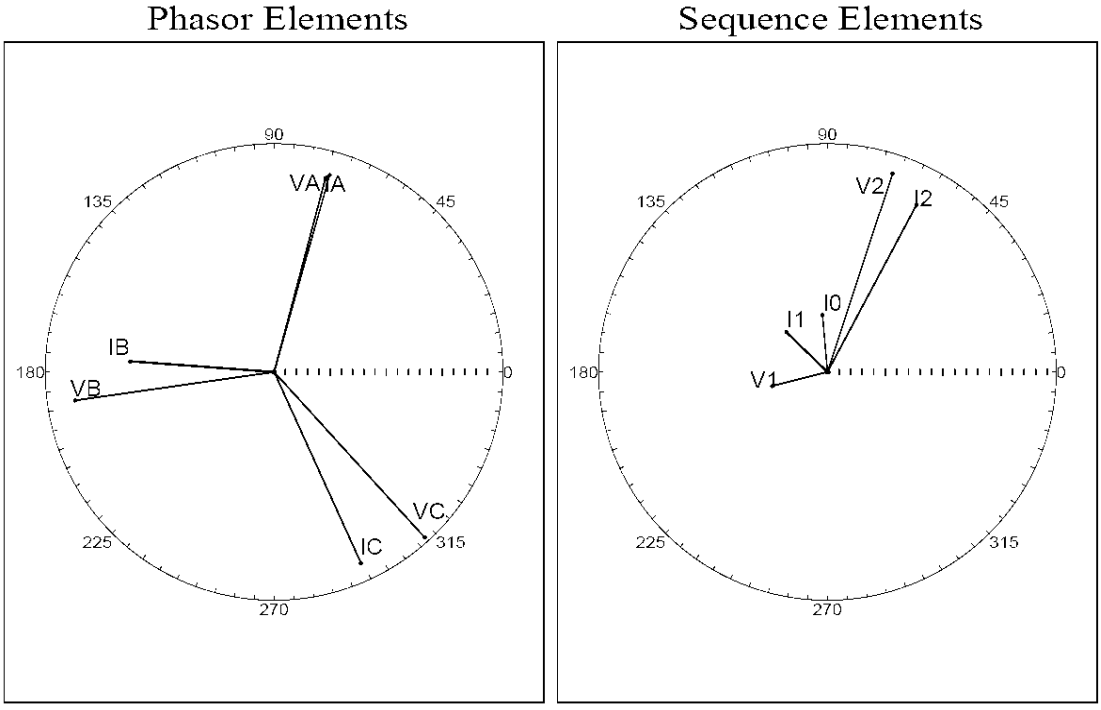

Figure 5.1: Measured data on low side of the substation transformer at BU for Case 3

Phasor and Sequence Elements

Relay/Terminal ID: SEL-311C 21/79 BKUP BU-1017

Event date/time: Thursday, October 27, 2005 10:22:46.288000

Printed: 6/1/2006 2:41:49 PM

Event Report File= G:\5040&5010_DATA\SEL5040\2005\Archive\BU-1017 21-79 311C 2005 10 27 10 22 46.288.eve

Cycles: 5.250
Reference Phase: A

Channel	Mag	Angle	Scale	Show	Ref
IA	1097.9	80.2	1	1	
IB	268.1	165.6	1	1	
IC	257.2	269.6	1	1	
IP	4.5	227.7	1	0	
IG	894.9	94.8	1	0	
VA	65.2	167.6	1	1	
VB	78.8	287.3	1	1	
VC	79.7	50.2	1	1	
VS	0.0	344.3	1	0	
I0	298.3	94.8	1	1	
I1	318.2	87.8	1	1	
I2	507.5	66.9	1	1	
V0	3.6	0.0	1	1	1
V1	5.9	350.4	1	1	
V2	74.6	168.4	1	1	

Phasor Elements

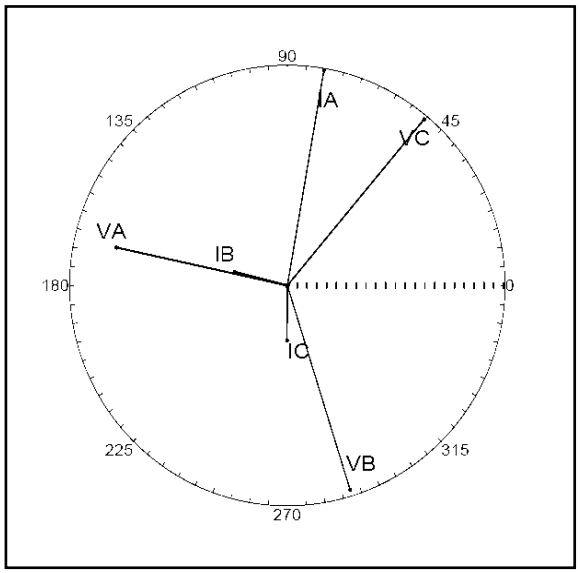

Sequence Elements

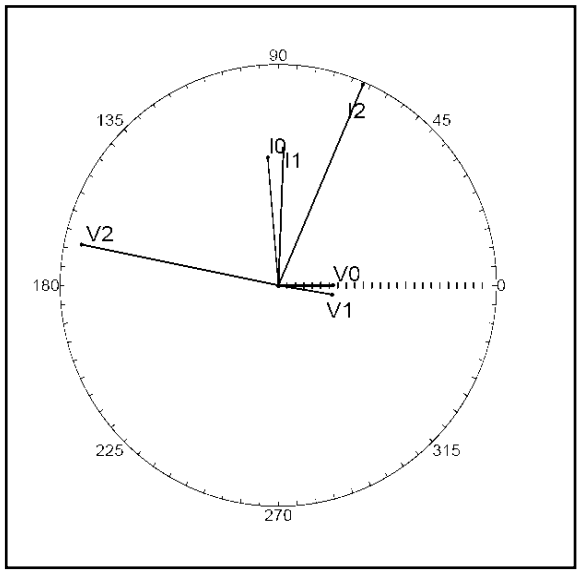

Figure 5.2: Measured data on high side of the substation transformer at BU for Case 3

A sample of the converted voltage sequence to phase components using ABC012 program is shown in Figure 5.3 below. The purpose of performing this step is to check the validity of the data in phase and sequence components on both, the high and the low side of a substation transformer recorded by the microprocessor relays. Phase or sequence voltage values can be inputted in either polar or rectangular and the program will display the converted data in all four formats. The program also allows up to 10 different tests to be stored for review and modifications.

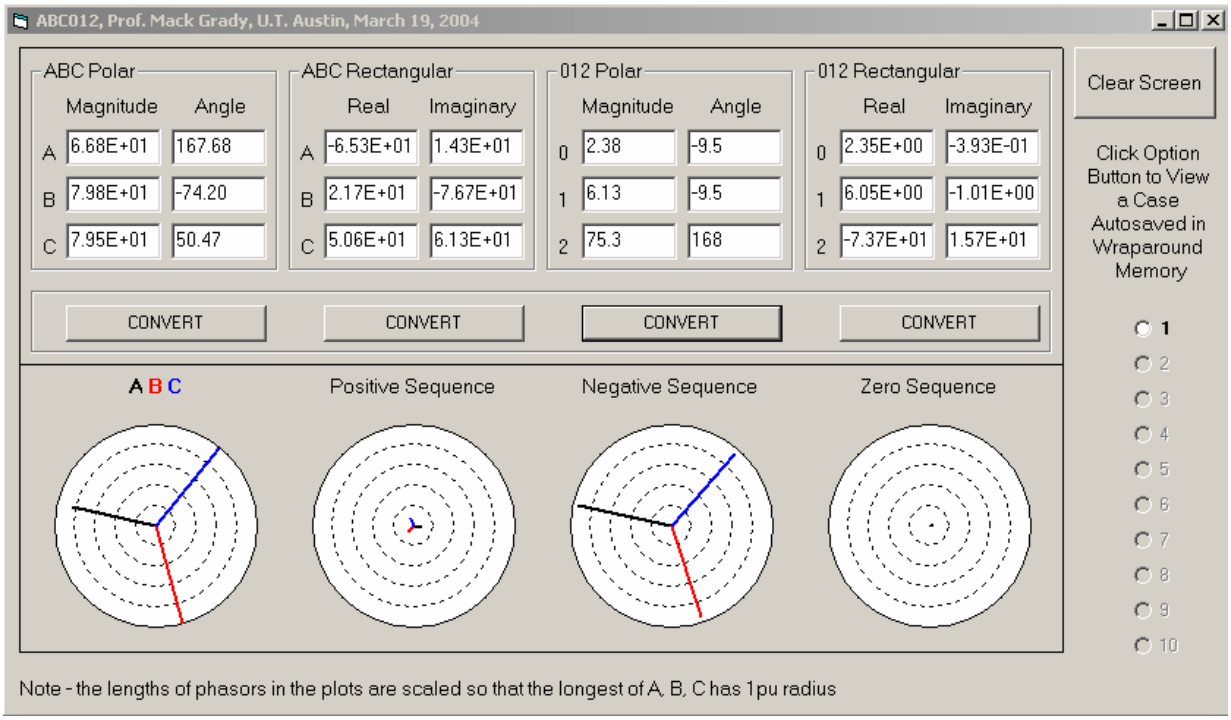

Figure 5.3: Voltage sequence to phase component conversion using ABC012

The data shown above is the actual analysis for the Event 3 described in Section 5.2 of the faulted phase a as an input, and the calculated phase values with their magnitude and phase angle by this program.

Table 5.1 below demonstrates the comparison of the phase voltage values on the high side resulted from the new algorithm in Chapter 1, ABC012 program in Figure 5.3, and the actual measured data by the SEL relay for this fault.

	Vabc calculated output		ABC012		Relay	
	Mag	Angle	Mag	Angle	Mag	Angle
Va	66.3	171.7	66.3	172.2	65.2	167.6
Vb	79.3	-69.6	79.3	-69.3	78.8	287.3
Vc	79.4	52.8	79.4	53.2	79.7	50.2

Table 5.1: Comparison of the calculated and the measured high side voltage values

5.2 Events

Seven actual faults were tested in this chapter to validate the theoretical techniques described in Chapter 4. All fault types: single-phase to ground, phase-phase, phase-phase to ground, and three-phase faults on 69kV and 138kV systems have been verified with the field data using the developed methodology. Due to the limited storage capacity of the relays on the distribution system, relays at 17 substations were modified to generate events for a fault on the transmission system which had caused voltage deviation at distribution level. These relays were set to initiate and capture voltage events when the voltage deviates by 10% from its normal value. The low side voltage data used for the seven cases in this section are for the faults used in Chapter 3.

The following describes the seven events with the data used from the distribution system. For each case, the tabulated results show the calculated voltage values using the above theory, their comparison with the actual measured data from the SEL relays, and the results of using ABC012 program. And finally the calculated high side voltage values are used as the meter data to estimate the fault on the transmission system as was described in Chapter 3.

Event 1: HL-456 Fault on 09/27/05 at 02:16:39 (Event 12 in Chapter 3)

This event was a b-phase to ground fault due to a transformer failure at HL substation. Using the template shown in Section 4.1, the fault data from the low side was transformed to high side of the substation transformer. The microprocessor relay on the low side of the distribution transformer at SU substation recorded voltage data for this fault. Microprocessor relay's phase and the sequence data, from the low and high side of transformer, were verified using the transformation matrix equations and the ABC012 program. Using the template the transformed voltage values on the high side were very close to the values recorded by the relay. Table 5.2 below shows the final phase voltage results at SU substation:

	Estimate of Trans. side Voltage Using Distribution side Relay Data		Measured Transmission Relay Data	
	Mag	Angle	Mag	Angle
Va	86.7	1.0	86.2	0.0
Vb	36.5	130.4	33.2	124.9
Vc	87.5	253.1	84.6	251.8

Table 5.2: Comparison of the calculated and the measured high side voltage for Event 1 at SU substation

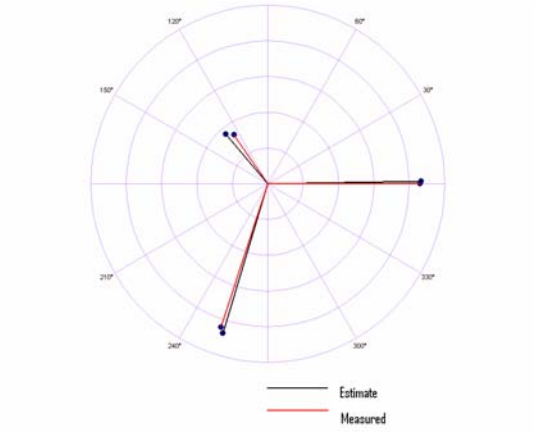

Figure 5.4: Visual comparison of the calculated and the measured high side voltage for Event 1 at SU substation

In this and some of the cases described below, the calculated phase angles showed to be negative numbers. However, the calculated would result in a close number to the measured value by the relay when added to 360 degrees. In this case the calculated c phase showed –106.9 degree and when added to 360 resulted in 251.8 degrees which is very close to the number measured by the relay.

Event 2: CKT 929 Fault on 9/11/2005 at 6:58:25 (Event 4 in Chapter 3)

This event was an a phase to ground fault due to a buzzard contacting the phase conductor of the 138 kV transmission line. Using the template shown in Section 4.1, the fault data from the low side was transformed to high side of the substation transformer. The microprocessor relay on the low side of the distribution transformer at BA substation recorded voltage data for this fault. Using the template the transformed voltage values on the high side were very close to the values recorded by the relay. Table 5.3 below shows the final phase voltage results at BA substation:

	Estimate of Trans. side Voltage Using Distribution side Relay Data		Measured Transmission Relay Data	
	Mag	Angle	Mag	Angle
Va	17.9	- 4.3	16.3	0.0
Vb	92.5	147.9	91.5	143.5
Vc	95.6	243.6	89.2	241.5

Table 5.3: Comparison of the calculated and the measured high side voltage for Event 2 at BA substation

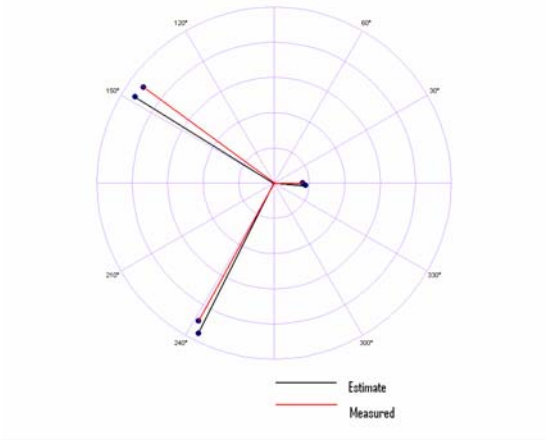

Figure 5.5: Visual comparison of the calculated and the measured high side voltage for Event 2 at BA substation

Event 3. CKT 974 Fault on 10/27/2005 at 10:22:46 (Event 14 in Chapter 3)

This event was an a phase to ground fault due to a buzzard contacting the phase conductor of this 138 kV transmission line. Using the template, the fault data from the low side was transformed to high side of the substation transformer. The microprocessor relay on the low side of the distribution transformer at two different locations: BU and OC substations recorded voltage data for this fault. Using the template the transformed voltage values on the high side were very close to the values recorded by the relay. Tables 5.4 and 5.5 below show the final phase voltage results at BU and OC substations:

	Estimate of Trans. side Voltage Using Distribution side Relay Data		Measured Transmission Relay Data	
	Mag	Angle	Mag	Angle
Va	66.3	171.7	65.2	167.6
Vb	79.3	290.4	78.8	287.3
Vc	79.4	52.8	79.7	50.2

Table 5.4: Comparison of the calculated and the measured high side voltage for Event 3 at BU substation

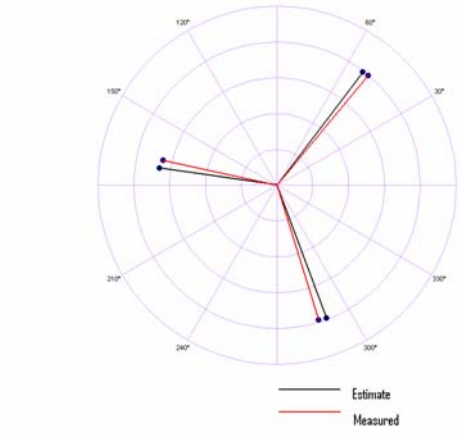

Figure 5.6: Visual comparison of the calculated and the measured high side voltage for Event 3 at BU substation

	Estimate of Trans. side Voltage Using Distribution side Relay Data		Measured Transmission Relay Data	
	Mag	Angle	Mag	Angle
Va	66.8	167.6	64.6	169.4
Vb	79.8	285.8	78.5	288.6
Vc	79.5	50.5	79.5	51.8

Table 5.5: Comparison of the calculated and the measured high side voltage for Event 3 at OC substation

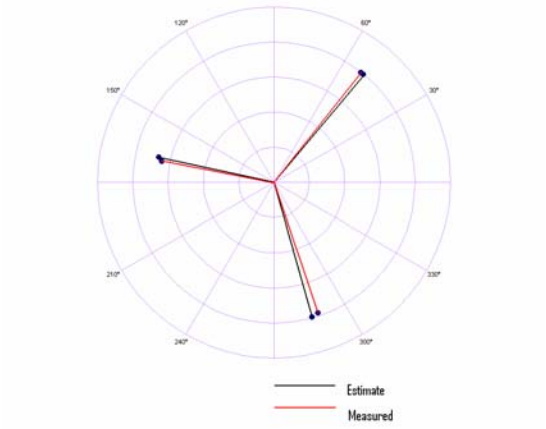

Figure 5.7: Visual comparison of the calculated and the measured high side voltage for Event 3 at OC substation

Event 4. CKT 924 Fault on 07/07/05 at 20:30:31 (Event 10 in Chapter 3)

This event was a c phase to ground fault during a thunderstorm. Using the template, the fault data from the low side was transformed to high side of the substation transformer. The microprocessor relay on the low side of the distribution transformer at BU substation recorded voltage data for this fault. Using the template, the transformed voltage values on the high side were very close to the values recorded by the relay. Table 5.6 below shows the final phase voltage results at BU:

	Estimate of Trans. side Voltage Using Distribution side Relay Data		Measured Transmission Relay Data	
	Mag	Angle	Mag	Angle
Va	79.0	1.4	78.8	0.0
Vb	78.9	121.9	79.5	123.2
Vc	47.3	237.2	48.8	236.0

Table 5.6: Comparison of the calculated and the measured high side voltage for Event 4 at BU substation

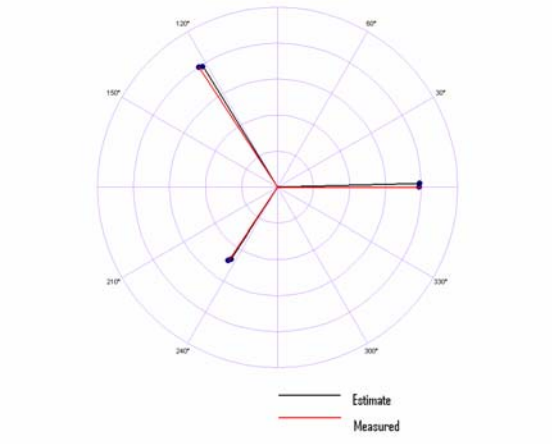

Figure 5.8: Visual comparison of the calculated and the measured high side voltage for Event 4 at BU substation

Event 5. CKT 979 Fault on 03/25/2005 at 23:19:03 (Event 15 in Chapter 3)

This event was a c phase to ground fault when a buzzard contacted the phase conductor of this circuit. Using the template, the fault data from the low side was transformed to high side of the substation transformer. The microprocessor relay on the low side of the distribution transformer at SU substation recorded voltage data for this fault. Using the template the transformed voltage values on the high side were very close to the values recorded by the relay. Table 5.7 below shows the final phase voltage results at SU substation:

	Estimate of Trans. side Voltage Using Distribution side Relay Data		Measured Transmission Relay Data	
	Mag	Angle	Mag	Angle
Va	89.1	-0.5	82.6	0.0
Vb	87.9	105.4	84.9	112.1
Vc	31.3	238.2	44.1	237.7

Table 5.7: Comparison of the calculated and the measured high side voltage for Event 5 at SU substation

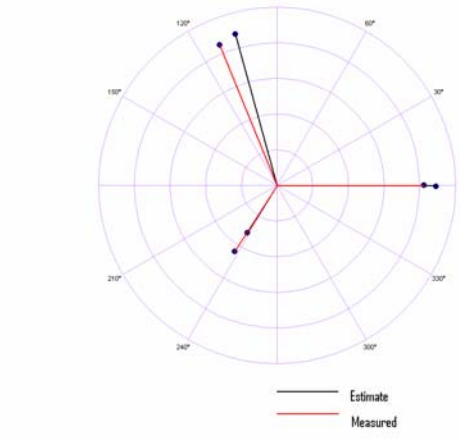

Figure 5.9: Visual comparison of the calculated and the measured high side voltage for Event 5 at SU substation

Event 6. HL-456 Fault on 09/27/05 at 02:16:39 (Event 13 in Chapter 3)

This event was a three-phase fault when the HL-456 transformer failed and caught on fire. The microprocessor relays on the low side of the distribution feeder transformer at 3 different locations initiated for this event and recorded the voltage values on the low side. Using the template, the fault data from the low side was transformed to high side of the substation transformer. The microprocessor relay on the low side of the distribution transformer at BU substation recorded voltage data for this fault. Using the template the transformed voltage values on the high side were very close to the values recorded by the relay. Tables 5.8, 5.9, and 5.10 below show the final phase voltage results at SU, OC, and DF locations:

	Estimate of Trans. side Voltage Using Distribution side Relay Data		Measured Transmission Relay Data	
	Mag	Angle	Mag	Angle
Va	32.8	96.7	30.2	109.0
Vb	29.6	216.4	27.3	232.6
Vc	31.5	331.6	29.5	346.6

Table 5.8: Comparison of the calculated and the measured high side voltage for Event 6 at SU substation

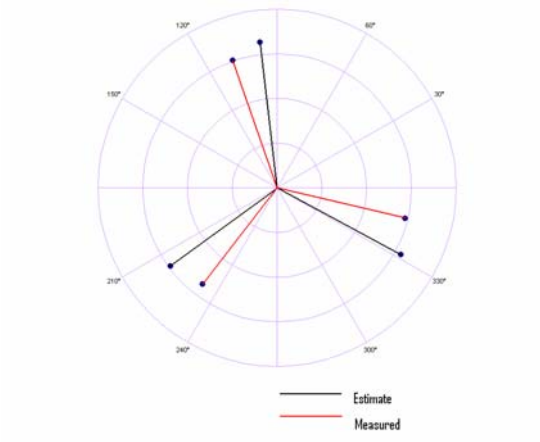

Figure 5.10: Visual comparison of the calculated and the measured high side voltage for Event 6 at SU substation

	Estimate of Trans. side Voltage Using Distribution side Relay Data		Measured Transmission Relay Data	
	Mag	Angle	Mag	Angle
Va	51.8	197.6	48.8	176.6
Vb	48.6	318.3	46.6	296.3
Vc	49.7	74.8	48.4	53.4

Table 5.9: Comparison of the calculated and the measured high side voltage for Event 6 at OC substation

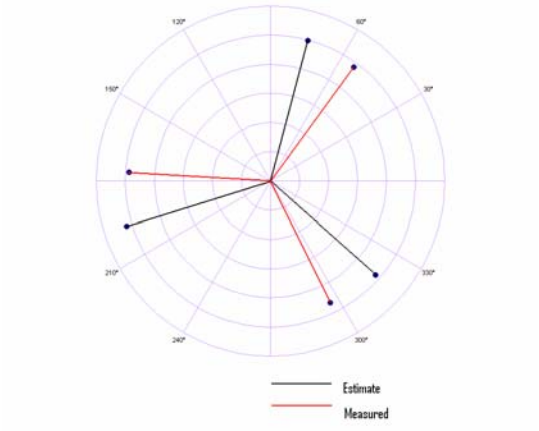

Figure 5.11: Visual comparison of the calculated and the measured high side voltage for Event 6 at OC substation

	Estimate of Trans. side Voltage Using Distribution side Relay Data		Measured Transmission Relay Data	
	Mag	Angle	Mag	Angle
Va	37.6	188.8	35.3	165.2
Vb	36.2	309.6	34.5	286.2
Vc	36.5	67.3	35.6	42.6

Table 5.10: Comparison of the calculated and the measured high side voltage for Event 6 at DG substation

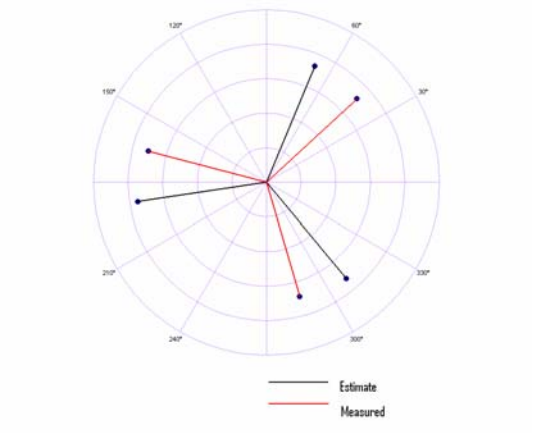

Figure 5.12: Visual comparison of the calculated and the measured high side voltage for Event 6 at DG substation

Event 7. JV Capacitor bank breaker failure on 12/11/2005 at 12:16:26

This event was a b phase to c phase to ground fault when the breaker serving the substation capacitor banks failed to operate. The microprocessor relays on the low side of the distribution feeder transformer at 2 different locations initiated for this event and recorder the voltage values on the low side of the transformer. Using the developed template in Section 4.1, the fault data from the low side was transformed to high side of the substation transformer. The transformed voltage values on the high side were very close to the values recorded by the relay. Table 5.11 and 5.12 below show the final phase voltage results at SU and OC locations:

	Estimate of Trans. side Voltage Using Distribution side Relay Data		Measured Transmission Relay Data	
	Mag	Angle	Mag	Angle
Va	82.8	11.0	81.7	8.3
Vb	42.5	137.6	41.6	138.3
Vc	42.3	245.6	44.8	242.0

Table 5.11: Comparison of the calculated and the measured high side voltage for Event 7 at SU substation

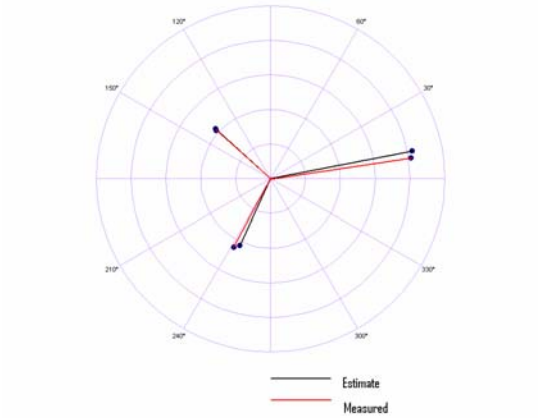

Figure 5.13: Visual comparison of the calculated and the measured high side voltage for Event 7 at SU substation

	Estimate of Trans. side Voltage Using Distribution side Relay Data		Measured Transmission Relay Data	
	Mag	Angle	Mag	Angle
Va	76.5	355.4	76.5	355.7
Vb	61.5	123.4	61.4	123.3
Vc	59.9	229.9	59.5	230.0

Table 5.12: Comparison of the calculated and the measured high side voltage for Event 7 at OC substation

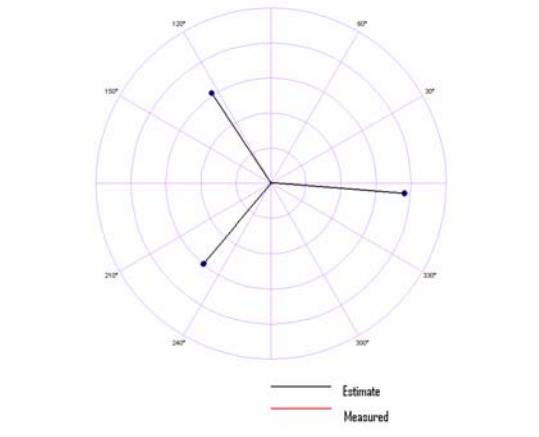

Figure 5.14: Visual comparison of the calculated and the measured high side voltage for Event 7 at OC substation

It is apparent from the above results that for all intents and purposes the calculated high side voltage is the same as the measured high side voltage.

We now apply the above calculated high side voltage values and estimate the fault location for a fault on the transmission system. As an example in this work, the transformed voltage magnitude from the low side to the high side for Event 6 was used. The data from the three substations included: SU with the calculated sag of 63.7%, DG with calculated sag value of 55.5%, and OC with the sag value of 40.4%; other meter data used in this case include NL with 54.4% and AU with 36.2% voltage sag.

Using these data with the algorithm developed in Chapter 4, we estimated the actual location of the fault with the third meters of data. However, the two meters of data estimated the fault at TR substation, one bus away (1.27 miles) from the actual fault location. A similar study for the same fault in Chapter 3, using the meter data on the transmission system, estimated the actual fault location with the second meter data. This difference in the accuracy of the fault estimation with two meter (using the transmission system sag data) and three meter data (using the low side sag data) is mainly due to the voltage drop across the substation transformer due to the impedance of the transformer. The measured voltage values directly on the high side of the transformer (as used in the studies in Chapter 3) are higher than the transformed voltage from the low to high side used in the studies in this chapter. The higher voltage values are also reflected in the difference between the measured sag values and the low side to high side calculated sag values.

Figure 5.4 below shows the meters' voltage sag values using the transformed voltage data from low to high side of the substation transformer, the actual and estimated fault location on the transmission system for Event 6.

The conclusion from this analysis is that, indeed, distribution-side voltage sag measurements can be used to pinpoint the location of transmission-side faults provided that transformer phase shift is properly handled. This conclusion is significant because there are many distribution-side monitors available, thus enhancing the accuracy of our predictions.

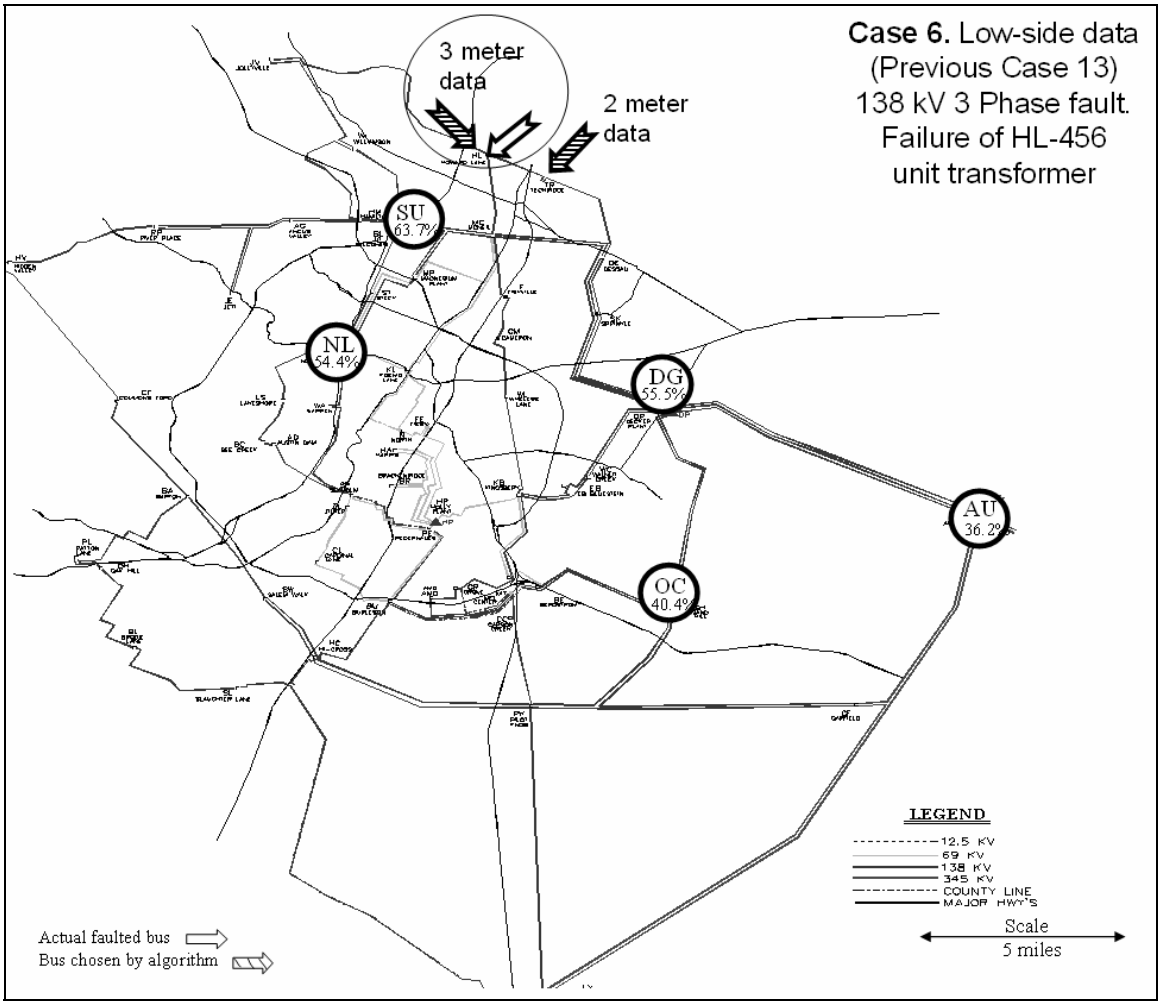

Figure 5.15: Meters and the estimated fault location for Case 6

Chapter 6: Conclusions and Suggestion for Future Work

This dissertation describes the need and significance of determining an accurate fault location in a timely manner in today's demanding electric power industry. Traditionally, fault location has been achieved by measuring rms short-circuit current magnitudes on both ends of a faulted line, and then comparing simulations with these measurements. However, these practices and the existing algorithm for fault location depends on many elements in which each element can introduce a source of error in these fault location methods. The new voltage-only based fault location procedure incorporates the system impedance matrices into the problem so that as few as three or four voltage recording devices can estimate the fault location over a wide area.

Chapter 1 presents the introduction and illustrates the current methods and practices for locating faults on transmission systems. Some of the importance of power system protection schemes and its application in estimating fault location is described in details. The two most common methods are fault location using the impedance characteristics of the line during a fault, and the traveling wave method. Fault location using line impedance calculations from both terminations of the faulted line, and using only one termination, are described in this chapter. The advantages and the problems with both methods are analyzed and explained. Several assumptions have to be made in these methodologies. Sources of error include the inherent characteristics of transmission lines, such as mutual impedance and three-terminal lines; the line terminal devices, such as C.T. saturation; and the characteristics of the fault itself, such as fault resistance, load flow, short-duration fault, and zero-sequence impedance error and mutual coupling. The traveling wave method of fault location and its merits and the causes of its inaccuracies are also explained in Chapter

1. The emphasis is on two terminal traveling waves where the relative time of arrival at both terminations is measured.

Chapter 2 presents a new voltage-only based algorithm for determining the location of all fault types in a power system. The formulation of the problem using the transmission system monitors was provided in detail. All step-by-step descriptions of the theories with their supporting equations used in this new methodology for each fault type were illustrated. For each fault type, required equations were generated and driven including balanced three-phase, single-phase to ground, phase-phase, and phase-phase to ground.

Chapter 3 describes the necessary tools and theories for this study. The types of the metering devices with their data calculation methods were described followed by the illustration of the meters' measured values. The new voltage-only method is successfully validated using 15 actual faults on Austin Energy's transmission system. For each case, data from five different meters were used. Not all cases have the same five meters because the faults occurred in different parts of the power system. Depending on threshold settings, remote meters may not respond to a fault. Eight of the studied 15 cases are single-phase to ground fault types due to the common occurrence of this type of faults. Two are phase-to-phase to ground, two phase-to-phase, and three are three-phase faults. The meters were either fault recorders or microprocessor relays at different locations in the system.

The actual event with the cause of the fault for each of these cases and related data was described followed by graphical presentation of the location of the meter, recorded voltage sag values used in this algorithm, and the actual and the estimated fault location. A table showing the meters and their measured voltage sag values (in per unit) for each case

was presented. For each case, the bus ranking and the error of actual fault bus determined by the algorithm and the error of the bus chosen by the algorithm for two, three, four, and five meter cases was shown in tabular format. An enhancement of the algorithm for locating phase-phase and phase-phase to ground fault types was presented, and the results of the enhanced algorithm were compared to the results of the original algorithm. Moreover, the goodness of the best choice was explored by comparing the least-squared error of the chosen bus to that of the next four most likely candidates.

Chapter 4 describes a methodology, theories, and calculations for extension of the problem formulation described in Chapter 2. In Chapter 4, the meter data in distribution system monitoring is used rather than the meter data on the transmission system. Application of symmetrical components in this theory and the type of the meters used on the low side of the substation transformer were explained in detail. The theories for such transformation for each type of faults with their equations were described. The phase and sequence voltage values measured by the meters on the low and high side were checked against the results of the calculated values using theoretical equations. These data were also checked using ABC012 program. A template was developed to check the measured sequence and phase values of voltage quantities by each meter. The template was devised to also calculate the high side voltage from the low side measured voltage data. After validation of these measured values, the developed equations for each fault type were used to determine the high side voltage values using the low side data of substation transformer.

Once the calculated high side voltage sag values were compared and validated with the actual measured values, then the methodology developed in Chapter 2 was applied with this transformed data to estimate a fault on the transmission system.

In Chapter 5, the theory of the low to high side voltage transformation and the developed formulas were successfully validated using seven actual faults on the Austin Energy system. Because of the availability of the relays on the low side to initiate and capture voltage data for a fault on transmission system, 17 substations were modified to capture events for a fault on the high side of a substation transformer. Normally, none or few of these relays would record an event for a fault on the transmission system due to their trigger settings and their distance from the fault. The results of the study for each of the seven cases were shown in tabular format with the following data: the calculated magnitude and phase angle values of the high side phase voltage, measured values from the relay, and the resulted output using ABC012 program. This chapter was concluded with applying the high side transformed voltage values with the methodology developed in the first phase to estimate location of a fault on transmission system. The sample case estimated the actual fault location with data from three meters. It can be concluded from this that distribution side data can be used to accurately estimate the location of transmission side faults, provided that the low to high side transformation is handled properly.

The sources of error and required assumptions for the three fault location methods described in this dissertation are summarized in Table 6.1 followed by the key advantages and disadvantages of the three fault location methods in Table 6.2 below.

Fault location method	Source of error	Required assumptions
1) Line impedance method One-termination data: Frequency domain: Time domain: Z-transform	Load flow, random value of fault resistance, mutual impedance. Accuracy not affected by the above source of error.	Line impedance is proportional to the fault distance.
Two-termination	Mutual impedance effects, load flow, fault resistance which must be assumed to be zero, line's positive/zero-sequence impedance data, three terminal lines and infeed effects, conductor size and circuit configuration which affects Z_0 and Z_1, CT saturation which causes reduction of fault current and consequently increases impedance to the fault. Series compensators (i.e., capacitors) on the bus and the line side of the transmission line can cause transient error in fault calculations. Some algorithm in this method require at least 4-5 cycles of the fault data for fault location calculations and for EHV lines the fault is cleared very fast less that 4 cycles.	
Simple Impedance	1Ω fault resistance causes large error in fault location.	Zero fault resistance at point of fault. Perfect line loading conditions.
2) Traveling Wave Method	Dependency on the arrival and reflection of the fault energy.	Transient travels assumed velocity of the speed of light. Significant part of the wave is reflected back into the faulty line. Constant wave propag. along the line. Frequency dependent of the wave propagation.
3) Voltage-only Method	Phase-phase and phase-phase to ground fault types requires alpha coefficient. Inaccuracies in system impedance matrix due to equivalency.	Positive-sequence has the same value as the negative-sequence. Perfect line loading conditions.

Table 6.1: Source of error and needed assumptions for the fault location methods

Fault location method	Advantage/Disadvantages
1) Line impedance method One-termination data: Frequency domain: Time domain: Z-transform Two-termination Simple Impedance	Adv. - Needs fault data from only one end of the faulted line. Dis. - Fault type must be determined for accurate fault location. - Requires the fault voltage and current to determine fault location. - Requires analog and digital filters to filter high frequency and dc offset. Adv. - Ground faults determined without Z_0 line impedance data. - Least sensitive to perfect line loading conditions. Dis. - Requires a skilled tech to locate the fault. Dis. - Most sensitive to perfect line loading conditions.
2) Traveling Wave Method	Adv. - More accurate fault location method than method 1. Dis. - Will not work for close-in faults and faults close to the zero crossing of the voltage waveform at the fault point. For close-in faults, attenuation at the remote end of the faulted line cause inaccuracy in fault location. - Requires very high sampling frequency.
3) Voltage-only Method	Adv. - Works regardless of the fault type. - No major assumptions are imposed for this algorithm. - Is not susceptible to the sources of errors in method 1 and 2. - Needs only voltage waveform of the faulted phase to determine fault location. Dis. - Acquisition of system impedance matrix.

Table 6.2: Advantages and disadvantages of the three fault location methods

A thorough evaluation and comparison of the fault location method using voltage-only measurements discussed in this dissertation reveals not only the superior accuracy, but also the lower number of assumptions needed in this method which consequently reduces possible sources of errors. Possible future improvements would be:

1. A set of guidelines for optimal siting of voltage only recorders in a system.
2. Using a large set of voltage sag measurements to detect improperly modeled transmission elements.
3. Utilizing system wide state estimator data to generate extremely accurate impedance matrices.
4. Predicting voltage sags system wide, or at specific customer locations, given certain faults.
5. A method for locating the fault on a line rather than at a bus.

Most utilities already have expensive fault recorders at a few of their most critical substations, and these data are telemetered back to a central control center. The procedure described in this dissertation can take advantage of these data at no extra cost, and supplement whatever existing fault location procedure is being utilized. The algorithm can be easily expanded to predict voltage sag levels through the entire system.

Appendix A: Procedure for Determining Power System Impedance Matrix Using PCFLO* Version 5.5

Introduction

There hardly exists any simple tool or software program that can calculate the impedance matrix of a power system. One of the available sources for such information is the commercially available loadflow and short-circuit programs used by electric utilities, such as PSS/E and ASPEN. However, the manufacturers consider the impedance matrix calculations in these programs as proprietary. The manufacturers of these programs can provide the impedance data for the utility users/owners of these programs for a price, ranging anywhere from $15,000 to $20,000.

PCFLO is free software (for academic use) and is available at www.ece.utexas.edu/~grady/. HOWDY.ZIP from this site needs to be downloaded and installed on the computer's hard drive. It contains all the information and programs needed to run PCFLO, including an instruction manual.

PCFLO performs load flow analysis, short circuit study and harmonics analysis. It reads column-formatted, comma-separated (CSV), or tab-separated (TSV) data. CSV/TSV data make it easy to use Microsoft Excel® for preparing input data and examining output results. Excel's sorting capabilities are especially helpful in reviewing, for example, total harmonic distortion at buses, or in finding transmission lines with overloads or buses with high or low voltages.

The following procedure outlined in this manual can provide impedance matrix data for any power system. All electric utilities are required by their regional governing bodies (such as ERCOT, Midwest ISO, etc.) to maintain and submit their load flow and short circuit case data on an annual basis. These data are recorded as RAW and SEQ data.

This document outlines the steps for determining the impedance matrix data using the impedance data available in RAW (system positive/negative-sequence data) and SEQ (system zero-sequence data) files in PTI (Power Technology, Inc.) format.

There are two input files needed for running PCFLO to determine the impedance matrix of a system – the BDAT file contains the system's bus and generation data, and the LDAT file contains the system's line and transformer data.

For BDAT, the bus data can be extracted from the top portion, "Bus Data", and the generator data from the third portion, "Generator Data", of the RAW file respectively (please note the difference in the bus type codes between the LDAT and RAW file formats).

For LDAT, the line and transformer data are extracted from the fourth portion, "Nontransformer Branch Data", and the next segment, "Transformer Data", of the RAW file respectively. The data for the transformers' connection type in LDAT is available in the "Zero-sequence Transformer Data" segment of the SEQ file (please note the difference in transformer connection codes between the LDAT and SEQ file formats).

Important notes when extracting data from RAW and SEQ into BDAT and LDAT:

- All R and X values should be converted from per unit to percentage.
- BDAT: bus data must contain a swing bus for the program to run properly.
- LDAT: 30 degree phase shift for all generator step-up (and distribution feeder) transformer and 0 degree for autotransformers.

- In LDAT, the transformer connection codes must follow the From and To in LDAT (column 1 and 2). Step-up and dist. feeder trans (Delta-Y) use code 8; all Delta-Delta and Y-Y like Auto uses code 1.

Below are the equitant fields between BDAT in PCFLO and RAW in PSS/E format:

BDAT

A 1	B 2	C 3	D 4	E 5	F 6	G 7	H 8
:Bus Data : : : :Bus :Number :(I)	Bus Name (A)	Bus Type (I)	Linear P Generation (%) (F)	Linear Q Generation (%) (F)	Linear P Load (%) (F)	Linear Q Load (%) (F)	Desired Voltage (%) (F)

RAW - Bus Data

I	NAME	IDE 3- load 2- gen 1- swing	PG	QG			100 for swing bus and all generators

BDAT

I 9	J 10	K 11	L 12	M 13	N 14	O 15	P 16
Shunt Reactive Q Load (%) (F)	Maximum Q Generation (%) (F)	Minimum Q Generation (%) (F)	Bus Control Area (I)	Remote- Controlled Bus No. (I)	Connection Type for Shunt Reactive Q Load (I)	Positive Sequence Subtransient R (%) (F)	Positive Sequence Subtransient X (%) (F)

RAW - Generator Data

						ZR	ZX; 0.01 swing

BDAT

Q 17	R 18	S 19	T 20	U 21	V 22	W 23	X 24
Negative Sequence Subtransient R (%) (F)	Negative Sequence Subtransient X (%) (F)	Zero Sequence Subtransient R (%) (F)	Zero Sequence Subtransient X (%) (F)	Connection Type for Subtransient R and X (I)	Grounding Impedance R for Subtransient Impedances (%) (F)	Grounding Impedance X for Subtransient Impedances (%) (F)	Nonlinear Device P Gen (%) (F)

RAW – Generator Data

	0.01 swing		**0.01 swing**				

BDAT

Y 25	Z 26	AA 27	AB 28	AC 29
Nonlinear Device P Load (%) (F)	Nonlinear Device Displacement Power Factor (%) (F)	Nonlinear Device Type (I)	Nonlinear Device Phase Shift (Degrees) (F)	Linear Load Connection Type (I)

RAW - Bus Data

				0

Format: (I) Integer, (F) Floating point, including E±00, (L) Logical, (A) Character
Note: The header lines must begin with a colon so that they will be properly treated as comments.
Any line beginning with a colon is treated as a comment.

LDAT

A 1	B 2	C 3	D 4	E 5	F 6	G 7	H 8
:Line and Transformer Data							
:			Positive	Positive	Pos/Neg		Min.
:			Sequence	Sequence	Sequence		Tap (pu), or
:From	To	Circuit	R	X	Charging	Rating	Min. Phase
:Bus	Bus	Number	(%)	(%)	(%)	(%)	Angle (Deg.)
:(I)	(I)	(I)	(F)	(F)	(F)	(F)	(F)

RAW – Nontransformer Branch Data

I	J	CKT	R	X	B 0- line only; blank trans	RATEA Line only; blank trans	

LDAT

I 9	J 10	K 11	L 12	M 13	N 14	O 15	P 16
	Tap					Desired Volt. at	
Max.	Step Size (pu)			Voltage-	Voltage-	V-Cont. Bus (%)	Zero
Tap (pu), or	or Phase Shift	Fixed	Phase	Cont.	Cont.	or Desired P	Sequence
Max. Phase	Step Size	Tap	Shift	Bus	Bus	in Phase Shifter	R
Angle (Deg.)	(Deg.)	(pu)	(Deg.)	Number	Side	FROM-TO (%)	(%)
(F)	(F)	(F)	(F)	(I)	(I)	(F)	(F)

RAW – Transformer Data

		1 - Trans only	* 0 and 30 - Trans only				

* 30 degree phase shift for all delta-Y transformers (generator step-up and distribution feeder) and 0 degree for all Y-Y, delta-delta (auto-transformers).

LDAT

Q 17	R 18	S 19	T 20	U 21	V 22	W 23
Zero Sequence X (%) (F)	Zero Sequence Charging (%) (F)	Connect. Type for Trans. and Shunt Elements (I)	Grounding R (%) (F)	Grounding X (%) (F)	Pos/Neg Resistive Skin Effect Factor (F)	Zero Resistive Skin Effect Factor (F)

SEQ – Zero-sequence Transformer Data

		CC	0	0		

Format: (I) Integer, (F) Floating point, including E±00, (L) Logical, (A) Character
Note: The header lines must begin with a colon so that they will be properly treated as comments.
Any line beginning with a colon is treated as a comment.

The results of executing the PCFLO program, following the above instructions, are the OUT1 and OUT2 files. PCFLO builds impedance matrices ZBUS0, ZBUS1, and ZBUS2 for zero/positive/negative sequences, respectively. ZBUS1 is always built, but ZBUS0 and ZBUS2 are built only if sufficient data are provided in BDAT and LDAT.

Appendix B: Equivalencing

Austin Energy and Electric Reliability Council of Texas (ERCOT) System

Austin Energy's system was extracted from the entire ERCOT (the regional electric grid governing body). All other adjacent systems were thevenin equivalenced. Area 9 is the Austin Energy's system bus numbers with ties with Lower Colorado River Authority, LCRA (Area 7) which is a local retail power company in Austin. Most of the electric ties are in 138 kV level with a couple of 345 kV. The ties are at north, south, east and west part of Austin Energy's system with two jointly owned power plants. The other electrical tie with Austin Energy is with CenterPoint with Area 5. The only tie is in 345 kV level.

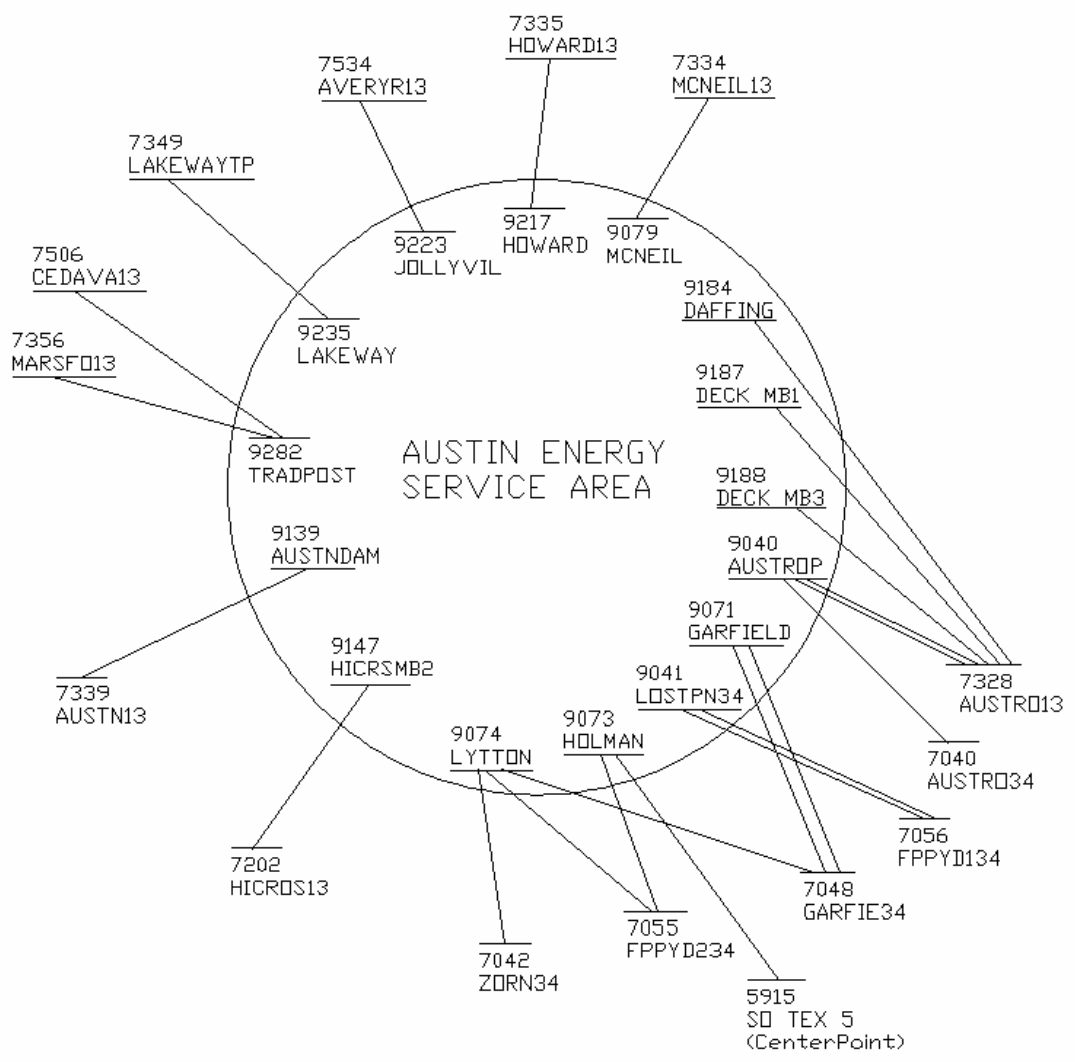

Figure A.1: Austin Energy interconnection with LCRA and CenterPoint Energy

Bibliography/References

[1] J. Lewis Blackburn, Protective Relaying Principles and Applications, Marcel Dekker, New York, 1987.

[2] T. Takagi, Y. Yamakoshi, M, Yamaura, R. Kondow, T. Mastsushima, "Development of a New Type Fault Location Using the One-Terminal Voltage and current Data", IEEE Transactions on Power Apparatus and Systems, Vol. Pas-101, No. 8, August 1982, PP. 2892-2898.

[3] E.O. Schweitzer, III, "Evaluation and Development of Transmission Line Fault-Locating Techniques which use Sinusoidal Steady Stare Information", Ninth Annual Western Protection Relay Conference, October 26-28, 1982, Spokane, Washington.

[4] Gill G. Richards and Owen T. Tan, "An Accurate Fault Location for Transmission Line", IEEE Transactions and Apparatus and Systems. Vol. Pas-101, No. 4, April 1982, PP. 945-950.

[5] Sachdev, M.S., Agarwal, R., "A Technique for Estimating Transmission Line Fault Location from Distance Relay Measurements", Power Delivery, IEEE Transactions on, Vol. 3 Issue: 1, Jan. 1988, PP. 121-129.

[6] W. Mack Grady, lecture notes, hptt://www.ece.utexas.edu/~grady/, 10/24/98, Section8-short Circuit.pdf, PP. 8-4 through 8-5.

[7] Lawrence, D.J., Waser. D.L., "Transmission Line Fault Locating Using Digital Fault Recorders", Power Delivery, IEEE Transaction on, Vol. 3, Issue 2. April 1988, PP. 496-502.

[8] Zhang Qingchao, Zhang Yao, Song Wennan, Fang Dazhong, "Transmission Line Fault Location for Single-Phase-Earth Fault on Non-Direct-Ground Neutral System", Power Delivery, IEEE Transactions on, Vol. 13, Issue 4, October 1998, PP. 1086-1092.

[9] Zhang Qingchao, Zhang Yao, Song Wennan, Fang Dazhong, "Transmsssion Line Fault Location for Double-Phase-Earth Fault on Non-Direct-Ground Neutral System", Power Delivery, IEEE Transactions on, Vol. 15, Issue 2, April 2000, PP. 520-524.

[10] Lawrence, D.J., Cabeza, L.Z., Hochberg, L.T., "Development of an Advanced Transmission Line Fault Location System Algorithm Development and Simulation", IEEE Transaction on Power Delivery, Vol. 7, Issue 4, October 1992, PP. 1972-1983.

[11] Dr. Edmund O. Schweitzer, III, "A Review of Impedance-based Fault Locating Experience", Fourteenth Annual Iowa-Nebraska System Protection Seminar, October 16, 1990, Omaha, Nebraska.

[12] Gale, P.F., Crossley, P.A., Xu Binggin, Ge Yaozhong, B.J. Baker, J.R., "Fault Location Based on Traveling Wave", Development in Power System Protection, 1993, International Conference on, PP. 54-59.

[13] Harry Lee, Abdul M. Mouse, "GPS Traveling Wave Fault Locator System: Investigation Into the Anomalous Measurements Related to Lightning Strikes", IEEE Transaction on Power Delivery, Volume:11, Issue:3, July 1996, PP. 1214-1223.

[14] Harry Lee, "Development of an Accurate Traveling Wave Fault Location Using the Global Position System Satellites", Presented to the Spring Meeting of the Canadian Electrical Association, Montreal, Quebec, March 1993, Paper No. 77.

[15] Ancell, G.B., Pahalawaththa, N.C., "Maximum Likelihood Estimate of Fault Location on Transmission Line Using Traveling Wave", Power Delivery, IEEE Transactions on, Volume: 9, Issue: 2, April 1994, PP. 680-689.

[16] Tawfik, M.M.; Morcos, M.M., "A Novel Approach for Fault Location on Transmission Lines", IEEE Power Engineering Review, Volume: 18, Issue:

[17] W. Mack Grady, Department of Electrical and Computer Engineering, University of Texas at Austin, www.ece.utexas.edu/~grady, lecture notes 3/28/99, Section 3-Transformers, Transmission Line, and UG cables.pdf, PP. 3-6 through 3-8.

[18] John J. Grainger and William D. Stevenson, Jr., Power System Analysis, McGraw-Hill Inc., 1994.

[19] Arthur R. Bergen and Vijay Vittal, Power System Analysis, Prentice Hall, 2000.

[20] PSS/E Power System Simulator for Engineering, Siemens Power Transmission & Distribution, Inc., Schenectady, NY.

[21] W. M. Grady, PCFLO (loadflow, short circuit, and harmonics analysis program), Department of Electrical and Computer Engineering, University of Texas at Austin, www.ece.utexas.edu/~grady.

[22] William D. Stevenson, Jr., Elements of Power System Analysis, McGraw-Hill Inc., 1982.

[23] Paul M. Anderson, Analysis of Faulted Power Systems, Iowa State University Press, 1978.

[24] M.F. McGranaghan, D. R. Muller, and M. J. Samotyj, "Voltage sags in industrial systems, "IEEE Transaction Ind. Application, Vol. 29, pp. 397-403, Mar./Apr. 1993.

[25] Vladimir Galouchko, www.field.hypermart.net, 2006.

[26] SEL Manual, Section 12: Standard Event Reports, Sag/swell/interruption Report, and SER.

[27] W. M. Grady, Department of Electrical and Computer Engineering, University of Texas at Austin, www.ece.utexas.edu/~grady, Free Power System Software, ABC012.

Vita

Mehrdad Vatani was born in Shahi, Iran on August 21, 1959, the son of the late Seyyed Abbasgholi Vatani and Rezvanieh Freshtian Vatani. After completing his work at Razi High School, in 1978, he attended Galveston College, San Jacinto College, and the University of Houston in Texas during 1980 and 1981. In 1982, he entered The University of Texas at Austin where he received the degree of Bachelor of Science in Electrical Engineering in May 1985. Upon his graduation, he was employed by Austin Energy, an electric utility company that provides electricity for the City of Austin, Texas. In 1989, he entered Saint Edward's University to pursue his M.B.A. and graduated in May 1992. In 1998, he entered The University of Texas at Austin to continue his graduate studies in the Electrical and Computer Engineering Department. He completed his MSEE in May 2001 and continued in the Ph.D. program.

He is a registered Professional Engineer in the State of Texas since 1992 and a member of IEEE since 1985. His work experiences are in power system protection, system control and reliability, and power quality areas. He is currently manager of the Reliability & Power Quality Engineering group at Austin Energy.

Permanent Address: 2006 Oakglen Drive
Austin, Texas 78745
U.S.A.

This dissertation was typed by the author.